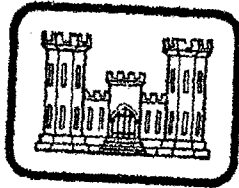


LEVEL



12
8.5



TECHNICAL REPORT GL-79-6

A TERRAIN-VEHICLE INTERACTION MODEL FOR ANALYSIS OF STEERING PERFORMANCE OF TRACK-LAYING VEHICLES

by

George Y. Baladi and Behzad Rohani

Structures Laboratory
U. S. Army Engineer Waterways Experiment Station
P. O. Box 631, Vicksburg, Miss. 39180

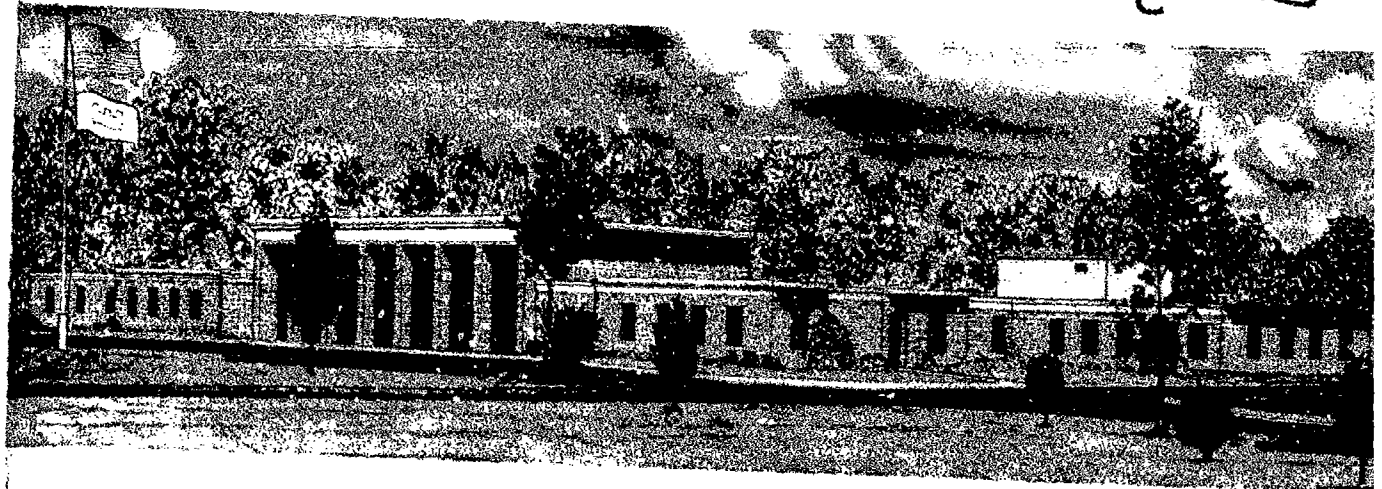
May 1979
Final Report

Approved For Public Release; Distribution Unlimited

DDC
RECEIVED
AUG 16 1979
RECEIVED
C

A TERRAIN-VEHICLE INTERACTION MODEL FOR ANALYSIS OF STEERING PERFORMANCE

DA072815



Prepared for Office, Chief of Engineers, U. S. Army
Washington, D. C. 20314

Under Project 4A161102AT24
Task A3/E3, Work Unit 003

Monitored by Geotechnical Laboratory
U. S. Army Engineer Waterways Experiment Station
P. O. Box 631, Vicksburg, Miss. 39180

79 08 16 003

Destroy this report when no longer needed. Do not return
it to the originator.

The findings in this report are not to be construed as an official
Department of the Army position unless so designated
by other authorized documents.

Unclassified

SECURITY CLASSIFICATION OF THIS PAGE (When Data Entered)

REPORT DOCUMENTATION PAGE		READ INSTRUCTIONS BEFORE COMPLETING FORM
1. REPORT NUMBER Technical Report GL-79-6	2. GOVT ACCESSION NO.	3. RECIPIENT'S CATALOG NUMBER
4. TITLE (and Subtitle) A TERRAIN-VEHICLE INTERACTION MODEL FOR ANALYSIS OF STEERING PERFORMANCE OF TRACK-LAYING VEHICLES.		5. TYPE OF REPORT & PERIOD COVERED Final report. 317-51
7. AUTHOR(s) George V/Baladi Behzad/Rohani		6. PERFORMING ORG. REPORT NUMBER
9. PERFORMING ORGANIZATION NAME AND ADDRESS U. S. Army Engineer Waterways Experiment Station Structures Laboratory P. O. Box 631, Vicksburg, Miss. 39180		8. CONTRACT OR GRANT NUMBER(s)
11. CONTROLLING OFFICE NAME AND ADDRESS Office, Chief of Engineers, U. S. Army Washington, D. C. 20314		10. PROGRAM ELEMENT, PROJECT, TASK AREA & WORK UNIT NUMBERS Project 4A161102AT24 Task A3/E3 Work Unit 003
14. MONITORING AGENCY NAME & ADDRESS (if different from Controlling Office) Geotechnical Laboratory U. S. Army Engineer Waterways Experiment Station P. O. Box 631, Vicksburg, Miss. 39180		12. REPORT DATE May 1979
16. DISTRIBUTION STATEMENT (of this Report) Approved for public release; distribution unlimited.		13. NUMBER OF PAGES 139
17. DISTRIBUTION STATEMENT (of the abstract entered in Block 20, if different from Report)		15. SECURITY CLASS. (of this report) Unclassified
18. SUPPLEMENTARY NOTES		15a. DECLASSIFICATION/DOWNGRADING SCHEDULE
19. KEY WORDS (Continue on reverse side if necessary and identify by block number) AGIL (Computer program) Soil-track interaction Mathematical models Terrain-vehicle interaction Military vehicles Track-laying vehicles Rheological models Vehicle performance		
20. ABSTRACT (Continue on reverse side if necessary and identify by block number) This report documents the development of a mathematical model for predicting the steering performance of track-laying vehicles in environments ranging from soft soils to hard surfaces such as rigid pavements. The tractive forces between the terrain and the vehicle track are simulated by a rheological model that accounts for nonlinear shear-stress/shear-deformation relation, the effect of deformation rate on shearing resistance, and the effect of pressure		

(Continued)

Unclassified

SECURITY CLASSIFICATION OF THIS PAGE(When Data Entered)

20. ABSTRACT (Continued).

on shear resistance and plastic yielding. The rheological model is coupled with the kinematics and the characteristics of the vehicle to develop the equations governing the transient motion of a vehicle on a level flat surface and the steady-state turning motion on a sloping terrain.

A computer program, named AGIL, numerically integrates and solves these equations of motion in terms of the kinematics of the problem. The computer program is used to investigate parametrically the steering performance of a specific vehicle on different types of terrain and to examine the effect of vehicle characteristics on steering performance.

Appendix A of this report presents a procedure for determining the coefficient of rolling resistance. Appendix B gives recommended stability criteria for uniform turning motion. The field direct shear device is described in Appendix C.

Accession For	
NTIS GRA&I	<input checked="" type="checkbox"/>
DDC TAB	<input type="checkbox"/>
Unannounced	
Justification	
By _____	
Date _____	
Special Codes	
Dist	Special
A	

Unclassified

SECURITY CLASSIFICATION OF THIS PAGE(When Data Entered)

PREFACE

The investigation reported herein was conducted for the Office, Chief of Engineers, U. S. Army, by personnel of the Geomechanics Division (GD), Structures Laboratory (SL), U. S. Army Engineer Waterways Experiment Station (WES), CE, as a part of Project 4A161102AT24, Task A3/E3, Work Unit 003, "Soil Response to Nonlinear Loading Systems."

This investigation was conducted by Drs. G. Y. Baladi and B. Rohani during the period October 1976-October 1978 under the general direction of Mr. B. Mather, Acting Chief, SL; Dr. J. G. Jackson, Jr., Chief, GD; Mr. J. P. Sale, Chief, Geotechnical Laboratory (GL); and Mr. C. J. Nuttall, Jr., Project Leader, Mobility Systems Division, GL.

The field direct shear device described in Appendix C for measurements of soil properties was designed by Mr. J. Q. Ehrgott, GD. Numerical calculations were performed by Mr. D. E. Barnes, GD. Appendix C was prepared by Mr. Ehrgott. The report was written by Drs. Baladi and Rohani.

COL J. L. Cannon, CE, was Commander and Director of the WES during the investigation. Mr. F. R. Brown was Technical Director.

CONTENTS

	<u>Page</u>
PREFACE	1
CONVERSION FACTORS, U. S. CUSTOMARY TO METRIC (SI)	
UNITS OF MEASUREMENT	4
PART I: INTRODUCTION	5
Background and Objective	5
Scope	6
PART II: SOIL MODEL	7
Strength Components	7
Effect of Rate of Deformation	7
Shear-Stress/Shear-Deformation Relation	8
PART III: DERIVATION OF TERRAIN-VEHICLE MODEL	10
Background	10
Boundary Conditions	11
Stress Distribution Along the Tracks	12
Normal Stress Contributions Due to Track Tension	15
Kinematics of the Vehicle	19
Track Slip Velocity and Displacement	21
Inertial Forces	24
The Rolling Resistance	25
Equations of Motion	26
Terrain-Vehicle Model for Uniform Turning Motion	27
Treatment of Sloping Terrain under Uniform Turning Motion	31
Sprocket Power	33
PART IV: PARAMETRIC STUDIES OF TERRAIN-VEHICLE INTERACTION DURING STEERING	35
Vehicle and Terrain Characteristics	35
Steady-State Turning Motion	36
Transient Motion	43
PART V: SUMMARY AND RECOMMENDATIONS	45
REFERENCES	47
TABLES 1 and 2	
FIGURES 1-67	
APPENDIX A: PROCEDURE FOR DETERMINING THE COEFFICIENT OF ROLLING RESISTANCE	A1
APPENDIX B: RECOMMENDED STABILITY CRITERIA FOR UNIFORM TURNING MOTION	B1
FIGURES B1 and B2	

CONTENTS

	<u>Page</u>
APPENDIX C: DESCRIPTION OF THE FIELD DIRECT SHEAR DEVICE	C1
Background	C1
Direct Shear Device	C2
Measurement of Soil Parameters	C5
Limitation	C6
Conclusions	C7
FIGURES C1-C5	
APPENDIX D: NOTATION	D1

CONVERSION FACTORS, U. S. CUSTOMARY TO METRIC (SI)
UNITS OF MEASUREMENT

U. S. customary units of measurement used in this report can be converted to metric (SI) units as follows:

<u>Multiply</u>	<u>By</u>	<u>To Obtain</u>
horsepower per ton	82.82	watts per kilonewton
inches	25.4	millimetres
pounds (force) per square inch	6894.757	pascals
pounds (mass)	0.45359237	kilograms
pounds (mass) per cubic foot	16.01846	kilograms per cubic metre
tons (force) per square foot	95.76052	kilopascals

A TERRAIN-VEHICLE INTERACTION MODEL FOR ANALYSIS OF
STEERING PERFORMANCE OF TRACK-LAYING VEHICLES

PART I: INTRODUCTION

Background and Objective

1. Development of high-mobility/agility tracked combat vehicles has received considerable attention recently because of the possibilities they offer for increased battlefield survivability through the avoidance, by high-speed and violent maneuver, of hits by high-velocity projectiles and missiles. In order to design and develop such vehicles rationally, it is necessary to have a quantitative understanding of the interrelationship between the terrain factors (such as soil type, soil shear strength and compressibility, etc.) and the vehicle characteristics (weight, track length and width, location of center of gravity, velocity, etc.) during steering. The actual mechanism of terrain-vehicle interaction during steering is undoubtedly very complex. Thus, in order to study such an interrelationship, it is necessary to construct idealized mathematical models of the actual system. The accuracy and range of application of such models must, of course, be determined from actual mobility experiments and obviously must depend on the degree of relevance of the idealized model as an approximation to the real behavior. The object of this investigation is to develop a mathematical model of terrain-vehicle interaction for predicting the steering performance of tracked vehicles. The basic intent is to construct a deterministic model that includes the most pertinent elements of terrain-vehicle interaction and can be used for cause-and-effect studies and optimization problems. To this end, the tractive forces between the terrain and the vehicle track are first simulated by a rheological model. The rheologic model is then coupled with track slippage, centrifugal forces, and vehicle characteristics in order to develop the equations of motion for a vehicle during steering. The equations of motion are integrated

numerically in terms of the kinematics of the problem, e.g., vehicle turning radius (or trajectory of motion), track-terrain slip velocities, offset in the vehicle's instantaneous center of rotation, etc. The model has been applied in a parametric study concerning the steering performance and stability of M113A1 armored personnel carrier (APC).

Scope

2. The development of the rheological model is given in Part II. Complete mathematical derivation of the terrain-vehicle model is presented in Part III. Detailed parametric studies concerning the steering performance of track-laying vehicles are documented in Part IV. Part V contains a summary and presents recommendations. A procedure for determining rolling resistance is outlined in Appendix A. Recommended stability criteria for uniform turning motion are given in Appendix B. Fabrication of a field direct shear device for measurement of pertinent soil properties is documented in Appendix C.

PART II: SOIL MODEL

Strength Components

3. One of the most important properties of soil affecting trafficability is the in situ shear strength of soil. The shear strength of earth materials varies greatly for different types of soil and is dependent on the confining pressure and time rate of loading (shearing). This dependence, however, is not the same for all soils and varies with respect to two fundamental strength properties of soil: the cohesive and the frictional properties. It has been found experimentally that the shear strength of purely cohesive soils (soils without frictional strength) is independent of the confining stress and is strongly affected by the time rate of shearing. On the other hand, in the case of purely frictional soil (soils without cohesive strength), the shear strength is found to be independent of time rate of loading and is strongly dependent on the confining pressure. In nature, most soils exhibit shearing resistance due to both the frictional and cohesive components. The cohesive and frictional components of strength are usually added together in order to obtain the total shear strength of the material,* i.e.,

$$\tau_M = C + \sigma \tan \phi \quad (1)$$

where τ_M is the maximum shearing strength of the material, C is the cohesive strength of the material corresponding to static loading (very slow rate of deformation), σ is normal stress, and ϕ is the angle of internal friction of the material.

Effect of Rate of Deformation

4. As was pointed out previously, the cohesive strength of the

* Symbols used in this report are listed and defined in the Notation (Appendix D).

material is dependent on the time rate of loading (shearing); i.e., the cohesive component of strength increases with increasing rate of loading. Dynamic loading, therefore, does contribute to cohesive strength. For the range of loading rates associated with the motion of tracked vehicles, the contribution to cohesive strength due to dynamic loading can be expressed as $C_d [1 - \exp(-\Lambda \dot{\Delta})]$, where C_d and Λ are material constants, and $\dot{\Delta}$ is time rate of shearing deformation. (The dot denotes differentiation with respect to time.) In view of the above expression and Equation 1, the dynamic failure criterion takes the following form:

$$\tau_M = C + C_d [1 - \exp(-\Lambda \dot{\Delta})] + \sigma \tan \phi \quad (2)$$

Equation 2 is shown graphically in Figure 1, and it is noted that when $\Lambda = 0$, it reduces to the static failure criterion (Equation 1).

Shear-Stress/Shear-Deformation Relation

5. Prior to failure, the shear-stress/shear-deformation characteristics of a variety of soils can be expressed by the following mathematical expression:

$$\tau = \frac{G \tau_M \Delta}{\tau_M + G |\Delta|} \quad (3)$$

The behavior of Equation 3 is shown graphically in Figure 2. As indicated in Figure 2, τ denotes shearing stress, Δ is shearing deformation, and G is the initial shear stiffness coefficient. In view of Equation 2, the proposed shear-stress/shear-deformation relation for soil (Equation 3) becomes

$$\tau = \frac{G [C + C_d - C_d \exp(-\Lambda \dot{\Delta}) + \sigma \tan \phi] \Delta}{G |\Delta| + C + C_d - C_d \exp(-\Lambda \dot{\Delta}) + \sigma \tan \phi} \quad (4)$$

For purely cohesive soils, $\phi = 0$ and τ is only a function of Δ and $\dot{\Delta}$. For granular materials, C and C_d are zero and τ is a function of Δ and σ . For mixed soils, τ is dependent on Δ , $\dot{\Delta}$, and σ . The qualitative behavior of Equation 4 for these three conditions is shown in Figure 3. It should be pointed out that Equation 4 reduces to the rigid plastic soil model often used in mobility studies when an extremely large value is specified for G and Λ is set to zero.

6. The most appropriate test for determining the numerical values of the five material constants in Equation 4 is an in situ direct shear test. A field direct shear device has been developed at the U. S. Army Engineer Waterways Experiment Station (WES), CE, for this purpose and is documented in Appendix C. It is also useful to conduct dynamic tri-axial tests on undisturbed soil samples taken from locations of interest to more conclusively determine the numerical values of Λ and C_d . The parameters in Equation 4 should be dimensionally consistent. For example, in English units (U. S. Customary)* and in SI units (International System of Units), the parameters have the following dimensions:

<u>Soil Model Parameters</u>	<u>English Units</u>	<u>SI Units</u>
G	lb/in. ² /in.	newton/m ² /m
C	lb/in. ²	newton/m ²
C_d	lb/in. ²	newton/m ²
σ	lb/in. ²	newton/m ²
Δ	in.	m
$\dot{\Delta}$	in./sec	m/sec
Λ	sec/in.	sec/m
τ	lb/in. ²	newton/m ²

7. In the next part, the equations of motion for a track-laying vehicle during steering are developed using the proposed soil model (Equation 4) in conjunction with track slippage, centrifugal forces, and vehicle characteristics.

* A table of factors for converting U. S. customary units of measurement to metric (SI) units is presented on page 4.

PART III: DERIVATION OF TERRAIN-VEHICLE MODEL

Background

8. The recent history of the theory of terrain-vehicle interaction begins with the work of Bekker on the theory of land locomotion (Bekker, 1963). In this classic work, Bekker laid the general framework for analytical approach to the mobility problems. His work includes an analysis of the stability and steering performance of tracked vehicles. By assuming various load distributions along the track, Bekker was able to develop several mathematical expressions relating the characteristics of the vehicle and the tractive effort of the terrain during steering. Hayashi (1975) gives the development of simple equations for practical analysis of steering of tracked vehicles by considering both the lateral and longitudinal coefficients of friction between the track and the ground. However, Hayashi's work did not include the effect of the centrifugal forces on the steering performance of the vehicle. Kitano and Jyozaki (1976) developed a more comprehensive model for uniform turning motion including the effects of centrifugal forces. This model, however, is based on the assumption that ground pressure is concentrated under each road wheel (i.e., the ground is assumed to be very hard, such as concrete pavement) and the terrain-track interaction is simulated by Coulomb-type friction in both the longitudinal and transverse directions (i.e., the distribution of shear stresses along the track is assumed). The above terrain-vehicle models are all limited to uniform turning motion (in general, for low vehicle velocity). The model given in Kitano and Jyozaki (1976) was extended by Kitano and Kuma (1977) to include nonuniform (transient) motion but the basic elements of the terrain-track interaction part of the model were retained. Since the distribution of shear stresses along the track is a function of the turning conditions (i.e., speed, radius of curvature, etc.), the need for a more general terrain-vehicle model is evident.

9. The present terrain-vehicle model (a) is based on a more comprehensive soil model (presented in Part II) than previously reported,

(b) does not make any assumption regarding the distribution of shear stress along the track (the distribution of shear stresses is the outcome of the solution), and (c) treats the complete transient motion (uniform turning motion is a special case). The following assumptions have been made in developing the terrain-vehicle models:

- a. The soil response is simulated by a rheological model, and it is assumed that complete interaction exists between the tracks and the soil.
- b. The normal stress distribution is obtained by assuming that the vehicle track system is rigid.
- c. The center of gravity of the vehicle is displaced by some distance along the longitudinal axis from the center of geometry of the vehicle.
- d. Aerodynamic forces during the turning motion of the vehicle are neglected.
- e. Track sinkage is neglected.
- f. Sloping terrain is included only in the special case of uniform turning motion.

Boundary Conditions

10. The geometry of the vehicle and the boundary condition of the proposed model are shown schematically in Figure 4. The XYZ coordinates are the local coordinate system of which X is always the longitudinal axis of the vehicle and Y is a transverse axis parallel to the ground. These axes intersect at the center of geometry of the vehicle O. The Z axis is a vertical axis passing through the origin O. The center of gravity of the vehicle (CG) lies on the X axis and is displaced by a distance C_X from the origin. The numerical value of C_X is assumed to be positive if CG is displaced forward from the center of geometry of the vehicle. The XY coordinates of the instantaneous center of rotation ICR are $P + C_X$ and \tilde{R} , respectively, where P is the offset. The center of rotation and the radius of the trajectory of the CG are, respectively, CR and R_o . The height of the center of gravity measured from ground surface is denoted by H. The length of the track-ground contact, the track width, and the tread of the tracks are L, D, and B, respectively. As shown in Figure 4,

the components of the inertial force F_C in X and Y directions are, respectively, F_{CX} and F_{CY} . The weight of the vehicle is W.

Stress Distribution Along the Tracks

11. Two types of stress, i.e., normal and shear stresses, exist along the track. As indicated in Figure 4, the normal stresses under the outer and inner tracks are denoted by $R_1(X)$ and $R_2(X)$, respectively. The components of the shear stress in X and Y directions are, respectively, $T_1(X)$ and $Q_1(X)$ for the outer track, and $T_2(X)$ and $Q_2(X)$ for the inner track. These stresses are dependent on the terrain type, vehicle configuration, and speed and turning radius of the vehicle.

12. The magnitude of normal stresses $R_1(X)$ and $R_2(X)$ can be determined in terms of the components of the inertial force, the track tensions, and the characteristics of the vehicle by considering the balance of vertical stresses and their moments in Figure 4. Thus:

$$R_1(X) = \frac{W}{DL} \left[\frac{1}{2} + \frac{6XC_X}{L^2} - \frac{H}{WB} F_{CY} - \frac{6HX}{WL^2} F_{CX} + \frac{DLN_1(X)}{W} \right] \quad (5)$$

and

$$R_2(X) = \frac{W}{DL} \left[\frac{1}{2} + \frac{6XC_X}{L^2} + \frac{H}{WB} F_{CY} - \frac{6HX}{WL^2} F_{CX} + \frac{DLN_2(X)}{W} \right] \quad (6)$$

where the normal stresses $N_1(X)$ and $N_2(X)$ are the contributions due to track tension for the outer and the inner track, respectively.

13. For this class of problems, it is convenient to derive the solution in a dimensionless form. We can, therefore, rewrite Equations 5 and 6 in the following forms:

$$R_1(x) = \frac{W}{dL^2} \left[\frac{1}{2} + 6xc_x - \frac{h}{b} \frac{F_{CY}}{W} - 6hx \frac{F_{CX}}{W} + \frac{dL^2 N_1(x)}{W} \right] \quad (7)$$

$$R_2(x) = \frac{W}{dL^2} \left[\frac{1}{2} + 6xc_X + \frac{h}{b} \frac{F_{CY}}{W} - 6hx \frac{F_{CX}}{W} + \frac{dL^2 N_2(x)}{W} \right] \quad (8)$$

where

$$\left. \begin{aligned} h &= H/L \\ b &= B/L \\ d &= D/L \\ c_X &= C_X/L \\ x &= X/L \\ y &= Y/L \\ z &= Z/L \end{aligned} \right\} \quad (9)$$

14. The components of the shear stress in the X and Y directions along both the outer and inner tracks can be obtained by combining Equations 4, 7, and 8. Thus (it is noted that R_1 and R_2 replace the normal stress σ in Equation 4):

$$T_1(x) = \frac{W}{L^2} \left\{ \frac{\mu [dc + dc_d - dc_d \exp(-\lambda \delta_1) + r_1(x) \tan \phi] \delta_1}{\mu |\delta_1| d + dc + dc_d - dc_d \exp(-\lambda \delta_1) + r_1(x) \tan \phi} \right\} \cos \gamma_1 \quad (10)$$

$$T_2(x) = \frac{W}{L^2} \left\{ \frac{\mu [dc + dc_d - dc_d \exp(-\lambda \delta_2) + r_2(x) \tan \phi] \delta_2}{\mu |\delta_2| d + dc + dc_d - dc_d \exp(-\lambda \delta_2) + r_2(x) \tan \phi} \right\} \cos \gamma_2 \quad (11)$$

$$Q_1(x) = \frac{W}{L^2} \left\{ \frac{\mu [dc + dc_d - dc_d \exp(-\lambda \delta_1) + r_1(x) \tan \phi] \delta_1}{\mu |\delta_1| d + dc + dc_d - dc_d \exp(-\lambda \delta_1) + r_1(x) \tan \phi} \right\} \sin \gamma_1 \quad (12)$$

$$Q_2(x) = \frac{W}{L^2} \left\{ \frac{\mu [dc + dc_d - dc_d \exp(-\lambda \delta_2) + r_2(x) \tan \phi] \delta_2}{\mu |\delta_2| d + dc + dc_d - dc_d \exp(-\lambda \delta_2) + r_2(x) \tan \phi} \right\} \sin \gamma_2 \quad (13)$$

where

$$\left. \begin{aligned}
 r_1(x) &= \frac{dL^2}{W} R_1(x) \\
 r_2(x) &= \frac{dL^2}{W} R_2(x) \\
 \delta_1 &= \Delta_1/L \\
 \dot{\delta}_1 &= \dot{\Delta}_1/L \\
 \delta_2 &= \Delta_2/L \\
 \dot{\delta}_2 &= \dot{\Delta}_2/L \\
 \mu &= GL^3/W \\
 \lambda &= \Lambda L \\
 c &= CL^2/W \\
 c_d &= C_d L^2/W
 \end{aligned} \right\} \quad (14)$$

The values of γ_1 and γ_2 in Equations 10 through 13 can be determined from Figure 5 as

$$\left. \begin{aligned}
 \gamma_1 &= \tan^{-1} \frac{X - P - C_X}{C_1} = \tan^{-1} \frac{x - p - c_X}{\xi_1} \\
 \text{and} \\
 \gamma_2 &= \tan^{-1} \frac{X - P - C_X}{C_2} = \tan^{-1} \frac{x - p - c_X}{\xi_2}
 \end{aligned} \right\} \quad (15)$$

where

$$\left. \begin{aligned}
 \xi_1 &= \frac{C_1}{L} \\
 \xi_2 &= \frac{C_2}{L} \\
 p &= \frac{P}{L}
 \end{aligned} \right\} \quad (16)$$

The parameter C_1 is the distance between the instantaneous center of rotation of the outer track IC_1 and its axis of symmetry, and C_2 is the distance between the instantaneous center of rotation of the inner track IC_2 and its axis of symmetry (Figure 5).

15. In order to use Equations 10 through 15, the normal stress contributions due to track tensions $N_1(x)$ and $N_2(x)$, the track slip velocities and displacements (i.e., $\dot{\Delta}_1$, Δ_1 , $\dot{\Delta}_2$, and Δ_2), and the inertial forces F_{CX} and F_{CY} , have to be determined. These are the subjects of the following three sections.

Normal Stress Contributions Due to Track Tension

16. The effect of track tension on the normal stress distribution is influenced considerably by the motion of the vehicle. At relatively low speed, tractive effort is applied to the outer track, while braking force is applied to the inner track (Figure 6a). At high speed, on the other hand, tractive efforts are applied to both tracks (Figure 6b).

17. The angles θ_a and θ_d in Figure 6 are the approach and departure angles of the track envelope, respectively. The forces \bar{T}_1 and \bar{T}_2 are the track tension in the outer and inner track, respectively. These forces can be obtained by integrating Equations 10 and 11, respectively. Thus

$$\bar{T}_1 = L^2 \int_{-\frac{1}{2}}^{\frac{1}{2}} T_1(x) dx \quad (17)$$

$$\bar{T}_2 = L^2 \int_{-\frac{1}{2}}^{\frac{1}{2}} T_2(x) dx \quad (18)$$

The normal stress distributions are influenced, however, by the vertical components of the forces \bar{T}_1 and \bar{T}_2 , namely n_1 , n_2 , and n_2' . The values of n_1 , n_2 , and n_2' are

$$n_1 = \bar{T}_1 \sin \theta_d$$

$$n_2 = \begin{cases} \bar{T}_2 \sin \theta_d & \text{if } \xi_2 \geq 0 \\ 0 & \text{if } \xi_2 < 0 \end{cases}$$

$$n_2' = \begin{cases} -\bar{T}_2 \sin \theta_d & \text{if } \xi_2 < 0 \\ 0 & \text{if } \xi_2 \geq 0 \end{cases}$$

With the determination of the forces n_1 , n_2 , and n_2' , the normal stress contributions due to track tension may be determined.

18. Since the tracks are assumed to be rigid, the normal stresses due to track tension may be distributed according to the following equations (Figure 7):

$$\left. \begin{aligned} N_1(x) &= ax + m_0 & \text{for } \frac{\ell}{L} - \frac{1}{2} \leq x \leq \frac{1}{2} \\ N_1(x) &= ax + m_0 + \frac{2n_1}{d\ell^2} \left(x + \frac{1}{2} - \frac{\ell}{L} \right) & \text{for } -\frac{1}{2} \leq x \leq \frac{\ell}{L} - \frac{1}{2} \end{aligned} \right\} \quad (22)$$

and

$$\left. \begin{aligned} N_2(x) &= ax + m_I - \frac{2n_2}{d\ell^2} \left(x - \frac{1}{2} + \frac{\ell}{L} \right) & \text{for } \frac{1}{2} - \frac{\ell}{L} \leq x \leq \frac{1}{2} \\ N_2(x) &= ax + m_I & \text{for } \frac{\ell}{L} - \frac{1}{2} \leq x \leq \frac{1}{2} - \frac{\ell}{L} \\ N_2(x) &= ax + m_I + \frac{2n_2'}{d\ell^2} \left(x + \frac{1}{2} - \frac{\ell}{L} \right) & \text{for } -\frac{1}{2} \leq x \leq \frac{\ell}{L} - \frac{1}{2} \end{aligned} \right\} \quad (23)$$

where ℓ is the distance between two adjacent wheels, and a , m_0 ,

and m_I can be determined by considering the equation of equilibrium of normal stresses and the moments of these stresses. Thus

$$\int_{-\frac{1}{2}}^{\frac{1}{2}} (ax + m_o) dx + \int_{-\frac{1}{2}}^{\frac{\ell}{L} - \frac{1}{2}} \frac{2n_1}{d\ell^2} \left(x + \frac{1}{2} - \frac{\ell}{L}\right) dx = 0 \quad (24)$$

$$\int_{-\frac{1}{2}}^{\frac{1}{2}} (ax + m_I) dx - \int_{\frac{1}{2} - \frac{\ell}{L}}^{\frac{1}{2}} \frac{2n_2}{d\ell^2} \left(x - \frac{1}{2} + \frac{\ell}{L}\right) dx +$$

$$\int_{-\frac{1}{2}}^{\frac{\ell}{L} - \frac{1}{2}} \frac{2n'_2}{d\ell^2} \left(x + \frac{1}{2} - \frac{\ell}{L}\right) dx = 0 \quad (25)$$

and

$$\int_{-\frac{1}{2}}^{\frac{1}{2}} (2ax + m_I + m_o) \left(\frac{1}{2} + \frac{\ell}{L} - x\right) dx - \int_{\frac{1}{2} - \frac{\ell}{L}}^{\frac{1}{2}} \frac{2n_2}{d\ell^2} \left(x - \frac{1}{2} + \frac{\ell}{L}\right) \left(\frac{1}{2} + \frac{\ell}{L} - x\right) dx$$

$$+ \int_{-\frac{1}{2}}^{\frac{\ell}{L} - \frac{1}{2}} \frac{2(n_1 + n'_2)}{d\ell^2} \left(x + \frac{1}{2} - \frac{\ell}{L}\right) \left(\frac{1}{2} + \frac{\ell}{L} - x\right) dx = 0 \quad (26)$$

Equations 24 through 26 contain three unknowns a , m_o , and m_I .
Completing the integrations we obtain

$$a = \frac{1}{dL^2} \left[\left(3 - \frac{2\ell}{L}\right) (n_2 - n'_2 - n_1) \right] \quad (27)$$

$$m_o = \frac{1}{dL^2} n_1 \quad (28)$$

$$m_I = \frac{1}{dL^2} (n_2 + n_2') \quad (29)$$

Substitution of Equations 27 through 29 into Equations 22 and 23 leads to

$$\left. \begin{aligned} N_1(x) &= \frac{1}{dL^2} [(3 - 2\beta) (n_2 - n_2' - n_1)x + n_1] \quad \text{for } \beta - \frac{1}{2} \leq x \leq \frac{1}{2} \\ N_1(x) &= \frac{1}{dL^2} \left\{ \left[(3 - 2\beta) (n_2 - n_2' - n_1) + \frac{2n_1}{\beta^2} \right] x + \left(\frac{1 - \beta}{\beta} \right)^2 n_1 \right\} \\ &\quad \text{for } -\frac{1}{2} \leq x \leq \beta - \frac{1}{2} \end{aligned} \right\} (30)$$

and

$$\left. \begin{aligned} N_2(x) &= \frac{1}{dL^2} \left\{ \left[(3 - 2\beta) (n_2 - n_2' - n_1) - \frac{2n_2}{\beta^2} \right] x + \left(\frac{1 - \beta}{\beta} \right)^2 n_2 + n_2' \right\} \\ &\quad \text{for } \frac{1}{2} - \beta \leq x \leq \frac{1}{2} \\ N_2(x) &= \frac{1}{dL^2} [(3 - 2\beta) (n_2 - n_2' - n_1)x + n_2 + n_2'] \\ &\quad \text{for } \beta - \frac{1}{2} \leq x \leq \frac{1}{2} - \beta \\ N_2(x) &= \frac{1}{dL^2} \left\{ \left[(3 - 2\beta) (n_2 - n_2' - n_1) + \frac{2n_2'}{\beta^2} \right] x + \left(\frac{1 - \beta}{\beta} \right)^2 n_2' + n_2 \right\} \\ &\quad \text{for } -\frac{1}{2} \leq x \leq \beta - \frac{1}{2} \end{aligned} \right\} (31)$$

where

$$\beta = \frac{g}{L} \quad (32)$$

Note that Equations 20 and 21 dictate that either n_2 or n_2' in Equations 30 and 31 are zero.

Kinematics of the Vehicle

19. A tracked vehicle in transient motion is shown schematically in Figure 8. The XYZ coordinates are the local coordinate systems that are fixed with respect to the moving vehicle (also see Figure 4). The origin O of this coordinate system stays, for all time, at a distance C_X from the center of gravity of the vehicle. The $\Psi\phi$ coordinate system is fixed on level ground, and its origin coincides with the center of gravity at time zero. The vehicle can maneuver on the $\Psi\phi$ plane and the displacements of the center of gravity of the vehicle from this reference frame are $\Psi(t)$ and $\phi(t)$.

20. The velocities v_X and v_Y (relative to the origin of the $\Psi\phi$ coordinate system) as well as the velocities v_Ψ and v_ϕ are related to the instantaneous velocity v of the CG by

$$v = \sqrt{v_X^2 + v_Y^2} = \sqrt{v_\Psi^2 + v_\phi^2} \quad (33)$$

The side-slip angle α , which is the angle between the velocity vector v and the longitudinal X axis of the vehicle, is related to the velocities v_X and v_Y as

$$\alpha = \tan^{-1} \frac{v_Y}{v_X} \quad (34)$$

Hence

$$\frac{d\alpha}{dt} = \left(v_X \frac{dv_Y}{dt} - v_Y \frac{dv_X}{dt} \right) / v^2 \quad (35)$$

The yaw angle ω and the directional angle θ are related to α as

$$\theta = \omega - \alpha \quad (36)$$

Hence

$$\frac{d\theta}{dt} = \frac{d\omega}{dt} - \frac{d\alpha}{dt} \quad (37)$$

Substitution of Equation 35 into Equation 37 leads to

$$\frac{d\theta}{dt} = \frac{d\omega}{dt} - \left(v_X \frac{dv_Y}{dt} - v_Y \frac{dv_X}{dt} \right) / v^2 \quad (38)$$

21. The radius of curvature of the trajectory of the center of gravity (i.e., the distance between CR and CG, Figures 5 and 9) is

$$R_o = v / \frac{d\theta}{dt} \quad (39)$$

Substitution of Equation 38 into Equation 39 leads to

$$R_o = \frac{v^3}{v^2 \frac{d\omega}{dt} - v_X \frac{dv_Y}{dt} + v_Y \frac{dv_X}{dt}} \quad (40)$$

The coordinates of the trajectory of the center of gravity of the vehicle can be written as

and

$$\left. \begin{aligned} \psi(t) &= - \int_0^t v \cos \theta \, dt \\ \phi(t) &= \int_0^t v \sin \theta \, dt \end{aligned} \right\} \quad (41)$$

22. The coordinates of the instantaneous center of rotation (ICR) of the hull in the XY systems (X_I , Y_I) and the instantaneous radius of curvature are (Figures 5 and 9)

$$\left. \begin{aligned} X_I &= P + C_X = v_Y / \frac{d\omega}{dt} + C_X \\ Y_I &= \tilde{R} = v_X \frac{d\omega}{dt} \\ R_I &= \sqrt{\tilde{R}^2 + P^2} \end{aligned} \right\} \quad (42)$$

and

The instantaneous velocities of an arbitrary point e of the hull are shown in Figure 9 and can be written as

$$v_{eX} = v_X + Y \frac{d\omega}{dt} \quad (43)$$

$$v_{eY} = v_Y - (X - C_X) \frac{d\omega}{dt} \quad (44)$$

$$v_e = \sqrt{\left(v_X + Y \frac{d\omega}{dt}\right)^2 + \left[v_Y - (X - C_X) \frac{d\omega}{dt}\right]^2} \quad (45)$$

Track Slip Velocity and Displacement

23. Assume that v_{s1} ($v_{s1} = \dot{\Delta}_1$) is the slip velocity of an arbitrary point e_1 of the outer track and v_{s2} ($v_{s2} = \dot{\Delta}_2$) is the slip velocity at point e_2 (e_1 and e_2 have the same abscissa) of the inner track (Figure 5). The X and Y components of these velocities are

$$\left. \begin{aligned} v_{sX1} &= C_1 \frac{d\omega}{dt} = \xi_1 L \frac{d\omega}{dt} \\ v_{sY1} &= (X - P - C_X) \frac{d\omega}{dt} = L(x - c_X) \frac{d\omega}{dt} - v_Y \end{aligned} \right\} \text{For the outer track} \quad (46)$$

$$\left. \begin{aligned} v_{sX2} &= C_2 \frac{d\omega}{dt} = \xi_2 L \frac{d\omega}{dt} \\ v_{sY2} &= v_{sY1} \end{aligned} \right\} \text{For the inner track} \quad (47)$$

As indicated in Figure 10, the angular velocity $d\omega/dt$ and the value of \tilde{R} can be written as

$$\left. \begin{aligned} \frac{d\omega}{dt} &= \frac{1}{bL} (v_{X1} - v_{sX1} - v_{X2} + v_{sX2}) \\ \tilde{R} &= \frac{1}{2 \frac{d\omega}{dt}} (v_{X1} - v_{sX1} + v_{X2} - v_{sX2}) \end{aligned} \right\} \quad (48)$$

where

v_{X1} = the velocity of the outer track in X direction

v_{X2} = the velocity of the inner track in X direction

The ratio of v_{X1} and v_{X2} is defined as the steering ratio ϵ . Thus

$$\epsilon = v_{X1}/v_{X2} \quad (49)$$

Substitution of Equations 42 and 49 into Equation 48 leads to

$$v_{sX1} = \epsilon v_{X2} - \left(v_X + \frac{bL}{2} \frac{d\omega}{dt} \right) \text{ For the outer track} \quad (50)$$

$$v_{sX2} = v_{X2} - \left(v_X - \frac{bL}{2} \frac{d\omega}{dt} \right) \text{ For the inner track} \quad (51)$$

Comparison between Equations 50 and 51 and Equations 46 and 47 results in

$$\xi_1 = (\epsilon v_{X2} - v_X) / \left(L \frac{d\omega}{dt} \right) - \frac{b}{2} \quad (52)$$

$$\xi_2 = (v_{X2} - v_X) / \left(L \frac{d\omega}{dt} \right) + \frac{b}{2} \quad (53)$$

The slip velocities of the outer and inner tracks can be obtained from Equations 46, 47, 50, and 51. Thus

$$v_{s1} = \sqrt{\left[\epsilon v_{X2} - \left(v_X + \frac{bL}{2} \frac{d\omega}{dt} \right) \right]^2 + \left[(x - c_X) L \frac{d\omega}{dt} - v_Y \right]^2} = \dot{\Delta}_1 \quad (54)$$

and

$$v_{s2} = \sqrt{\left[v_{X2} - \left(v_X - \frac{bL}{2} \frac{d\omega}{dt} \right) \right]^2 + \left[(x - c_X) L \frac{d\omega}{dt} - v_Y \right]^2} = \dot{\Delta}_2 \quad (55)$$

or in dimensionless form

$$\frac{v_{s1}}{\sqrt{Lg}} = \sqrt{\frac{L}{g}} \frac{d\omega}{dt} \sqrt{\xi_1^2 + \left[(x - c_X) - \frac{v_Y}{L} \frac{d\omega}{dt} \right]^2} \quad (56)$$

and

$$\frac{v_{s2}}{\sqrt{Lg}} = \sqrt{\frac{L}{g}} \frac{d\omega}{dt} \sqrt{\xi_2^2 + \left[(x - c_X) - \frac{v_Y}{L} \frac{d\omega}{dt} \right]^2} \quad (57)$$

The displacements along the outer and the inner tracks can be obtained by integrating Equations 54 and 55, or 56 and 57, respectively. Thus

$$\Delta_1 = \int_0^{t_1} v_{s1} dt + \Delta_{I1}$$

and

$$\Delta_2 = \int_0^{t_2} v_{s2} dt + \Delta_{I2}$$

where

$$t_1 = (L/2 - X)/v_{X1}$$

$$t_2 = (L/2 - X)/v_{X2}$$

Δ_{I1} = initial displacement of the outer track

Δ_{I2} = initial displacement of the inner track

The values of Δ_{I1} and Δ_{I2} depend on the balance between all forces and moments applied on the vehicle at zero velocity. The forces applied on the vehicle at zero velocity are in turn dependent on the rolling resistance. Within the framework of the present model, the balance of forces and moments dictates that the initial displacements be numerically equal to the coefficient of rolling resistance δ (i.e., $\Delta_{I1} = \Delta_{I2} = \delta$). Equations 58 and 59 can be written in dimensionless form as

$$\frac{\Delta_1}{L} = \int_0^{t_1} \frac{v_{s1}}{L} dt + \frac{\Delta_{I1}}{L} \quad (60)$$

$$\frac{\Delta_2}{L} = \int_0^{t_2} \frac{v_{s2}}{L} dt + \frac{\Delta_{I2}}{L} \quad (61)$$

Inertial Forces

24. According to Figure 8, the relationship between the velocities v_ψ and v_ϕ , and the velocities v_X and v_Y can be written as

$$\left. \begin{aligned} v_\psi &= -v_X \cos \omega - v_Y \sin \omega \\ v_\phi &= v_X \sin \omega - v_Y \cos \omega \end{aligned} \right\} \quad (62)$$

The acceleration in ψ and ϕ direction, a_ψ and a_ϕ , can be written as

$$\left. \begin{aligned} a_{\psi} &= \frac{dv_{\psi}}{dt} \\ a_{\phi} &= \frac{dv_{\phi}}{dt} \end{aligned} \right\} \quad (63)$$

The forward and lateral accelerations, a_X and a_Y , can be written in terms of a_{ψ} and a_{ϕ} as

$$\left. \begin{aligned} a_X &= -a_{\psi} \cos \omega + a_{\phi} \sin \omega \\ a_Y &= -a_{\psi} \sin \omega - a_{\phi} \cos \omega \end{aligned} \right\} \quad (64)$$

Substitution of Equations 62 and 63 into Equation 64 leads to

$$\left. \begin{aligned} a_X &= \frac{dv_X}{dt} + v_Y \frac{d\omega}{dt} \\ a_Y &= \frac{dv_Y}{dt} - v_X \frac{d\omega}{dt} \end{aligned} \right\} \quad (65)$$

and

Hence, the X and Y components of the inertial force can be written as

$$F_{CX} = \frac{W}{g} a_X = \frac{W}{g} \left(\frac{dv_X}{dt} + v_Y \frac{d\omega}{dt} \right) \quad (66)$$

and

$$F_{CY} = \frac{W}{g} a_Y = \frac{W}{g} \left(\frac{dv_Y}{dt} - v_X \frac{d\omega}{dt} \right) \quad (67)$$

The Rolling Resistance

25. The rolling resistance is a function of terrain type, vehicle speed, track condition, etc. Therefore, rolling resistance should be

measured for every specific condition. In this report, however, the rolling resistance is assumed to be proportional to normal load. Thus,

$$R_s = \frac{W}{dL^2} \int_{-\frac{1}{2}}^{\frac{1}{2}} [r_1(x) + r_2(x)] dx \quad (68)$$

Equations of Motion

26. Steerability and stability of tracked vehicles depend on the dynamic balance between all forces and moments applied on the vehicle. According to Figure 4, the following three equations govern the motion of the vehicle:

$$\int_{-\frac{1}{2}}^{\frac{1}{2}} [t_1(x) + t_2(x)] dx - \int_{-\frac{1}{2}}^{\frac{1}{2}} [r_1(x) + r_2(x)] dx = f_{CX} \quad (69)$$

$$\int_{-\frac{1}{2}}^{\frac{1}{2}} [q_1(x) + q_2(x)] dx = f_{CY} \quad (70)$$

$$\begin{aligned} \int_{-\frac{1}{2}}^{\frac{1}{2}} [q_1(x) + q_2(x)] (x - c_X) dx + \frac{b}{2} \int_{-\frac{1}{2}}^{\frac{1}{2}} [t_1(x) - t_2(x)] dx \\ + \frac{b}{2} \int_{-\frac{1}{2}}^{\frac{1}{2}} [r_2(x) - r_1(x)] dx = \frac{I_z}{LW} \frac{d^2 \omega}{dt^2} \quad (71) \end{aligned}$$

where

$$\left. \begin{aligned}
 t_1(x) &= \frac{dL^2}{W} T_1(x) \\
 t_2(x) &= \frac{dL^2}{W} T_2(x) \\
 q_1(x) &= \frac{dL^2}{W} Q_1(x) \\
 q_2(x) &= \frac{dL^2}{W} Q_2(x) \\
 f_{CX} &= \frac{F_{CX}}{W} \\
 f_{CY} &= \frac{F_{CY}}{W}
 \end{aligned} \right\} \quad (72)$$

and I_z = mass moment of inertia about an axis passing through the center of gravity of the vehicle and parallel to the Z axis (Figure 4). Equations 69 through 71 with the aid of Equations 10 through 68 constitute three equations that involve three unknowns. The three unknowns are either v_x , v_y , and $d\omega/dt$ or ξ_1 , ξ_2 , and p . In order to obtain a complete solution for either of the two sets of unknowns, one of the following driving conditions must be specified: (a) time history of the steering ratio $\epsilon(t)$ and the initial speed of the vehicle, (b) time history of the velocity of the individual tracks $v_{x1}(t)$ and $v_{x2}(t)$ and the initial speed of the vehicle, (c) time history of the velocity of the vehicle $v(t)$ and the trajectory of motion, (d) time history of the velocity of the vehicle and a constant value of steering ratio ϵ , or (e) the trajectory of motion and a determination of the maximum velocity time history at which the vehicle can traverse the specified trajectory. A computer program called AGIL was developed to solve Equations 69 through 71 using Newton's iteration technique.

Terrain-Vehicle Model for Uniform Turning Motion

27. For uniform turning motions, Equations 1 through 33 remain

unchanged. The side-slip angle α (Equation 34), however, becomes constant. Hence, Equations 35 and 37 become, respectively

$$\frac{d\alpha}{dt} = 0 \quad (73)$$

$$\frac{d\theta}{dt} = \frac{d\omega}{dt} = \text{constant} \quad (74)$$

Therefore, Equations 39 and 40 become

$$R_o = \frac{v}{\frac{d\omega}{dt}} \quad (75)$$

Equation 41 can be written

$$\left. \begin{aligned} \psi(t) &= -\int_0^t v \cos \theta \frac{dt}{d\theta} d\theta \\ \phi(t) &= \int_0^t v \sin \theta \frac{dt}{d\theta} d\theta \end{aligned} \right\} \quad (76)$$

Substitution of Equations 74 and 75 into Equation 76 leads to

$$\left. \begin{aligned} \psi(\theta) &= -\int_0^\theta R_o \cos \theta d\theta \\ \phi(\theta) &= \int_0^\theta R_o \sin \theta d\theta \end{aligned} \right\} \quad (77)$$

The integral of Equation 77 is

$$\left. \begin{aligned} \psi(\theta) &= -R_o \sin \theta \\ \phi(\theta) &= -R_o \cos \theta \end{aligned} \right\} \quad (78)$$

Hence

$$\psi^2 + \phi^2 = R_o^2 \quad (79)$$

Equation 79 indicates, as was expected, that the trajectory under uniform turning motion is a circle. Equations 43 through 61 remain unchanged. Equations 60 and 61, however, can be integrated analytically to yield

$$\begin{aligned} \Delta_1 = \frac{L}{2} \left\{ A_1 - (x - p - c_X) \sqrt{(x - p - c_X)^2 + \xi_1^2} - \xi_1^2 \ln \left[x - p - c_X \right. \right. \\ \left. \left. + \sqrt{(x - p - c_X)^2 + \xi_1^2} \right] \right\} \left[\frac{\epsilon - 1}{\epsilon(b + \xi_1 - \xi_2)} \right] + \Delta_{I1} \quad (80) \end{aligned}$$

and

$$\begin{aligned} \Delta_2 = \frac{L}{2} \left\{ A_2 - (x - p - c_X) \sqrt{(x - p - c_X)^2 + \xi_2^2} - \xi_2^2 \ln \left[x - p - c_X \right. \right. \\ \left. \left. + \sqrt{(x - p - c_X)^2 + \xi_2^2} \right] \right\} \left[\frac{\epsilon - 1}{(b + \xi_1 - \xi_2)} \right] + \Delta_{I2} \quad (81) \end{aligned}$$

in which

$$\begin{aligned} A_1 = \left(\frac{1}{2} - p - c_X \right) \sqrt{\left(\frac{1}{2} - p - c_X \right)^2 + \xi_1^2} + \xi_1^2 \ln \left[\frac{1}{2} - p - c_X \right. \\ \left. + \sqrt{\left(\frac{1}{2} - p - c_X \right)^2 + \xi_1^2} \right] \quad (82) \end{aligned}$$

and

$$A_2 = \left(\frac{1}{2} - p - c_X\right) \sqrt{\left(\frac{1}{2} - p - c_X\right)^2 + \xi_2^2} + \xi_2^2 \ln \left[\frac{1}{2} - p - c_X + \sqrt{\left(\frac{1}{2} - p - c_X\right)^2 + \xi_2^2} \right] \quad (83)$$

The inertial forces F_{CX} and F_{CY} , Equations 66 and 67, become

$$F_{CX} = \frac{W}{g} v_Y \frac{d\omega}{dt} = \frac{W}{Lg} \frac{pv^2}{\left(\frac{R_0}{L}\right)^2} \quad (84)$$

and

$$F_{CY} = -\frac{W}{g} v_X \frac{d\omega}{dt} = -\frac{W}{g} \frac{\tilde{R}v^2}{R_0^2} \quad (85)$$

It is noted that Equations 84 and 85 correspond to components of centrifugal force in the X and Y directions.

28. Since, in uniform turning motion, the angular velocity $d\omega/dt$ (Equation 74) is constant, equations of motion (Equations 69 through 71) become

$$\int_{-\frac{1}{2}}^{\frac{1}{2}} [t_1(x) + t_2(x)] dx - \delta \int_{-\frac{1}{2}}^{\frac{1}{2}} [r_1(x) + r_2(x)] dx - f_{CX} = 0 \quad (86)$$

$$\int_{-\frac{1}{2}}^{\frac{1}{2}} [q_1(x) + q_2(x)] dx - f_{CY} = 0 \quad (87)$$

$$\int_{-\frac{1}{2}}^{\frac{1}{2}} [q_1(x) + q_2(x)] (x - c_X) dx + \frac{b}{2} \int_{-\frac{1}{2}}^{\frac{1}{2}} [t_2(x) - t_1(x)] dx + \frac{b}{2b} \int_{-\frac{1}{2}}^{\frac{1}{2}} [r_1(x) - r_2(x)] dx = 0 \quad (88)$$

Treatment of Sloping Terrain under Uniform Turning Motion

29. Figure 11 shows schematically a tracked vehicle under (momentary) uniform turning motion on a terrain with slope angle η . In this case, the weight of the vehicle W could be resolved into a normal component (normal to the terrain) W_N and a parallel component W_T . Thus

$$\left. \begin{aligned} W_N &= W \cos \eta \\ W_T &= W \sin \eta \end{aligned} \right\} \quad (89)$$

In general, the longitudinal axis of the vehicle X makes an angle χ with the component W_T (Figure 11). Therefore, the component W_T could be resolved into two components. The first component W_{TX} is parallel to the X axis of the vehicle and the second component W_{TY} is parallel to the Y axis. Thus

$$\left. \begin{aligned} W_{TX} &= W_T \cos \chi = W \sin \eta \cos \chi \\ W_{TY} &= W_T \sin \chi = W \sin \eta \sin \chi \end{aligned} \right\} \quad (90)$$

In view of Equations 89 and 90, the normal stresses under the outer and inner tracks (Equations 7 and 8) become:

$$R_1(x) = \frac{W}{dL^2} \left[\frac{\cos \eta}{2} + 6xc_X \cos \eta - \frac{h}{b} \left(\frac{F_{CY}}{W} - \sin \eta \sin \chi \right) \right. \\ \left. - 6hx \left(\frac{F_{CX}}{W} + \sin \eta \cos \chi \right) + \frac{DLN_1(x)}{W} \right] \quad (91)$$

$$R_2(x) = \frac{W}{dL^2} \left[\frac{\cos \eta}{2} + 6xc_X \cos \eta + \frac{h}{b} \left(\frac{F_{CY}}{W} - \sin \eta \sin \chi \right) \right. \\ \left. - 6hx \left(\frac{F_{CX}}{W} + \sin \eta \cos \chi \right) + \frac{DLN_2(x)}{W} \right] \quad (92)$$

Equations 10 through 34, 41 through 61, and 73 through 85 remain unchanged. Equations of motion (Equations 86 through 88), however, become

$$\int_{-\frac{1}{2}}^{\frac{1}{2}} [t_1(x) + t_2(x)] dx - \int_{-\frac{1}{2}}^{\frac{1}{2}} [r_1(x) + r_2(x)] dx = f_{CX} + \sin \eta \cos \chi \quad (93)$$

$$\int_{-\frac{1}{2}}^{\frac{1}{2}} [q_1(x) + q_2(x)] dx = f_{CY} - \sin \eta \sin \chi \quad (94)$$

$$\int_{-\frac{1}{2}}^{\frac{1}{2}} [q_1(x) + q_2(x)] (x - c_X) dx + \frac{b}{2} \int_{-\frac{1}{2}}^{\frac{1}{2}} [t_2(x) - t_1(x)] dx \\ + \frac{b}{2} \int_{-\frac{1}{2}}^{\frac{1}{2}} [r_1(x) - r_2(x)] dx = 0 \quad (95)$$

Sprocket Power

30. The steering performance of a tracked vehicle may be limited either by its stability or by the power available at the sprockets. The powers which must be available at the inner and outer track sprockets, PT1 and PT2, respectively, are

$$PT1 = D \int_{-\frac{L}{2}}^{\frac{L}{2}} [T_1(x) \dot{\Delta}_1 / \cos \gamma_1] dx + \delta v_{X1} W \cos \eta \frac{\int_{-\frac{L}{2}}^{\frac{L}{2}} R_1(x) dx}{\int_{-\frac{L}{2}}^{\frac{L}{2}} [R_1(x) + R_2(x)] dx} \quad (96)$$

$$PT2 = D \int_{-\frac{L}{2}}^{\frac{L}{2}} [T_2(x) \dot{\Delta}_2 / \cos \gamma_2] dx + \delta v_{X2} W \cos \eta \frac{\int_{-\frac{L}{2}}^{\frac{L}{2}} R_2(x) dx}{\int_{-\frac{L}{2}}^{\frac{L}{2}} [R_1(x) + R_2(x)] dx} \quad (97)$$

or in dimensionless form as

$$\frac{PT1}{W\sqrt{Lg}} = \frac{L}{\sqrt{Lg}} \int_{-\frac{1}{2}}^{\frac{1}{2}} [t_1(x) \dot{\delta}_1 / \cos \gamma_1] dx + \delta \cos \eta \frac{v_{X1}}{\sqrt{Lg}} \frac{\int_{-\frac{1}{2}}^{\frac{1}{2}} r_1(x) dx}{\int_{-\frac{1}{2}}^{\frac{1}{2}} [r_1(x) + r_2(x)] dx} \quad (98)$$

$$\frac{PT_2}{w\sqrt{Lg}} = \frac{L}{\sqrt{Lg}} \int_{-\frac{1}{2}}^{\frac{1}{2}} [t_2(x) \delta_2 / \cos \gamma_2] dx + \delta \cos \eta \frac{v_{X2}}{\sqrt{Lg}} \frac{\int_{-\frac{1}{2}}^{\frac{1}{2}} r_2(x) dx}{\int_{-\frac{1}{2}}^{\frac{1}{2}} [r_1(x) + r_2(x)] dx} \quad (99)$$

Therefore, the total power PT and the differential power PTD required are

$$PT = PT_1 + PT_2 \quad (100)$$

$$PTD = PT_1 - PT_2 \quad (101)$$

Equations 100 and 101 may be used to calculate the behavior of an actual steering mechanism.

PART IV: PARAMETRIC STUDIES OF TERRAIN-VEHICLE
INTERACTION DURING STEERING

31. In order to demonstrate the behavior of the terrain-vehicle model, the steering performance of a track-laying vehicle on different types of terrain is parametrically studied. In addition, the effect of vehicle characteristics on the steering performance is also investigated. The parametric studies are divided into two general areas: (a) steering performance during steady-state turning motion and (b) steering performance during transient motion. Under these two general areas five separate sets of parameter studies are conducted as outlined in the following tabulation:

<u>Steady-State Turning Motion</u>	<u>Transient Motion</u>
1. Effect of terrain type	1. Effect of terrain type
2. Effect of terrain slope	2. Effect of track tension
3. Effect of vehicle characteristics	

Vehicle and Terrain Characteristics

32. The characteristics of the tracked vehicle (M113A1 APC) used for the parametric studies are given in Table 1. As indicated in Equation 4, the tractive effort of the terrain material is characterized by five independent parameters. To determine the effects of these parameters on the steering performance of the vehicle, five different types of terrain are chosen for the analysis. The terrain soil types and the associated material constants are given in Table 2. In reality, Table 2 contains three basic types of soil, i.e., a soft clay, a dense sand, and a mixed soil having both cohesive and frictional strength (cases 1, 3, and 4, respectively). In order to include rate effects in the analysis, two extra cases are considered where the baseline properties of the soft clay (case 1) and the mixed soil (case 4) are modified (cases 2 and 5, respectively). It should be pointed out that the numerical values of the material constants in Table 2 are not for any specific site but are

chosen as "typical" numbers for the type of soil being simulated. For reference purposes and possible future use, Table 2 also includes the values of WES cone index (CI) for each material. The value of CI is calculated from empirical equations (see Appendix A) relating CI to C and ϕ and is, therefore, approximate. The coefficients of rolling resistance in Table 2 are determined based on the procedure outlined in Appendix A, using the characteristics of the vehicle shown in Table 1 and the calculated values of the cone index. The rolling resistance produces the initial displacements in Equations 58 through 61 or Equations 80 and 81.

33. In addition to the five different types of terrain, a firm surface is also considered for the steering performance analysis of the vehicle. The firm surface is simulated by equating the material constants C , C_d , and A to zero, allowing the initial shear stiffness coefficient to become infinitely large and replacing $\tan \phi$ by the friction coefficient between the track and the firm surface. The firm surface is denoted as case 6 in Table 2 and is represented by a friction coefficient of 0.7 (i.e., $\tan 35^\circ = 0.7$). The results of the parametric studies are presented in the following sections.

Steady-State Turning Motion

Effect of terrain type on steering performance

34. The results of the calculations for assessing the effect of terrain type on steering performance are presented in various forms in terms of dimensionless parameters in Figures 12 through 27. Relationships between vehicle speed and track slip velocities, turning radius, offset, and power requirement for two different values of steering ratio are given in Figures 12 through 17. Figures 18 through 21 show relationships between vehicle speed and track velocity and power requirement. Relationships between turning radius and steering ratio are given in Figure 22. Figure 23 presents relationships between offset and lateral components of centrifugal force for two different values of steering ratio. Using the stability criteria described in Appendix B,

relationships between steering ratio and turning radius, lateral acceleration, vehicle speed and corresponding power requirement are obtained and presented in Figures 24 through 27.

35. The steering performance of the vehicle on soft clay, with and without rate effect (cases 1 and 2 of Table 2), is shown in Figures 12 and 13 in terms of relationships between vehicle speed and track slip velocity, turning radius, offset, and power requirement for steering ratios of 1.1 and 1.75, respectively. In the case of soft clay without rate effect (case 1 of Table 2), it is observed that turning radius increases gradually with increasing velocity of the vehicle up to a critical velocity. Beyond this velocity, turning radius decreases rapidly with further increase in the vehicle speed, and the vehicle becomes unstable. For soft clay with rate effect (case 2 of Table 2), turning radius actually decreases with increasing vehicle velocity. As noted from Figures 12 and 13, the rate of decrease is very pronounced for lower velocities. The decrease in turning radius with increasing vehicle velocity is a direct consequence of the effect of the rate of shearing deformation on the cohesive strength of the material (Figure 1 and Equation 2). As the velocity of the vehicle increases, the rate of shearing deformation of the terrain material also increases. Consequently, the material would exhibit successively higher strengths (act as a harder material). A comparison between Figures 12 and 13 clearly shows that, with or without rate effect, the turning radius at which the vehicle is able to steer decreases as the steering ratio increases. It is also noted from Figures 12 and 13 that the slip velocity of the outer track (v_{sX1}) continuously increases with increasing vehicle velocity. This indicates that the outer track slips backward during steering and generates tractive effort. The slip velocity of the inner track (v_{sX2}) is practically zero at low vehicle velocities. As the velocity of the vehicle increases, the slip velocity of the inner track increases slightly (i.e., the inner track also slips backward). Both tracks slip backward because on soft clay the turning radius at which the vehicle is able to steer is relatively large. It will be shown later that on harder soil, where the turning radius is relatively small, the inner

track slips forward. This indicates that it is easy to oversteer the vehicle on soft soil. It is of interest to note that the rate of deformation has very little effect on the power requirement. This is due to the fact that rate effect has very little influence on the slip velocities from which the power is computed (Equations 96 and 97).

36. Relationships similar to Figures 12 and 13 are shown in Figures 14 and 15 for mixed soil. Relative to the shearing strength of soft clay, the mixed soil is considered hard. Comparisons of Figures 12 and 13 with Figures 14 and 15 indicate that the difference in the shearing strength of the material is reflected in the predicted steering performance and stability of the vehicle. In contrast to soft clay, the turning radius in the case of mixed soil is not strongly affected by rate of deformation. Since the mixed soil is already strong, the added strength due to rate effect does not affect the maneuverability of the vehicle. It is noted from Figures 14 and 15 that the inner track slips forward during steering. The slip velocity of the inner track increases with increasing vehicle velocity up to the critical velocity. Beyond this velocity, the slip velocity of the inner track decreases. At this point, the vehicle starts to oversteer. This behavior is more dramatic at a higher steering ratio (Figure 15). Kinematic relationships similar to those shown in Figures 12 and 13 are shown in Figures 16 and 17 for dense sand and firm surface, respectively, for steering ratios of 1.1 and 1.75. These relationships very closely resemble the corresponding curves for the mixed soil without rate effect (case 4). Comparison of Figure 16 with Figure 17 indicates that, within the framework of the present model, the steering performance of the vehicle on dense sand and firm surface is about the same. This is because the pertinent parameter describing the tractive effort of the material (i.e., ϕ , Table 2) is the same for both materials. It is anticipated that such similarity in steering performance will not be realized when soil compressibility and track sinkage are included in the model.

37. Relationships between vehicle speed and track velocity and power requirement for each track are given in Figures 18 through 21 for cases 1, 3, 4, and 6, respectively. Each figure contains relationships

for steering ratios of 1.1 and 1.75. These relationships are useful for determining the power required by each sprocket during steering. As anticipated, the difference in the power requirement for the outer track (PT1) and the inner track (PT2) increases as the steering ratio increases.

38. Figure 22 presents relationships between turning radius and steering ratio for all materials described in Table 2 at a relatively low velocity, $v/\sqrt{Lg} = 0.5$. Such a relationship, however, is weakly dependent on velocity as long as the velocity remains within the range at which the vehicle is stable. As was pointed out previously, turning radius decreases with increasing steering ratio. The rate of decrease in turning radius is greater for smaller values of steering ratio. It is of interest to note that the relationship between turning radius and steering ratio is independent of the strength of the terrain material for hard materials (cases 3, 4, 5, and 6). On the other hand, for soft soils (cases 1 and 2), this relationship is dependent on the strength of the material.

39. Relationships between offset and lateral components of the centrifugal force are shown in Figure 23 for steering ratios of 1.1 and 1.75 and for all materials described in Table 2. As the tractive effort of the material increases, the centrifugal force F_{CY} also increases. This is because the higher the tractive effort of the material is, the smaller the turning radius at which the vehicle is able to steer (Figures 12 through 15) will be and, consequently, the larger the centrifugal force. It is clear from Figure 23 that for a given material F_{CY} increases with increasing offset. The vehicle becomes unstable, as anticipated, when P/L exceeds 0.5.

40. Figures 24 through 27 contain relationships between steering ratio and turning radius, lateral acceleration, vehicle speed, and power requirements for soft clay, dense sand, mixed soil, and firm surface (cases 1, 3, 4, and 6, respectively). For each steering ratio, these quantities are calculated using the stability criteria presented in Appendix B. Since Figures 24 through 27 represent go-no-go situations, they are very useful for design and verification purposes.

Effect of terrain slope
on steering performance

41. The results of the parameter studies concerning the role of terrain slope on the steering performance of the vehicle for mixed soil (case 4, Table 2) are given in Figures 28 through 35. Two values of terrain slope (i.e., $\eta = 5^\circ$ and $\eta = 10^\circ$, Figure 11) are used for the calculations. For each value of η , results for four values of χ (i.e., $\chi = 0^\circ, 90^\circ, 180^\circ$, and 270°) are presented. As indicated in Figure 11, χ defines the vehicle's direction of motion on the sloping terrain ($\chi = 0^\circ, 90^\circ, 180^\circ$, and 270° correspond, respectively, to points 1, 2, 3, and 4 in Figure 11; $\chi = 0^\circ$ indicates upslope motion, $\chi = 180^\circ$ indicates downslope motion; $\chi = 90^\circ$ indicates cross-slope turning up; and $\chi = 270^\circ$ indicates cross-slope turning down). Figures 28 through 31 portray the effects of the parameters η and χ on the relationships between vehicle speed and slip velocity, turning radius, offset, and power requirement for steering ratio of 1.1. Relationships similar to Figures 28 through 31 are presented in Figures 32 through 35 for steering ratio of 1.75. For $\chi = 0^\circ$ (Figures 28 and 32) increasing the slope of the terrain causes the slip velocity of the outer track to increase and the slip velocity of the inner track to decrease. This indicates that, for this condition, as the slope of the terrain increases, the tractive efforts generated by the outer track increase, while the tractive efforts generated by the inner track decrease. For $\chi = 180^\circ$ (Figures 30 and 34), on the other hand, this trend is reversed. For $\chi = 90^\circ$ (Figures 29 and 33) the slip velocities of both the inner and the outer tracks decrease as the slope of the terrain increases. The decrease in slip velocities, however, is more pronounced for $\epsilon = 1.1$ (Figure 29) and higher vehicle velocities. For $\chi = 270^\circ$ (Figures 31 and 35) the slip velocities increase slightly as the slope of the terrain increases. In general, the effect of terrain slope on slip velocities is stronger for $\chi = 0^\circ$ and 180° than for $\chi = 90^\circ$ and 270° .

Effect of vehicle charac-
teristics on steering performance

42. Six vehicle characteristics are considered for this parameter

study. They are (a) weight W , (b) track length L , (c) track width D , (d) track tread B , (e) height of the center of gravity H , and (f) position of the center of gravity relative to the center of geometry C_x (Figure 4). The effects of these parameters on the steering performance of the vehicle are discussed in the following paragraphs.

43. Vehicle weight. The effect of vehicle weight on the steering performance is demonstrated in Figures 36 through 38 for steering on mixed soil (case 4) and firm surface (case 6). These figures contain results for the baseline weight W (Table 1) and $1.5W$. All other vehicle parameters are unchanged and correspond to those in Table 1. Increasing the weight while keeping other vehicle characteristics unchanged increases the lateral component of centrifugal force (Figure 36) and the power requirement (Figures 37 and 38). The vehicle velocity during steering, however, reduces (Figure 37). As a result of the decrease in vehicle velocity, the lateral acceleration also decreases (Figure 37). In the case of hard materials, such as the firm surface (case 6, Table 2), changing the weight of the vehicle does not change the results of the calculations, except for the power (Figure 38). This was expected since for firm surface the soil model (Equation 4) reduces to a friction-type model and weight drops out of the equations of motion for steady-state condition (Equations 86 through 88). It can be concluded, therefore, that friction models are not appropriate for studying the effect of vehicle weight on steering performance.

44. Track length. Figures 39 through 43 demonstrate the effect of track length on steering performance of the vehicle on mixed soil (case 4, Table 2). These figures contain results for the baseline length L (Table 1) and $1.5L$ for steering ratios of 1.1 and 1.75. All other vehicle parameters are unchanged and correspond to those in Table 1. Figures 39 and 41 indicate that the slip velocities of both the outer and inner tracks increase with increasing track length, causing an increase in the overall tractive efforts of the vehicle. This leads to an increase in the power required to steer the vehicle (Figures 39 through 42). Figures 39 and 41 also indicate that the ability of the vehicle to make a sharp turn reduces greatly as the length

of the track increases. This leads to a decrease in the lateral component of centrifugal force (Figure 43).

45. Track width. The effect of track width on steering performance is portrayed in Figures 44 through 48 for the baseline width D (Table 1) and $1.5 D$ and for steering ratios of 1.1 and 1.75. It is clear from these figures that, for mixed soil (case 4, Table 2), increasing the track width improves the overall stability of the vehicle. The velocity at which the vehicle becomes unstable increases as the track width increases. This increase in the velocity causes a corresponding increase in the lateral component of centrifugal force (Figure 48). Also, because of the increase in the slip velocities, the power required to steer the vehicle increases with increasing track width (Figures 44 through 47).

46. Track tread. Figures 49 through 53 demonstrate the effect of track tread on steering performance of the vehicle on mixed soil (case 4, Table 2). These figures contain results for the baseline track tread B (Table 1) and $2B/3$ for steering ratios of 1.1 and 1.75. All other vehicle parameters are unchanged and correspond to those in Table 1. Figures 49 and 51 indicate that decreasing the tread increases the slip velocities and the power requirement for steering the vehicle. The velocity at which the vehicle becomes unstable decreases slightly (Figures 49 and 51), causing a corresponding decrease in the lateral component of centrifugal force (Figure 53).

47. Height of center of gravity. The effect of the height of the center of gravity on the steering performance of the vehicle is demonstrated in Figure 54 in terms of relationships between the turning radius and the vehicle speed for the baseline $H/L = 0.367$, and for $H/L = 0.61$, and $H/L = 0.122$. The materials used in these calculations are dense sand and mixed soil (cases 3 and 4, Table 2). It is clear from Figure 54 that at low speeds the height of the center of gravity does not affect the turning radius because the load transfer to the outer track due to the centrifugal force is very small. As the velocity of the vehicle increases, however, the load transfer to the outer track increases proportionally to the height of the center of

gravity (Equations 7 and 8). This causes the vehicle to oversteer. The oversteering is more pronounced for sand.

48. Position of the center of gravity. Figures 55 through 57 demonstrate the effect of position of the center of gravity on steering performance of the vehicle on mixed soil (case 4, Table 2). From Figure 55 it is observed that moving the center of gravity in a forward ($C_x > 0$) or backward ($C_x < 0$) direction from the center of geometry of the vehicle causes the vehicle to oversteer as turning speed increases. The oversteering condition is more dramatic when $C_x < 0$. It can be concluded, therefore, that the steering performance of the vehicle is strongly affected by the position of the center of gravity. Figures 56 and 57 show that the velocity at which the vehicle becomes unstable increases as the center of gravity moves from a backward to a forward position.

Transient Motion

Effect of terrain type on steering performance

49. Two terrain types are chosen for this study: a dense sand and a mixed soil (cases 3 and 4, respectively, Table 2). The results of the calculations for the steering performance of M113A1 APC (Table 1) are given in Figures 58 through 62. At time zero the speed of the vehicle was specified to be $v_x/\sqrt{Lg} = 2.2$ and $v_y/\sqrt{Lg} = 0$ (Figure 59). Note that at time zero the speed of the vehicle is equal to the track velocity (Figure 58). The velocity of the inner track was gradually reduced to $v_{x2}/\sqrt{Lg} = 1.1$, while the outer track velocity was kept constant. The trajectories of motion of the center of gravity of the vehicle corresponding to these specified track velocities (Figure 58) are shown in Figure 60. Time histories of slip velocities and turning radius are shown in Figure 58. Time histories of the vehicle's forward and lateral velocities and accelerations are given in Figure 59. Figure 61 portrays the time histories of yaw rate, offset, side-slip angular velocity, and rate of directional angle. Time histories of

power requirements are shown in Figure 62. Figure 60 indicates that for both terrain materials the turning radius decreases rapidly and the trajectories spiral inward. At the same time the side-slip angle increases continuously, causing the vehicle to skid. This process is more pronounced for sand (case 3) than for mixed soil (case 4). Figure 60 also indicates that it is easier to steer the vehicle on mixed soil than on sand. The lateral accelerations increase initially with time and then decrease as the trajectories spiral inward and the vehicle skids (Figure 59). At later times, when the turning radius becomes constant (Figure 58), the lateral accelerations reach a constant value.

Effect of track tension
on steering performance

50. The effect of track tension on steering performance of M113A1 APC is demonstrated in Figures 63 through 67 for steering on a mixed soil (case 4). These figures are similar to Figures 58 through 62. In this case, however, the velocity of the vehicle at time zero is $v_x/\sqrt{Lg} = 1.0$ and $v_y/\sqrt{Lg} = 0$. From these figures it is clear that for this type of terrain and the specified initial velocity, the effect of track tension on the steering performance of the vehicle is very small. Including track tension in the calculations reduces the power requirements slightly, as indicated in Figure 67.

PART V: SUMMARY AND RECOMMENDATIONS

51. A mathematical model of terrain-vehicle interaction for predicting the steering performance of track-laying vehicles has been developed and computerized for numerical application. The model contains some of the basic parameters governing the steering performance of track vehicles, such as track slippage, centrifugal forces, vehicle characteristics, and soil type. The model has not been experimentally verified. However, the results obtained by utilizing the model for a specific vehicle and several types of soil are qualitatively in agreement with observed behavior of tracked vehicles during steering.

52. Based on a series of parameter studies conducted with the model, the following qualitative conclusions can be stated:

- a. The details of the stress-deformation characteristics of the terrain material strongly affect the steering performance of track-laying vehicles on soft soil. For such soils it appears that a single strength index (such as the cone index) is not sufficient to describe the tractive effort of the terrain material for studying the maneuverability of tracked vehicles.
- b. For hard soils the details of the stress-deformation characteristics very mildly affect the steering performance of the vehicle. For such soils the tractive effort can be described in terms of only the ultimate shearing strength of the material, including both the cohesive and frictional components.
- c. Increasing the weight of the vehicle (while keeping other vehicle parameters unchanged) reduces the velocity of the vehicle and increases the lateral component of centrifugal force and the power requirement during steering.
- d. Increasing the track length results in higher slip velocities for both the outer and the inner tracks during steering. This leads to an increase in power requirement during steering.
- e. Decreasing the track tread increases the slip velocities and the power requirement during steering. The velocity at which the vehicle becomes unstable decreases slightly, causing a corresponding decrease in the lateral component of centrifugal force.
- f. Increasing the track width improves the overall stability of the vehicle. The velocity at which the vehicle becomes

unstable increases as the track width increases. This increase in the velocity causes a corresponding increase in the lateral component of centrifugal force. Also, because of an increase in slip velocities, the power required to steer the vehicle increases with increasing track width.

- g. At low speeds the height of the center of gravity does not affect the turning radius of the vehicle because load transfer to the outer track due to centrifugal force is very small. As the velocity of the vehicle increases, the load transfer to the outer track increases proportionally to the height of the center of gravity. Therefore, increasing the height of the center of gravity causes the vehicle to oversteer as the velocity increases.
- h. The steering performance of the vehicle is strongly affected by the longitudinal position of the center of gravity. The velocity at which the vehicle becomes unstable increases as the center of gravity moves relative to the center of geometry of the vehicle from a rearward to a forward position.

53. Efforts are presently under way at WES to extend the model to include sloping terrains and track sinkage in the transient formulation. In order to quantitatively model the behavior of various types of soil, it is recommended that the soil model be extended to include (a) strain-softening behavior, (b) dependency of initial shear stiffness coefficient on pressure, and (c) dependency of angle of internal friction on pressure.

REFERENCES

Bekker, M. B. 1963. The Theory of Land Locomotion, The University of Michigan Press, Ann Arbor, Mich.

Hayashi, I. 1975. "Practical Analysis of Tracked Vehicle Steering Depending on Longitudinal Track Slippage," Proceedings, The International Society for Terrain Vehicle Systems Conference, Vol 2, p 493.

Kitano, M. and Jyozaki, H. 1976. "A Theoretical Analysis of Steerability of Tracked Vehicles," Journal of Terramechanics, The International Society for Terrain Vehicle Systems, Vol 13, No. 4, pp 241-258.

Kitano, M. and Kuma, M. 1977. "An Analysis of Horizontal Plane Motion of Tracked Vehicles," Journal of Terramechanics, The International Society for Terrain Vehicle Systems, Vol 14, No. 4, pp 221-225.

Rula, A. A. and Nuttall, C. J., Jr. 1971. "An Analysis of Ground Mobility Models (ANAMOB)," Technical Report M-71-4, U. S. Army Engineer Waterways Experiment Station, CE, Vicksburg, Miss.

Table 1
Characteristics of the Vehicle Used for Numerical Analysis

Weight (W) = 23,410 lb

Track length (L) = 105 in.

Track width (D) = 15 in.

Tread (B) = 90 in.

Height of center of gravity (H) = 38.5 in.

Moment of Inertia (I_z) = 200,000 lb-in.²

Distance between two adjacent wheels (ℓ) = 26.25 in.

Approach angle (θ_a) = 30 deg

Departure angle (θ_d) = 30 deg

Location of the center of gravity measured from the
geometrical center of the vehicle (C_x) = 0

Table 2
Matrix of Material Types and Associated Constants

Case No.	Material Simulated	Approximate Standard Cone Index CI*	C	C _d	A	G	φ	Remarks	
			lb/in. ²	lb/in. ²	sec/in.	lb/in. ² /in.	deg		
1	Soft clay	30	2.5	0	0	20	0	0.2	Baseline properties
2	Soft clay	30	2.5	2.5	0.03	20	0	0.2	Including rate effect
3	Dense sand	140	0	0	0	55	35	0.06	**
4	Mixed soil	120	4	0	0	50	20	0.06	Baseline properties
5	Mixed soil	120	4	4	0.04	50	20	0.06	Including rate effect
6	Firm surface	NA	0	0	0	∞	35	0.04	†

* CI corresponds to WES cone index (Rula and Nuttall, 1971).

** It is noted from Equation 4 that purely granular materials are assumed to be rate independent.

† The coefficient of rolling resistance ϕ for firm surface is calculated from Appendix A to be 0.045 by assuming an infinite value for CI. The value used for the calculations, however, was approximated to 0.04.

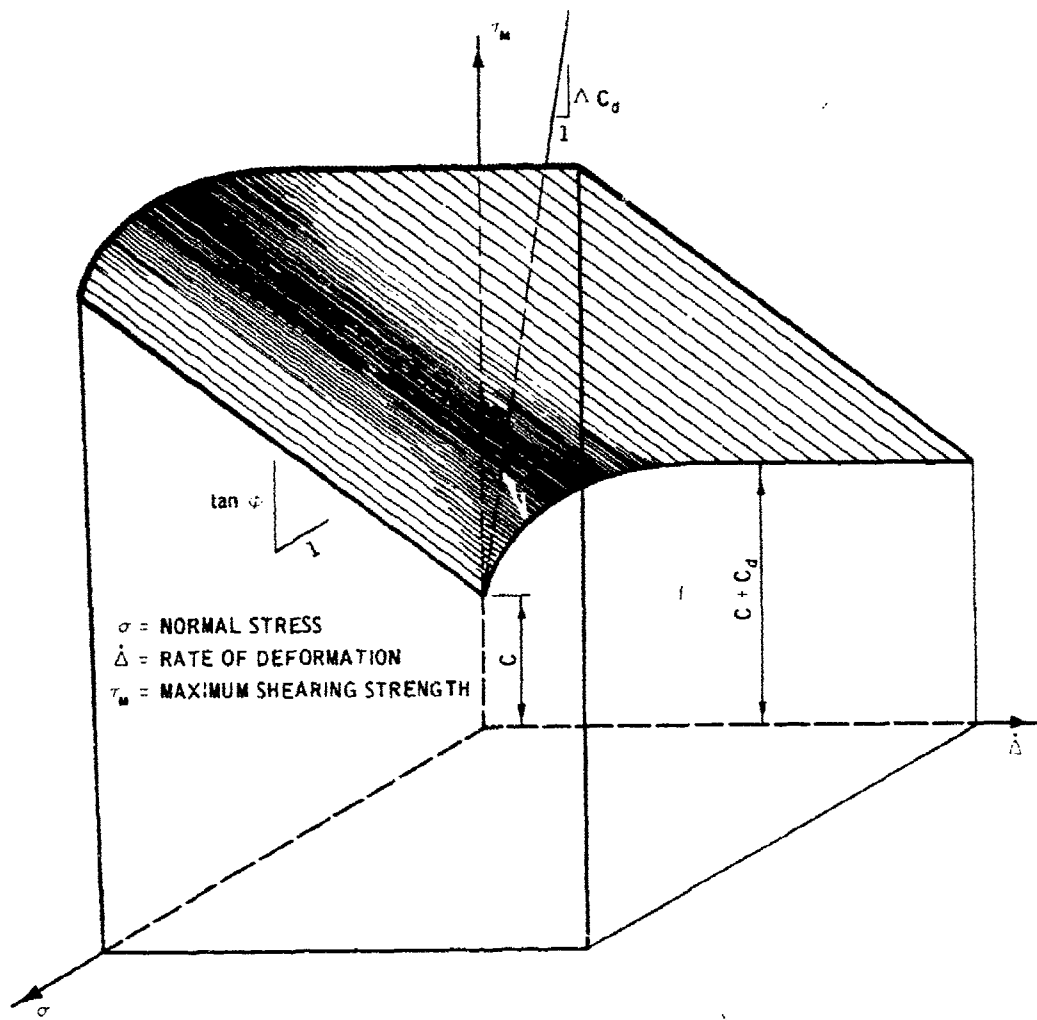


Figure 1. Proposed failure relation for soil

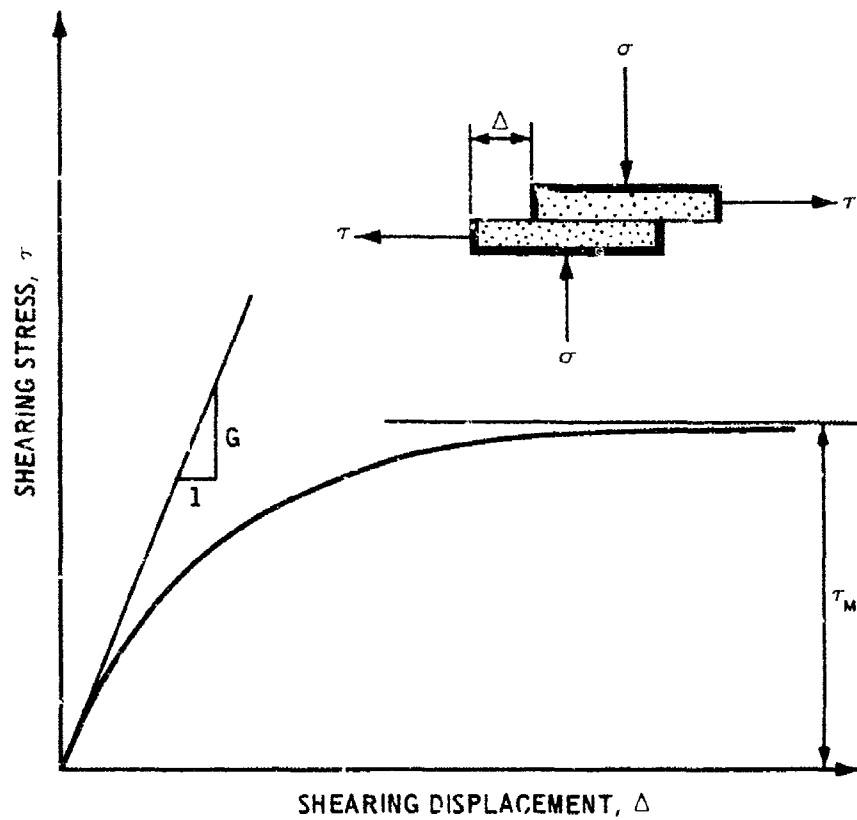
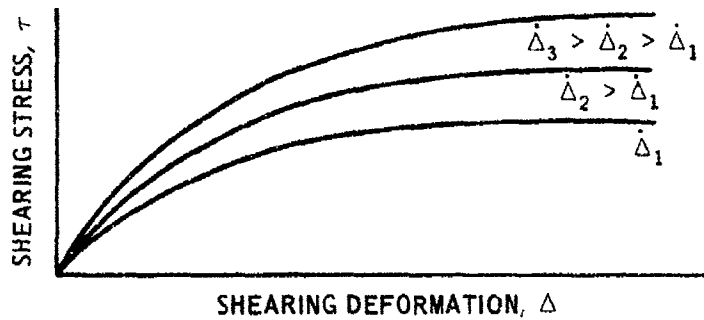


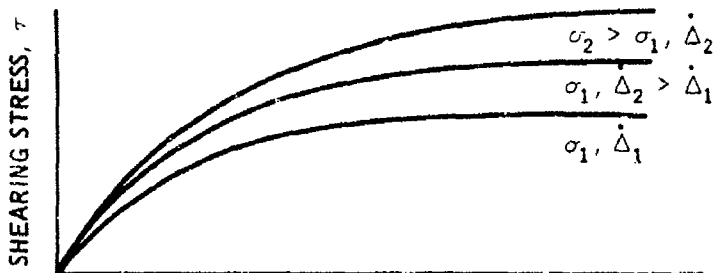
Figure 2. Proposed soil-stress/deformation relation during shearing process (Equation 3)



a. PURELY COHESIVE SOIL (τ INDEPENDENT OF σ)



b. GRANULAR SOIL (τ INDEPENDENT OF $\dot{\Delta}$)



c. MIXED SOIL (τ DEPENDENT ON BOTH σ AND $\dot{\Delta}$)

Figure 3. Qualitative behavior of the soil model (Equation 4) for various types of soil

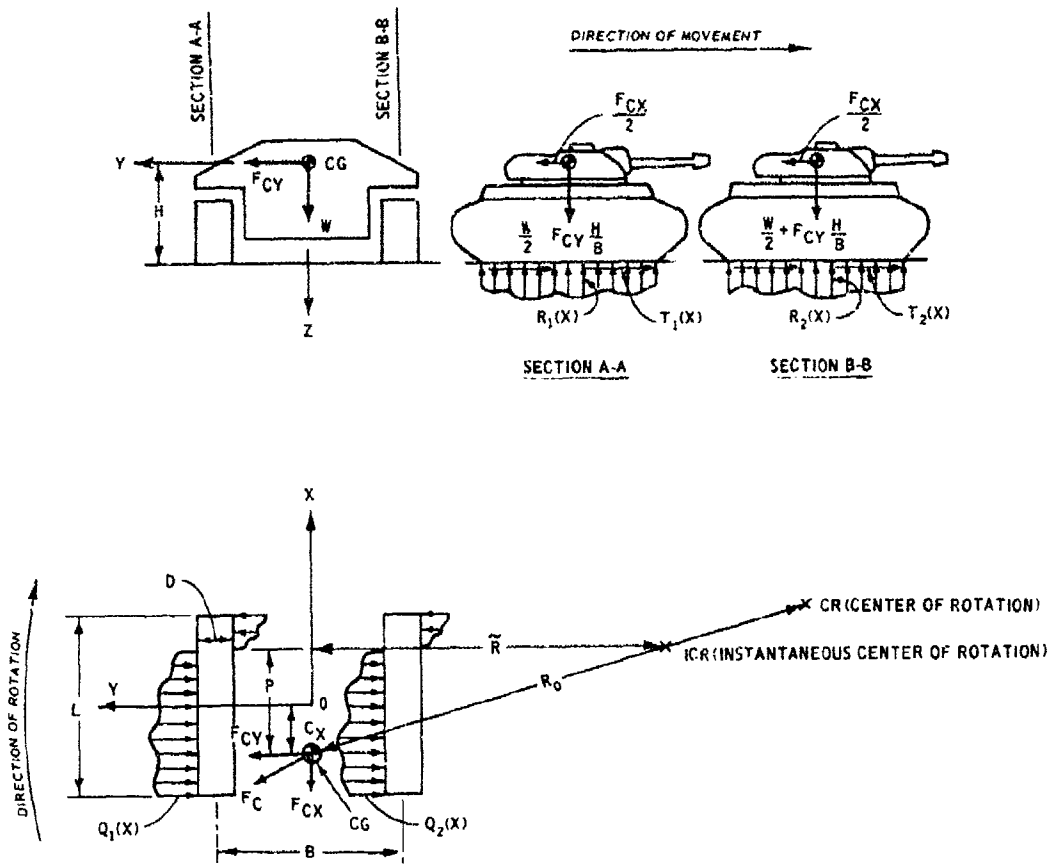
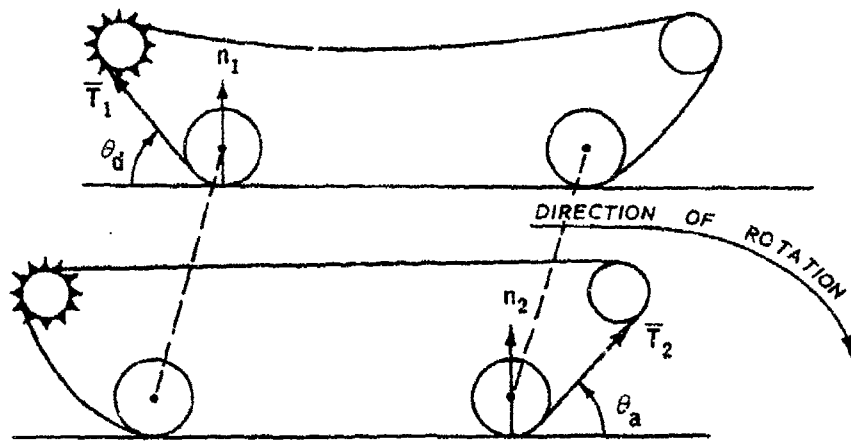
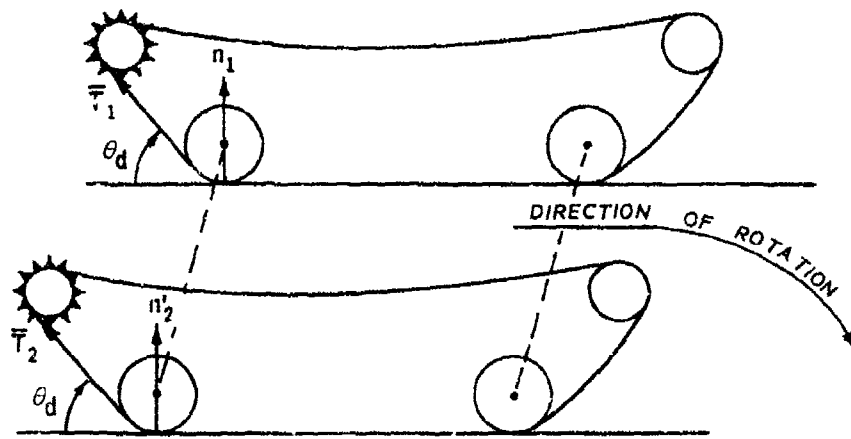


Figure 4. Geometry and boundary conditions of the terrain-vehicle model



a. LOW SPEED



b. HIGH SPEED

Figure 6. Track tension at low and high speeds

——— NORMAL STRESS DISTRIBUTION WITHOUT TRACK TENSION
 - - - - - NORMAL STRESS DISTRIBUTION WITH TRACK TENSION

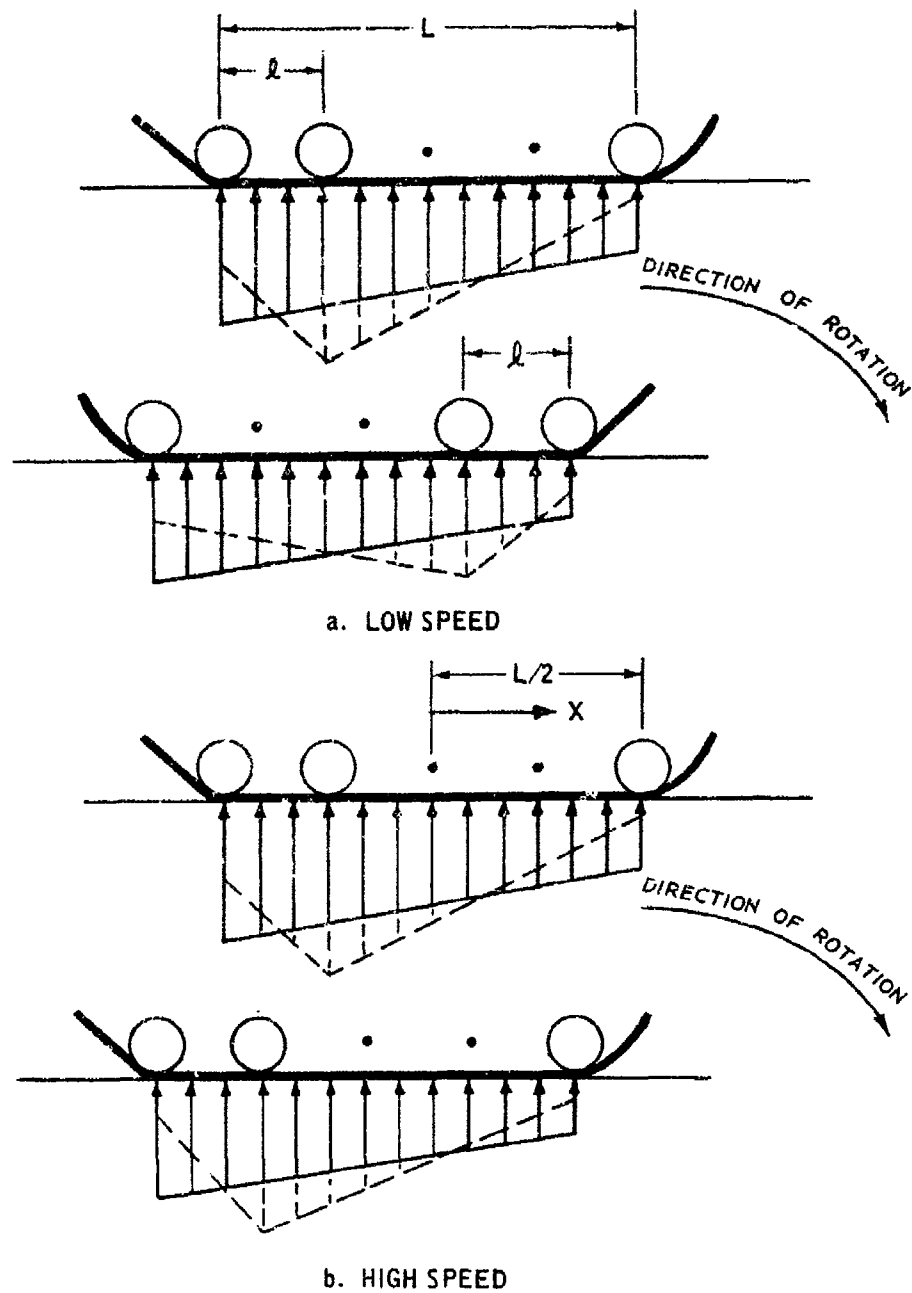


Figure 7. Effect of track tension on normal stress distribution

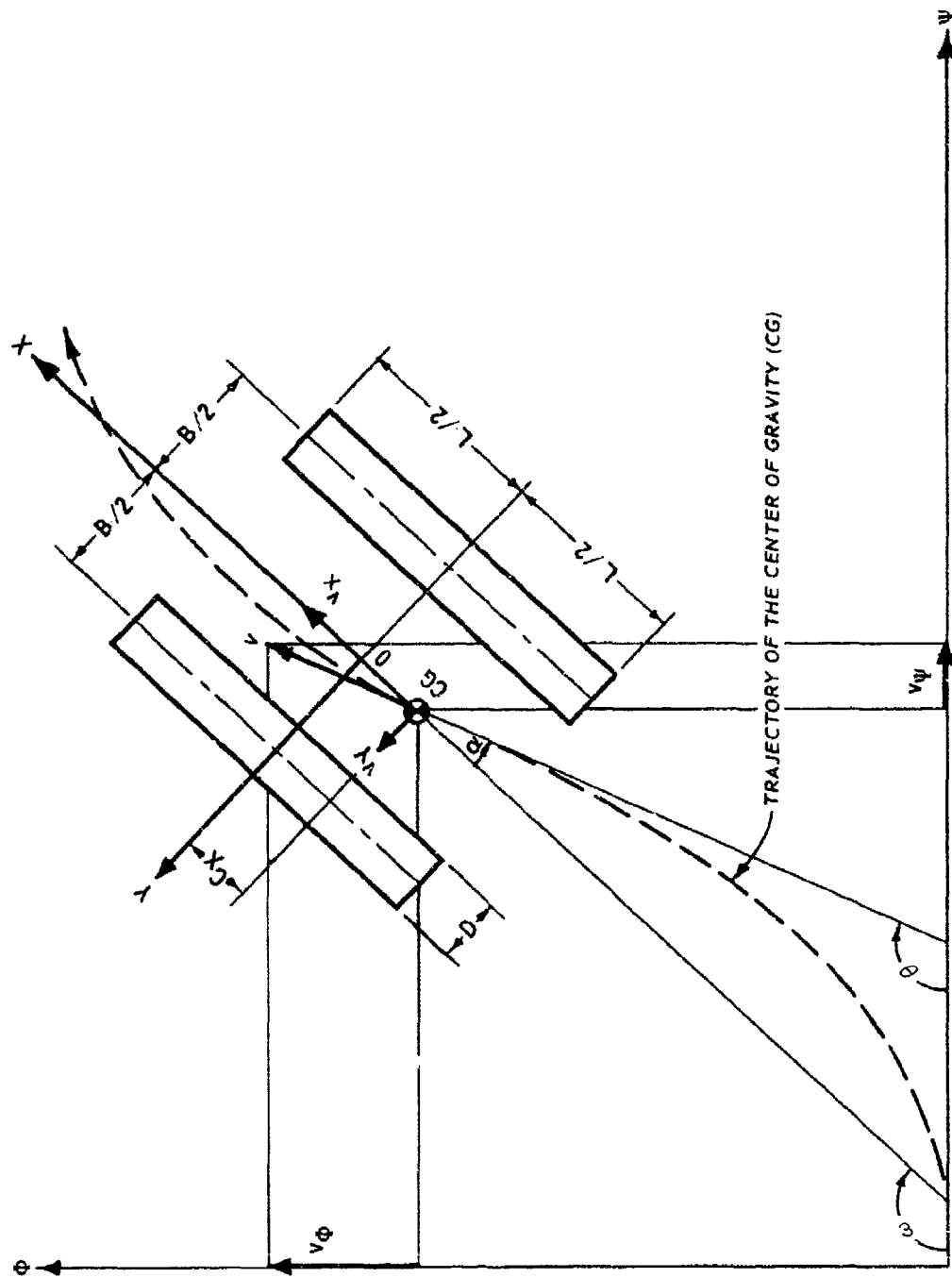


Figure 8. Tracked vehicle in transient motion

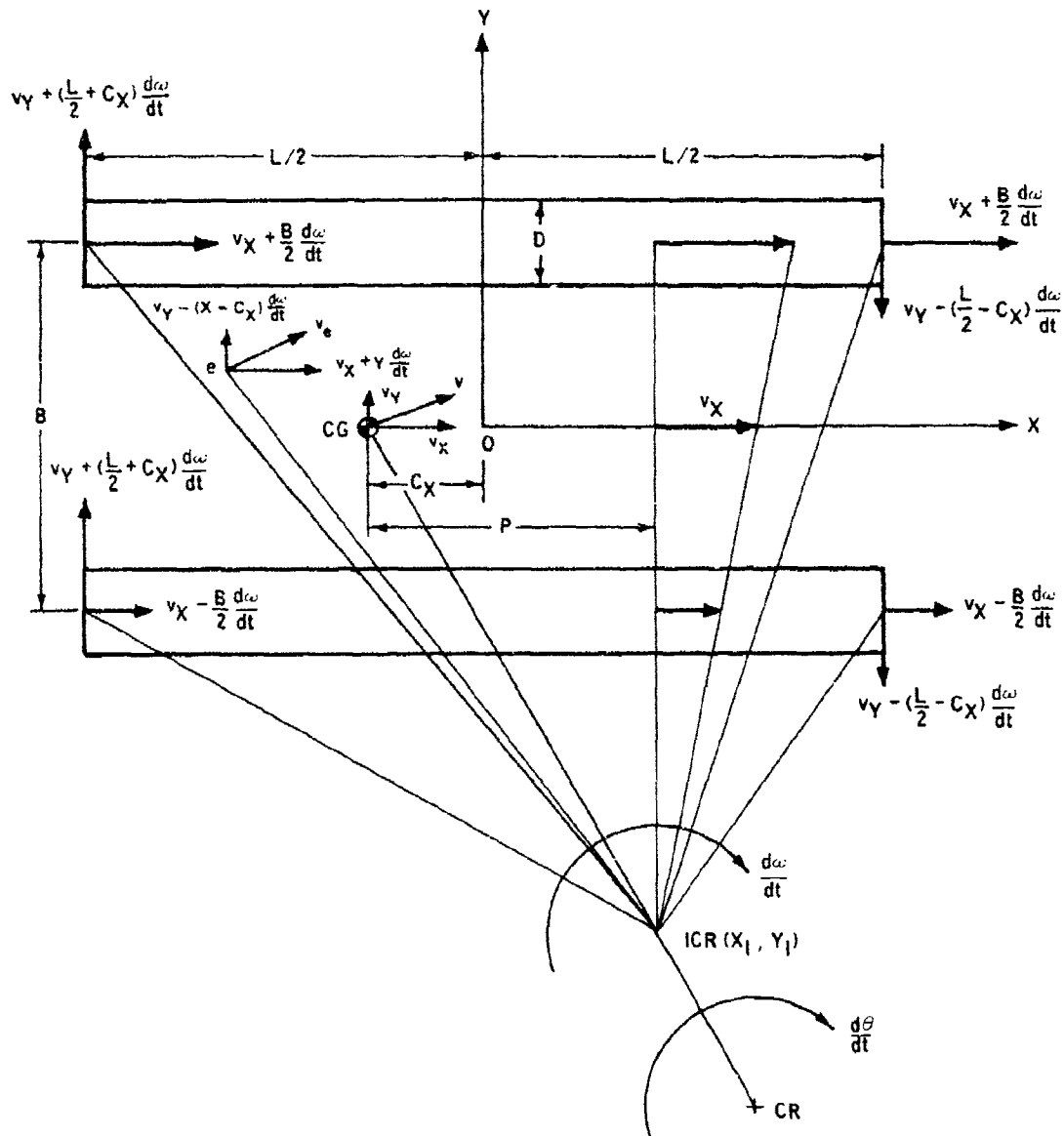


Figure 9. Track speeds and velocities of an arbitrary point of the hull

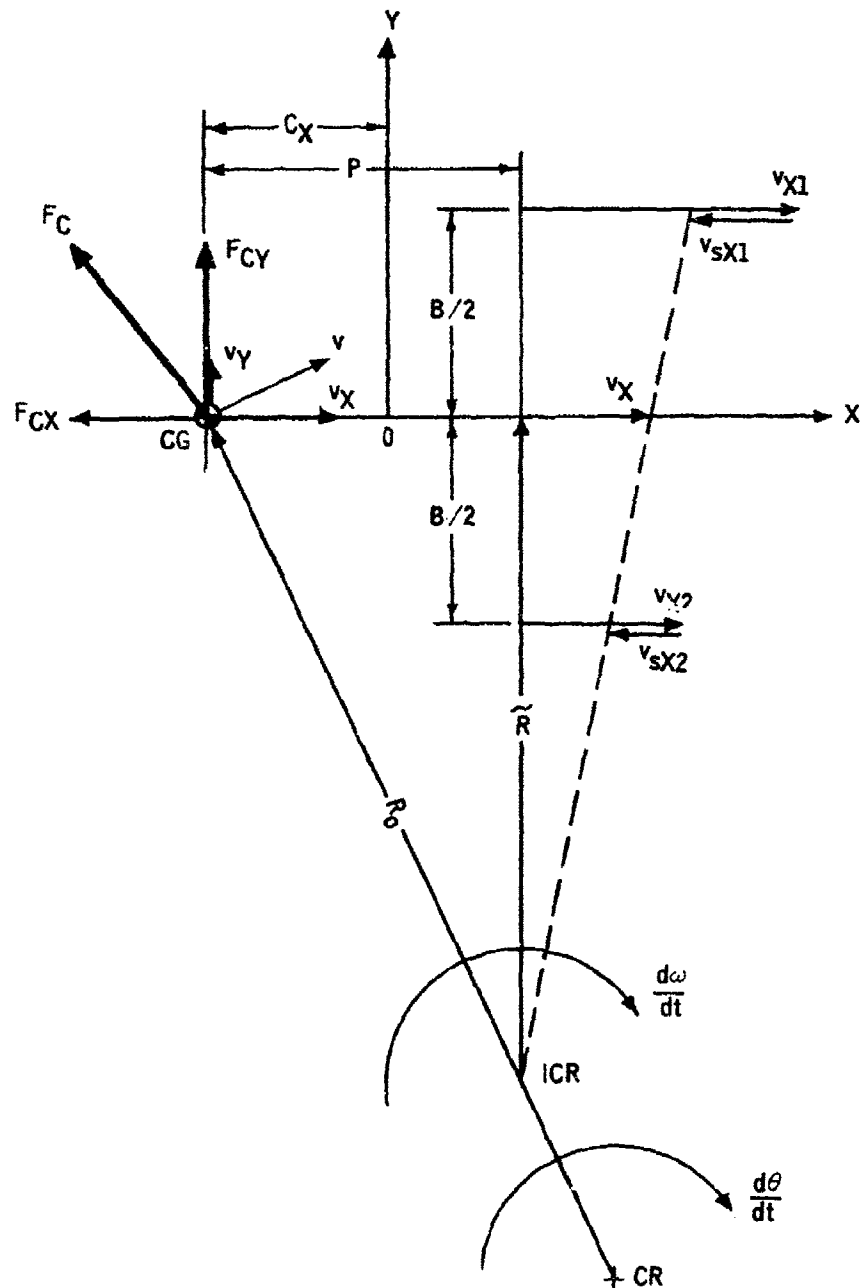


Figure 10. Schematic representation of vehicle and track speeds, track slip velocity, centrifugal forces, and turning radius

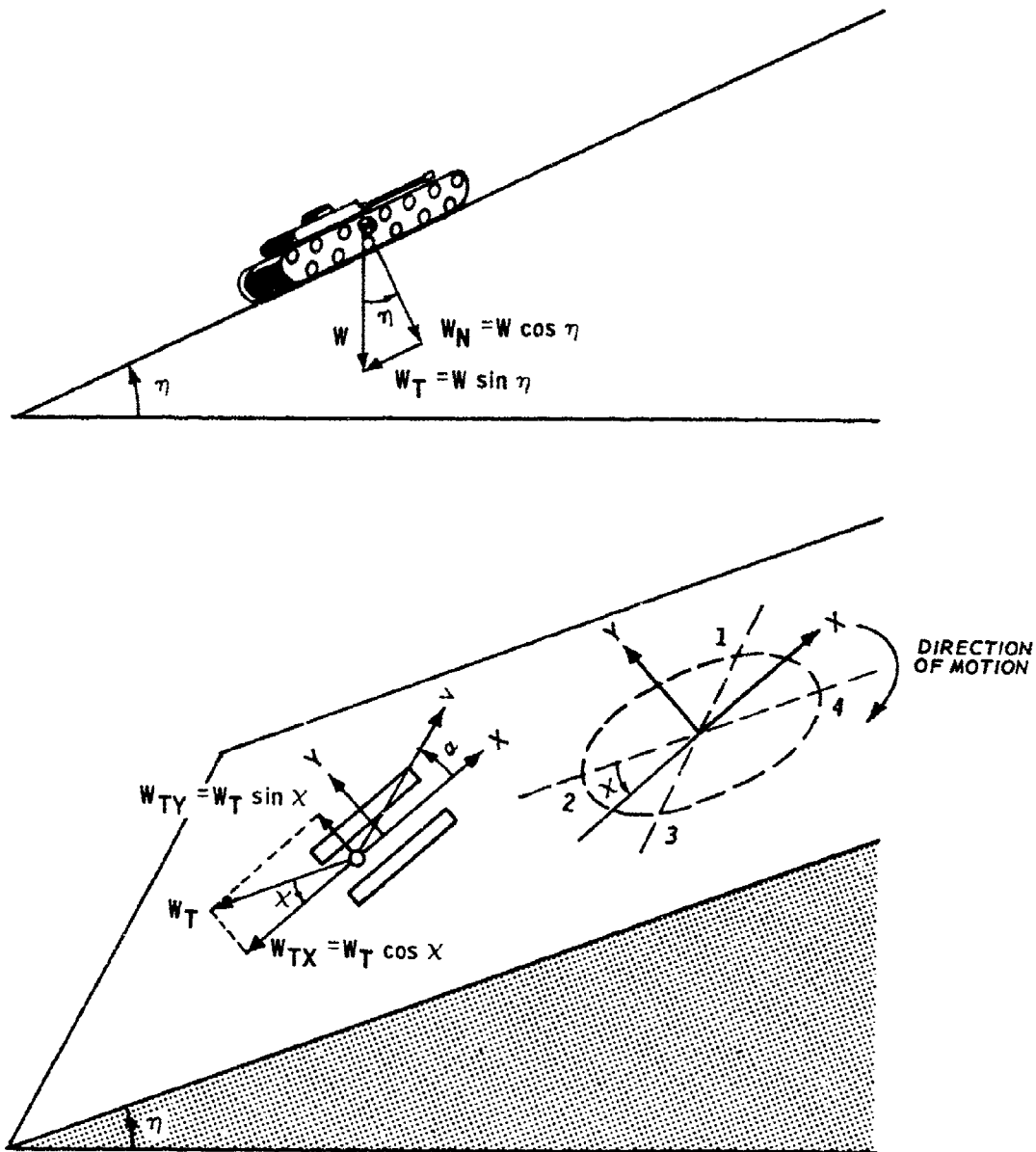


Figure 11. Effect of sloping terrain on uniform turning motion

CASE NO.	MATERIAL
— 1	SOFT CLAY WITHOUT RATE EFFECT
- - - 2	SOFT CLAY WITH RATE EFFECT

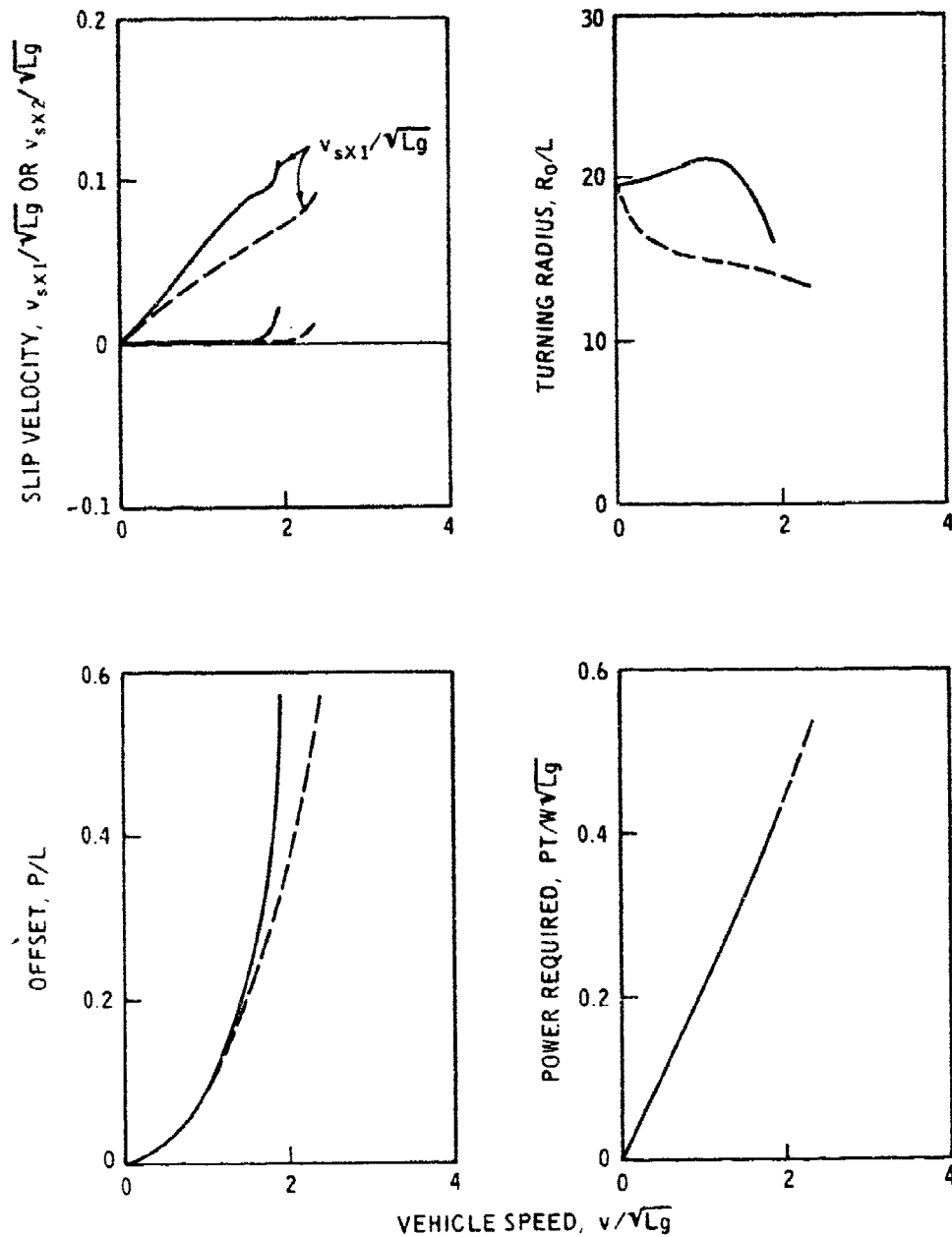


Figure 12. Relationships between vehicle speed and slip velocity, turning radius, offset, and power requirement (cases 1 and 2, $\epsilon = 1.1$)

LEGEND

CASE NO.	MATERIAL
— 1	SOFT CLAY WITHOUT RATE EFFECT
- - - 2	SOFT CLAY WITH RATE EFFECT

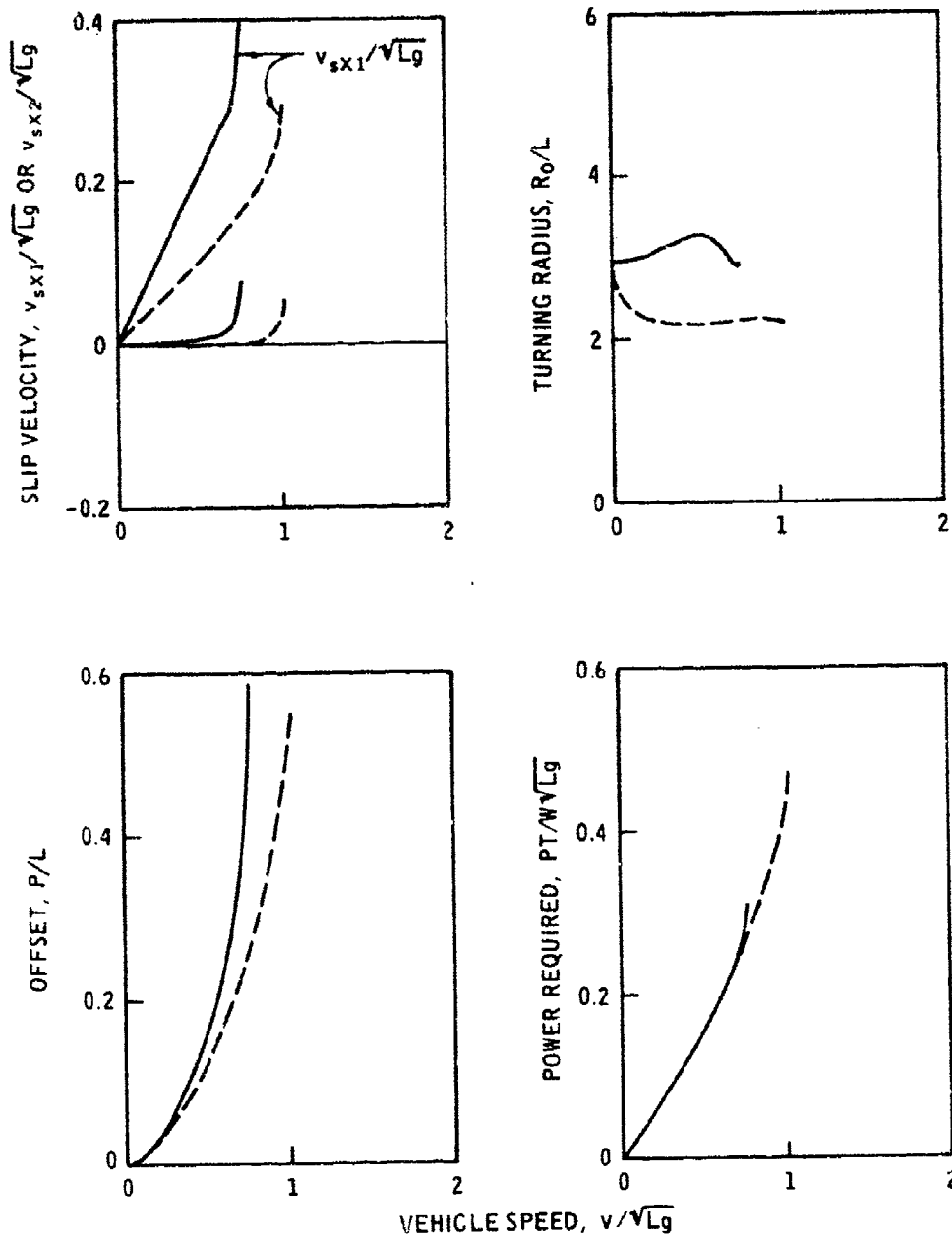


Figure 13. Relationships between vehicle speed and slip velocity, turning radius, offset, and power requirement (cases 1 and 2, $\epsilon = 1.75$)

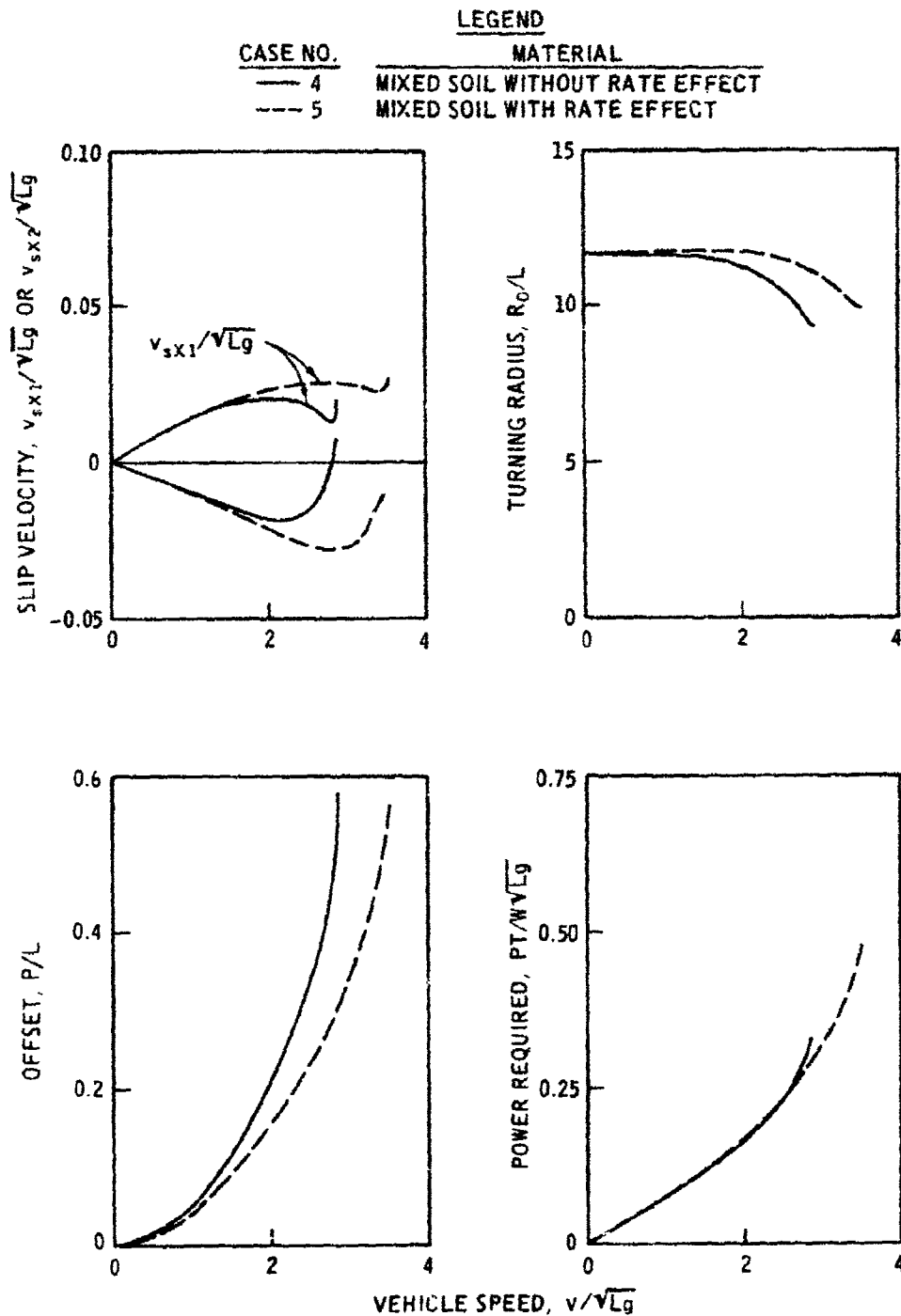


Figure 14. Relationships between vehicle speed and slip velocity, turning radius, offset, and power requirement (cases 4 and 5, $\epsilon = 1.1$)

LEGEND

CASE NO.	MATERIAL
— 4	MIXED SOIL WITHOUT RATE EFFECT
- - - 5	MIXED SOIL WITH RATE EFFECT

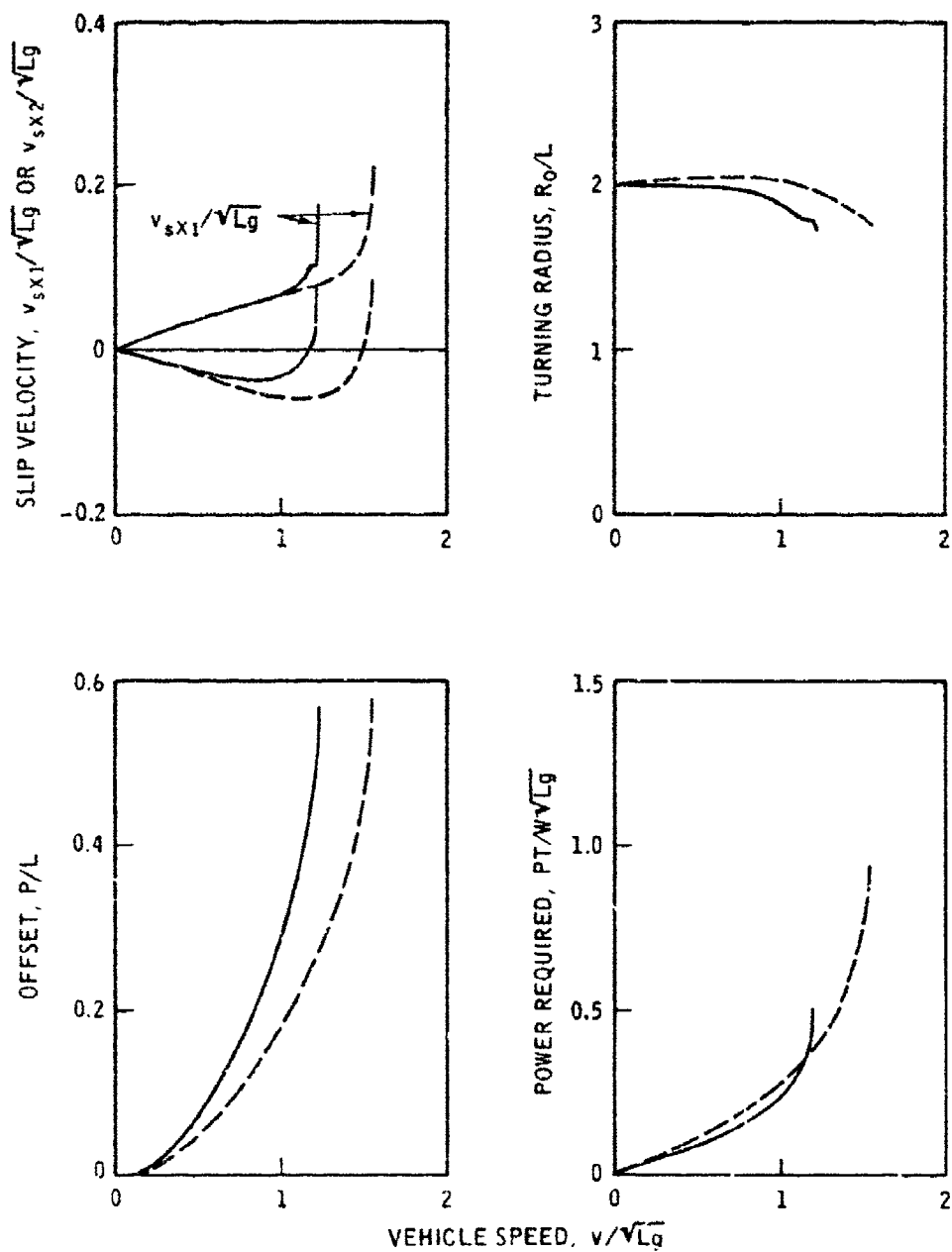


Figure 15. Relationships between vehicle speed and slip velocity, turning radius, offset, and power requirement (cases 4 and 5, $\epsilon = 1.75$)

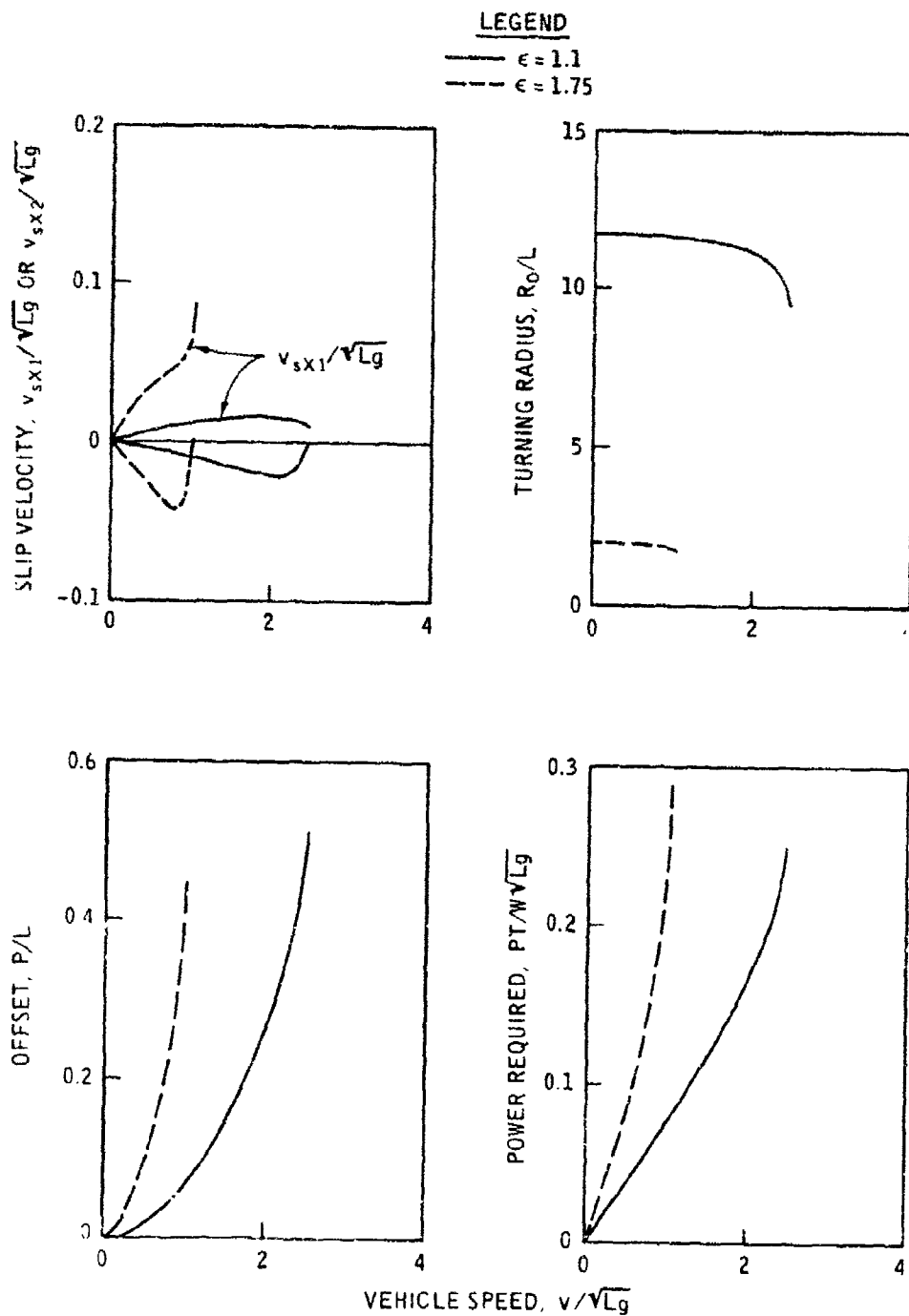


Figure 16. Relationships between vehicle speed and slip velocity, turning radius, offset, and power requirement (case 3, dense sand)

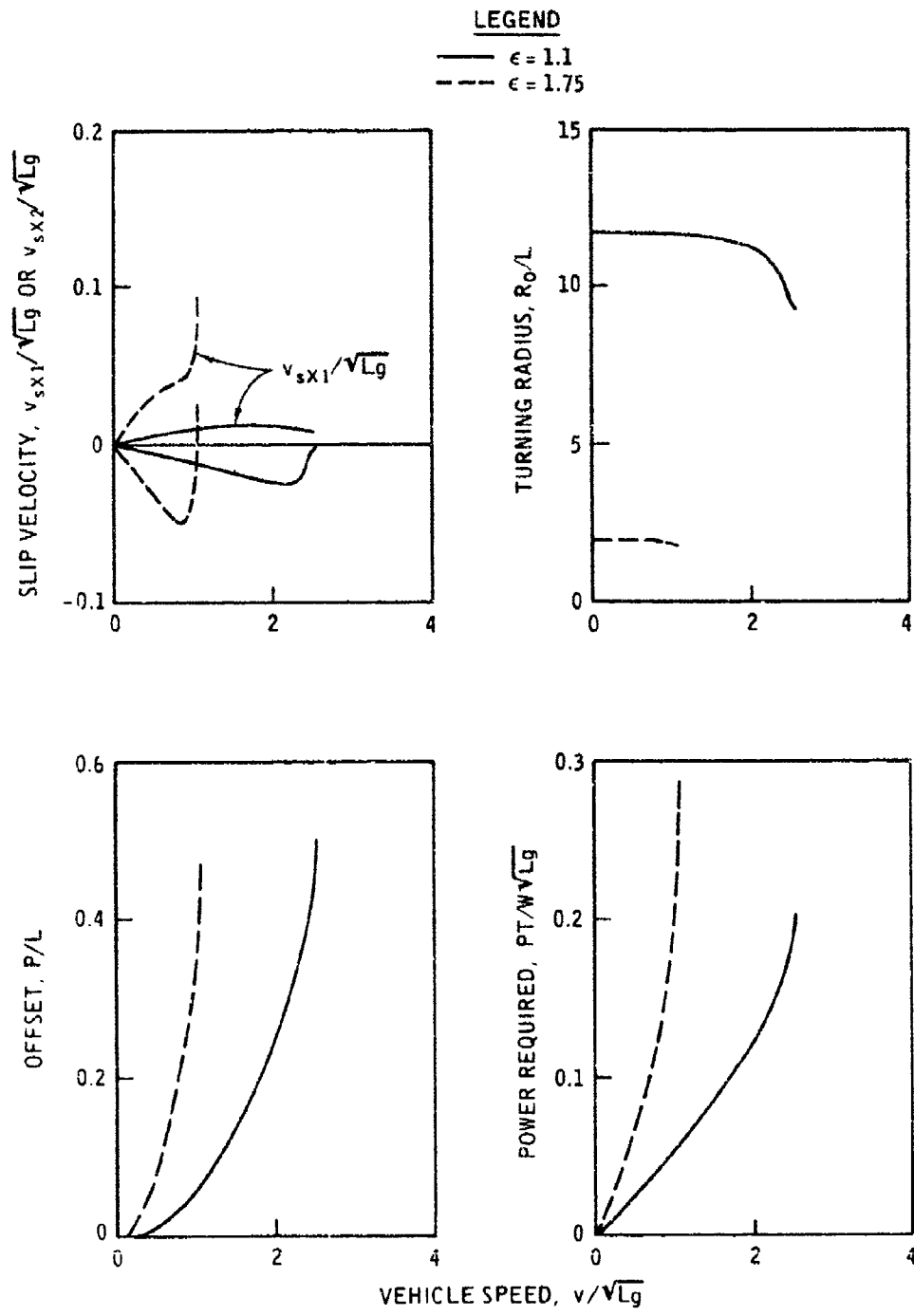


Figure 17. Relationships between vehicle speed and slip velocity, turning radius, offset, and power requirement (case 6, firm surface)

LEGEND

— $\epsilon = 1.1$
 - - - $\epsilon = 1.75$

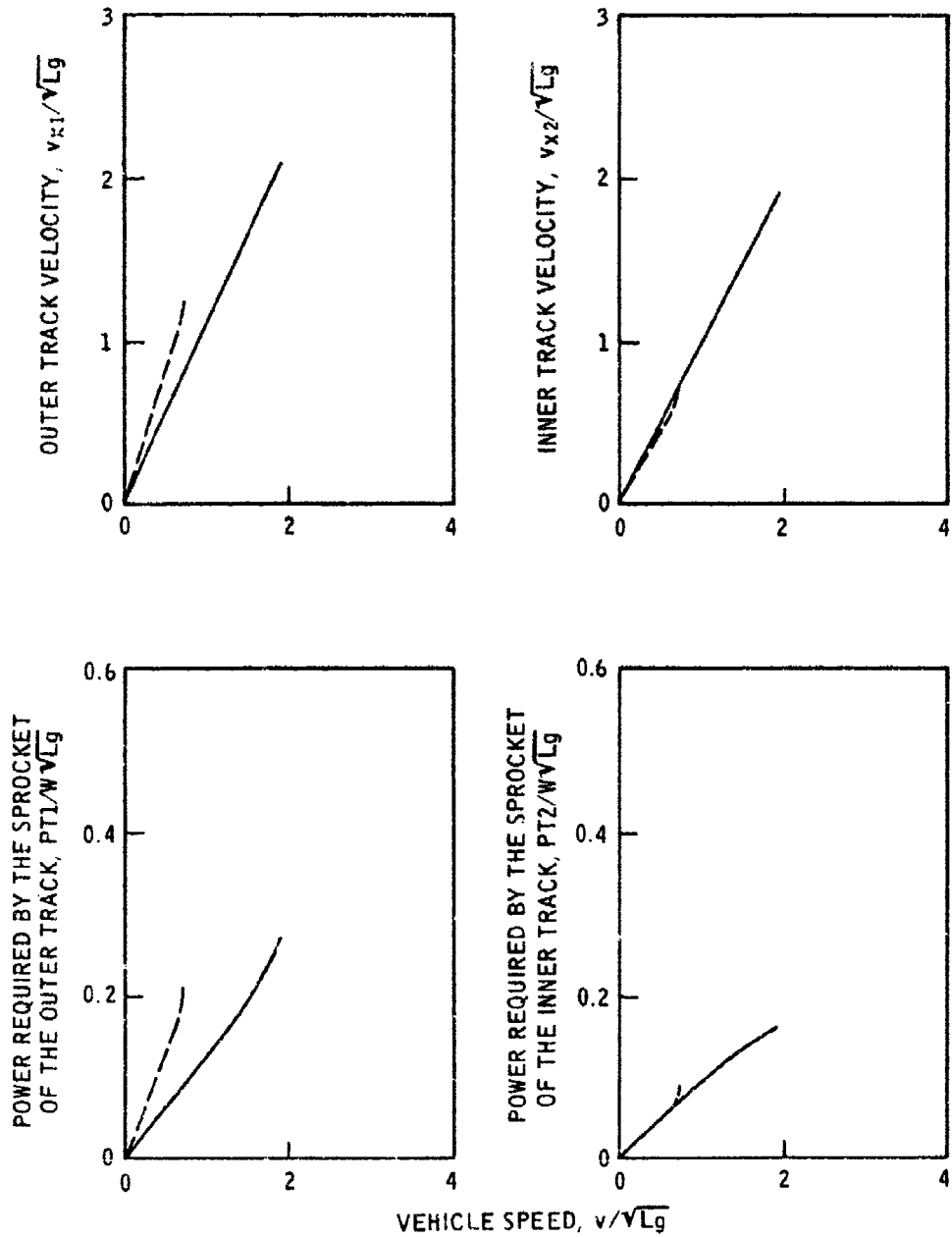


Figure 18. Relationships between vehicle speed and track velocity, and power requirement (case 1, soft clay without rate effect)

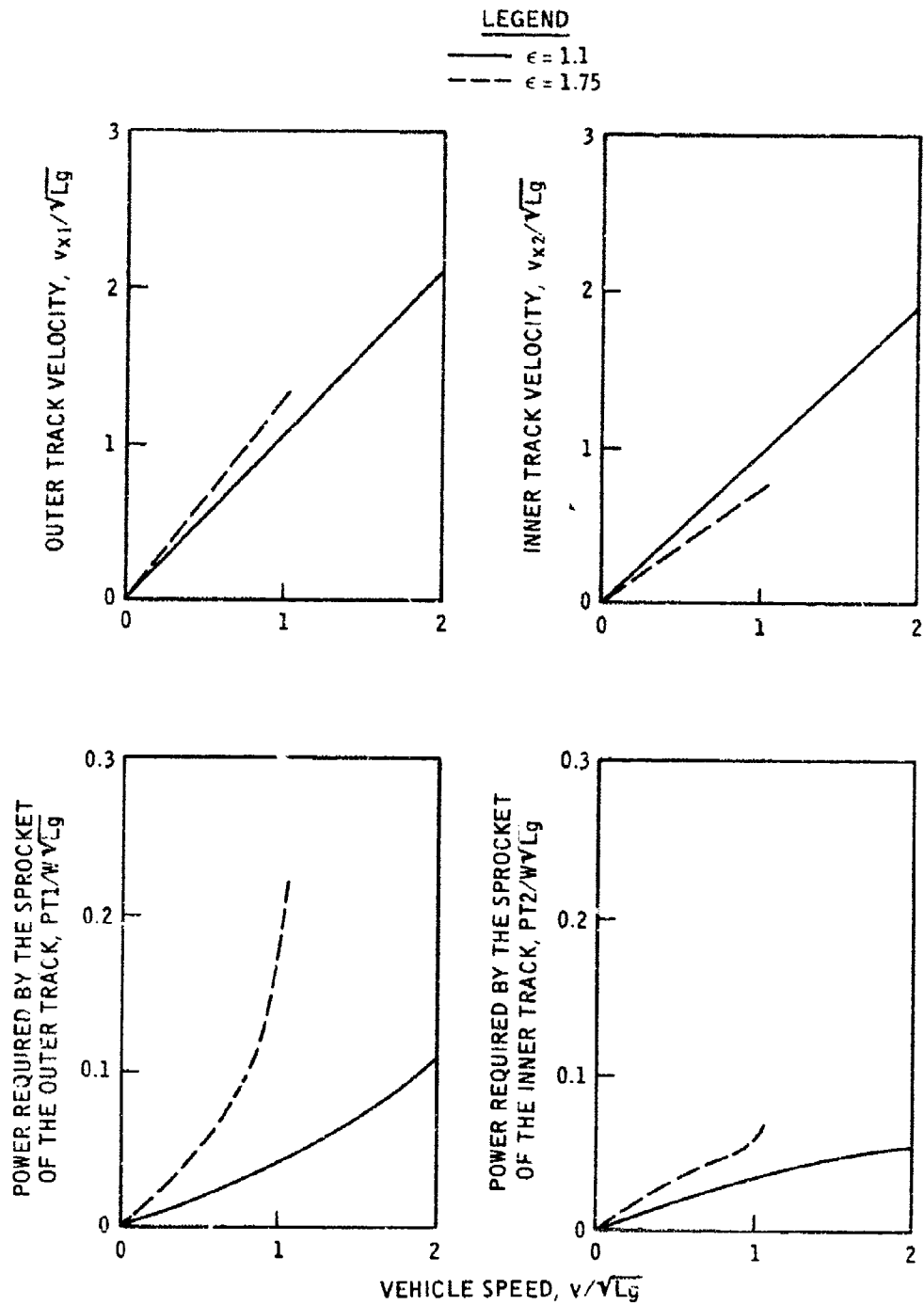


Figure 19. Relationships between vehicle speed and track velocity, and power requirement (case 3, dense sand)

LEGEND

— $\epsilon = 1.1$
 - - - $\epsilon = 1.75$

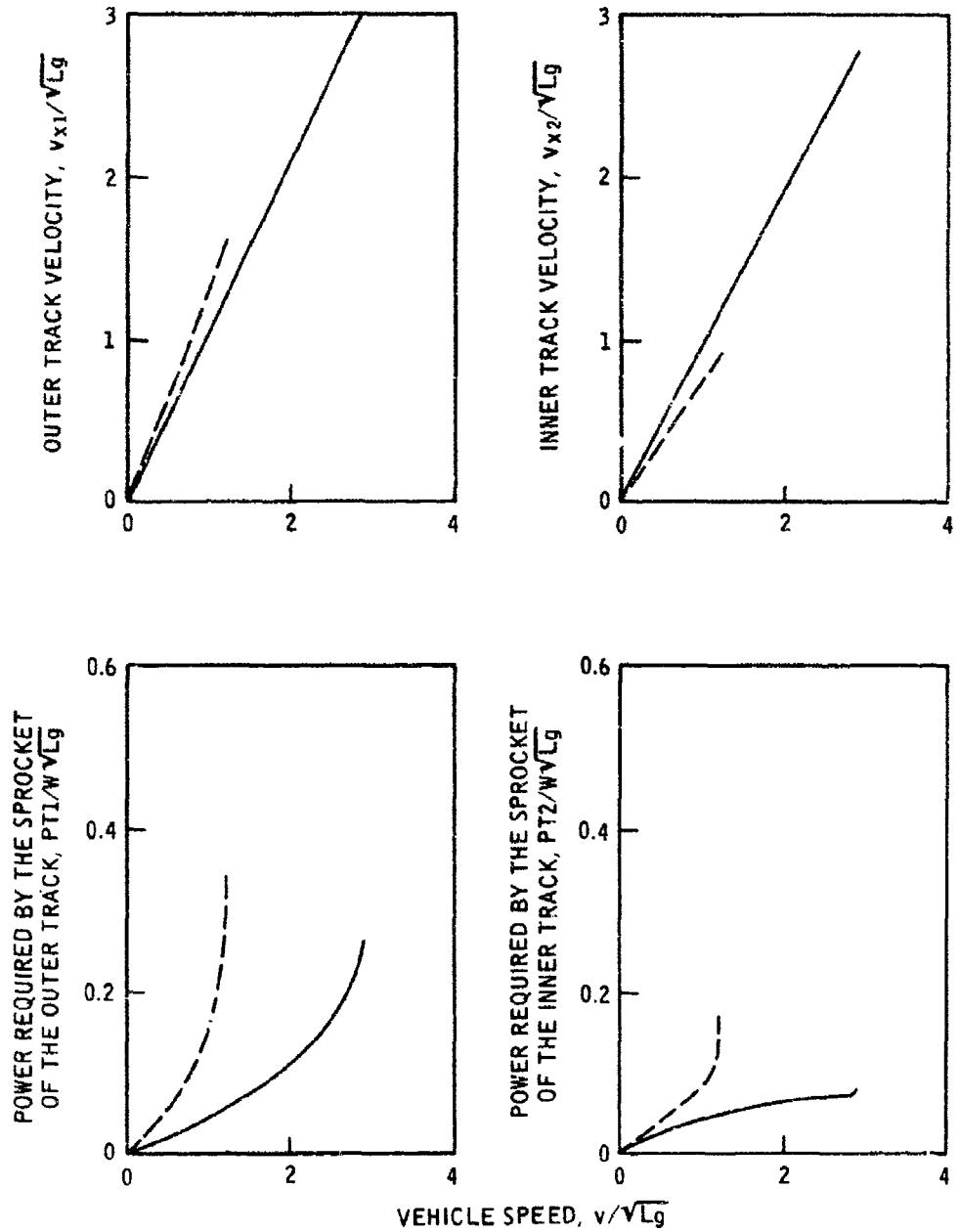


Figure 20. Relationships between vehicle speed and track velocity, and power requirement (case 4, mixed soil without rate effect)

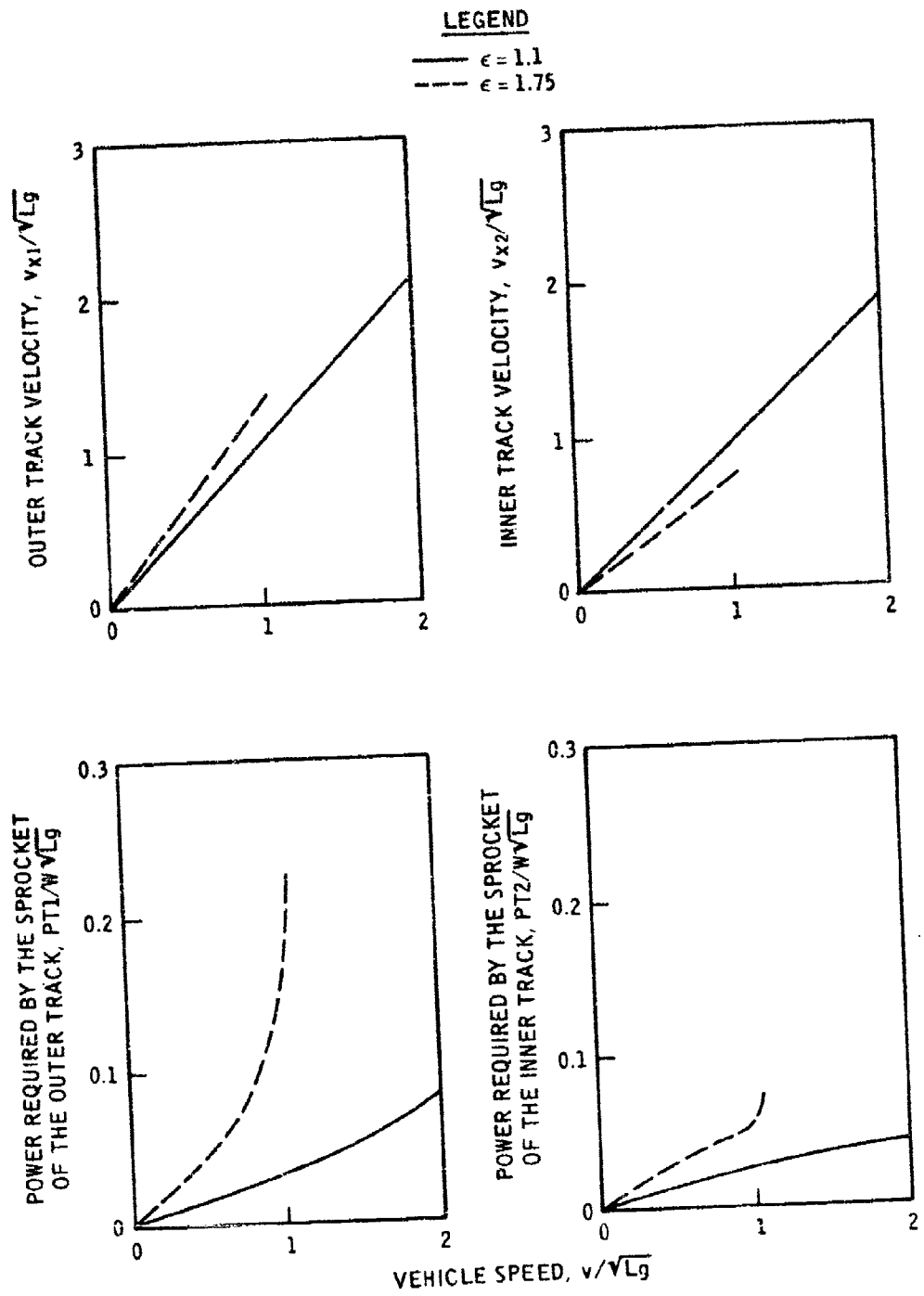


Figure 21. Relationships between vehicle speed and track velocity, and power requirement (case 6, firm surface)

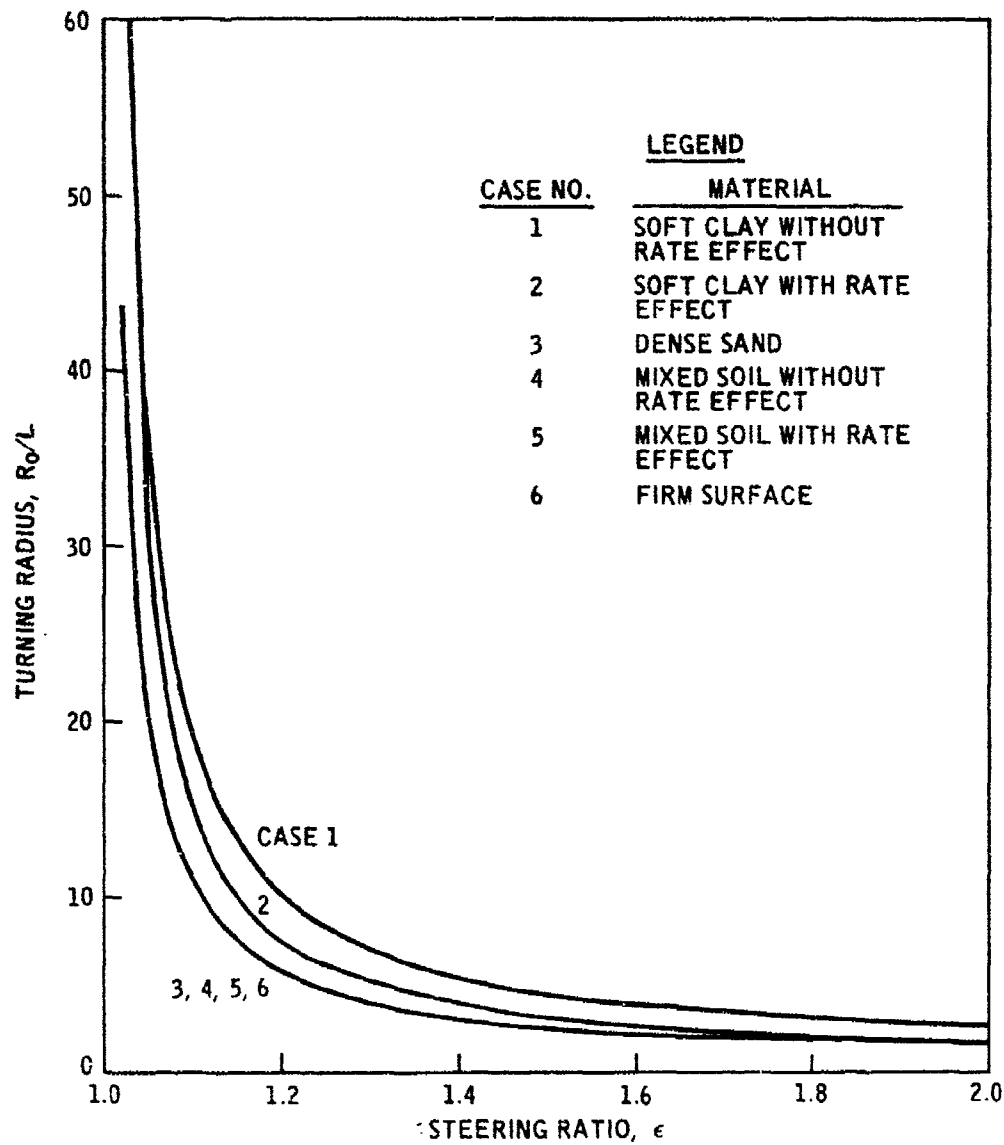


Figure 22. Relationships between turning radius and steering ratio

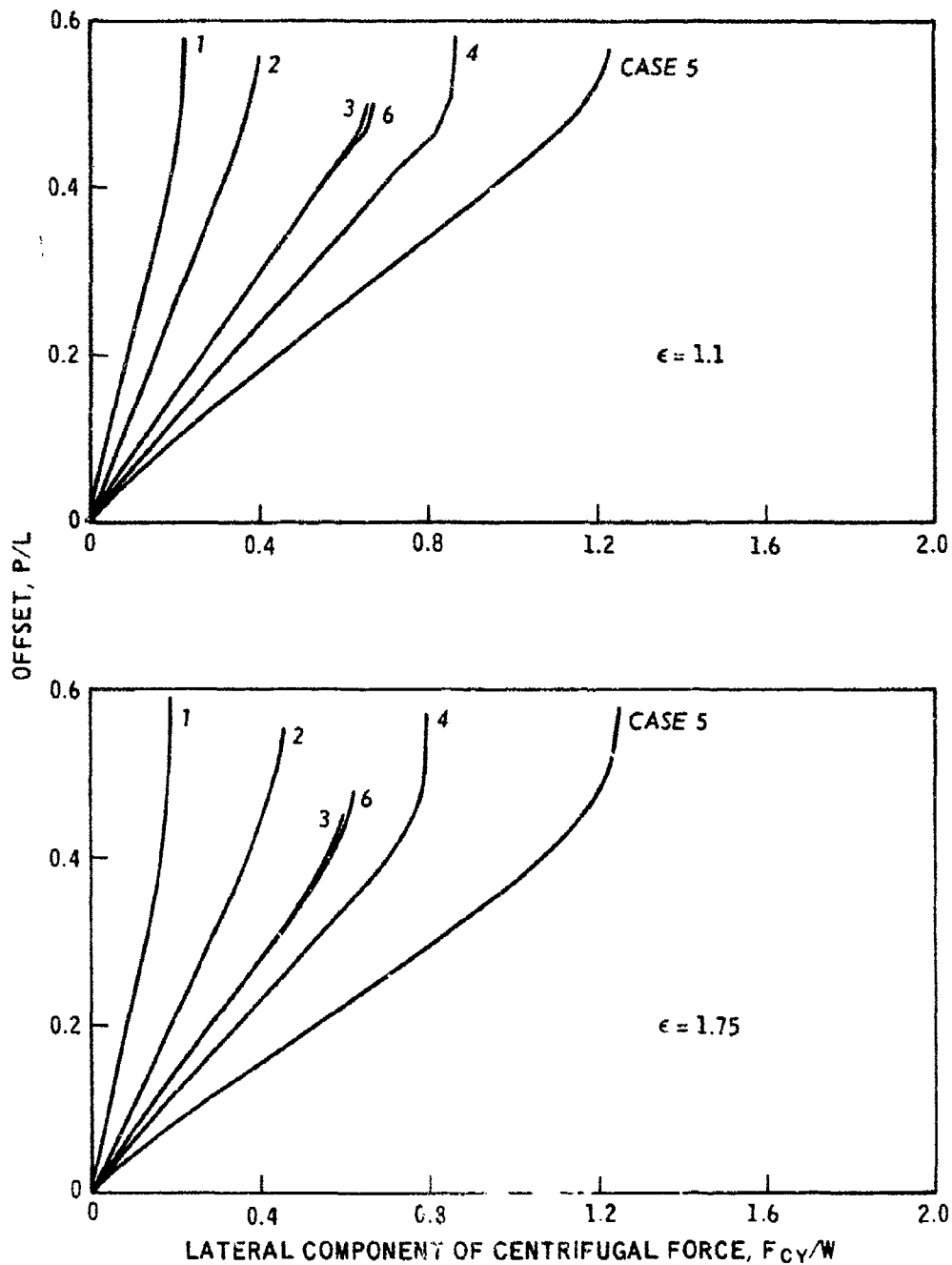


Figure 23. Relationships between offset and lateral components of centrifugal force

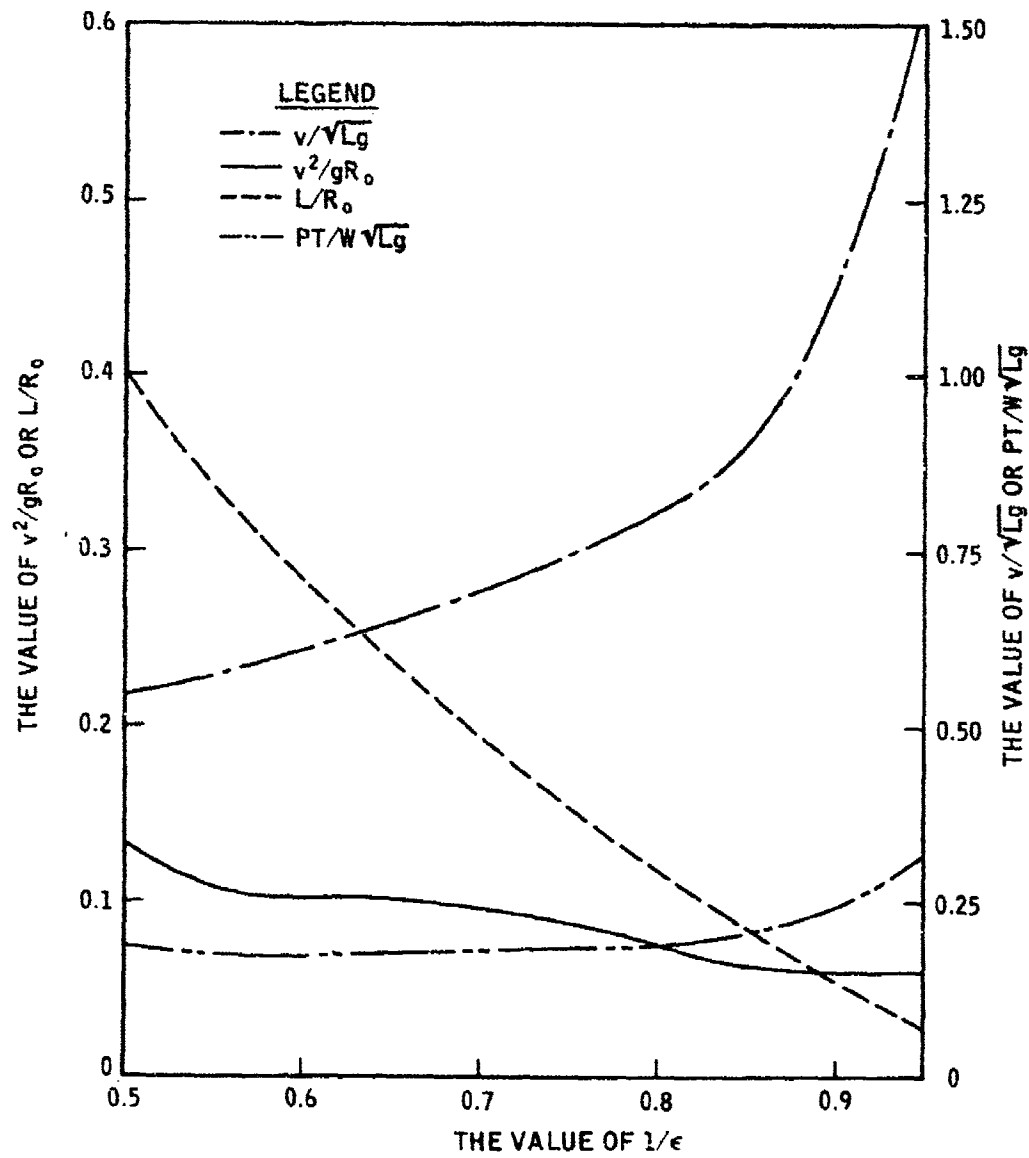


Figure 24. Relationships between steering ratio and turning radius, lateral acceleration, vehicle speed, and power requirement for soft clay without rate effect (case 1)

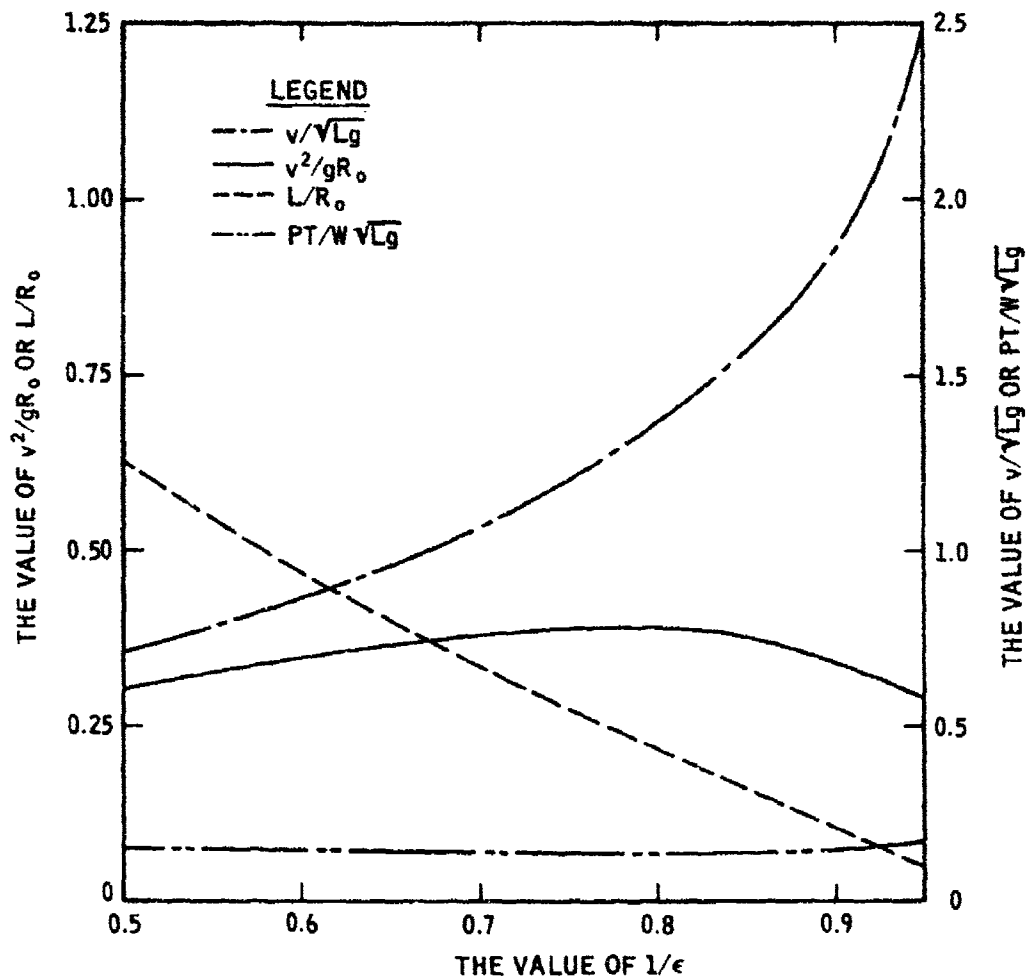


Figure 25. Relationships between steering ratio and turning radius, lateral acceleration, vehicle speed, and power requirement for dense sand (case 3)

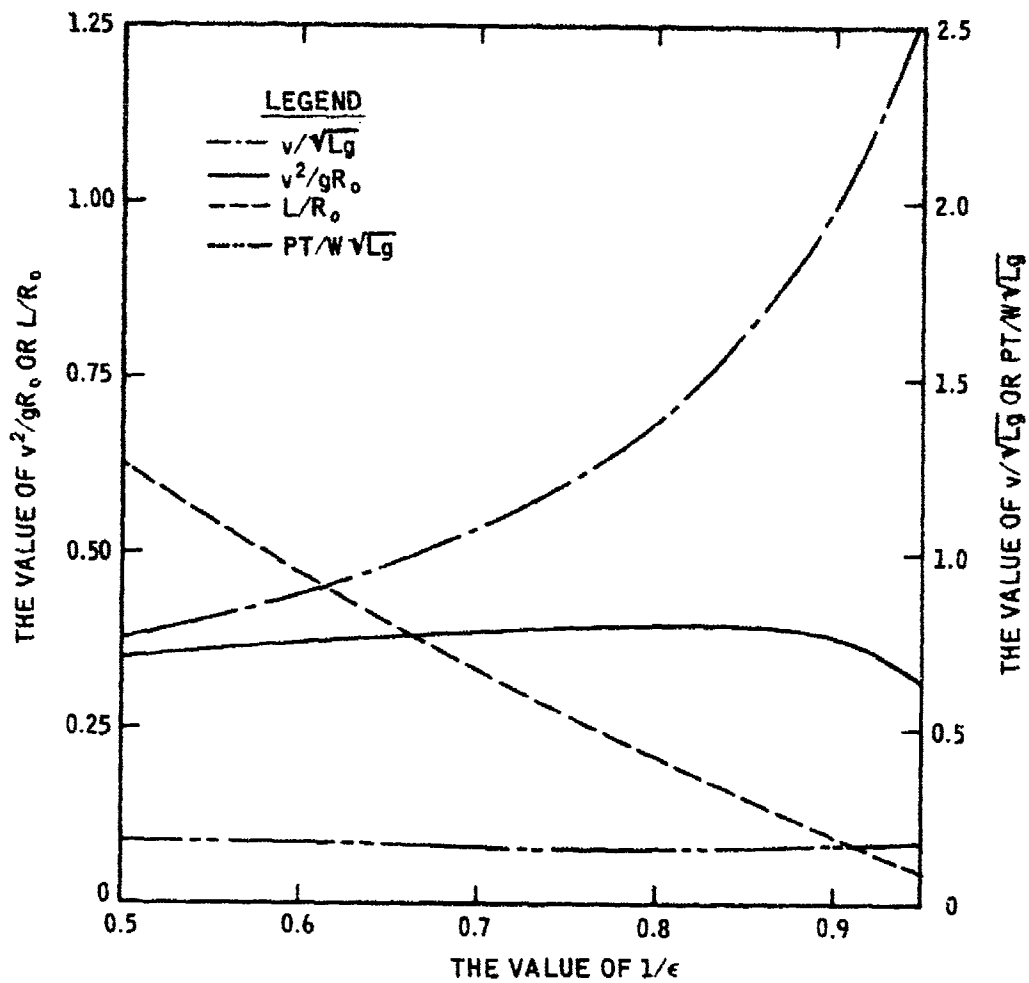


Figure 26. Relationships between steering ratio and turning radius, lateral acceleration, vehicle speed, and power requirement for mixed soil without rate effect (case 4)

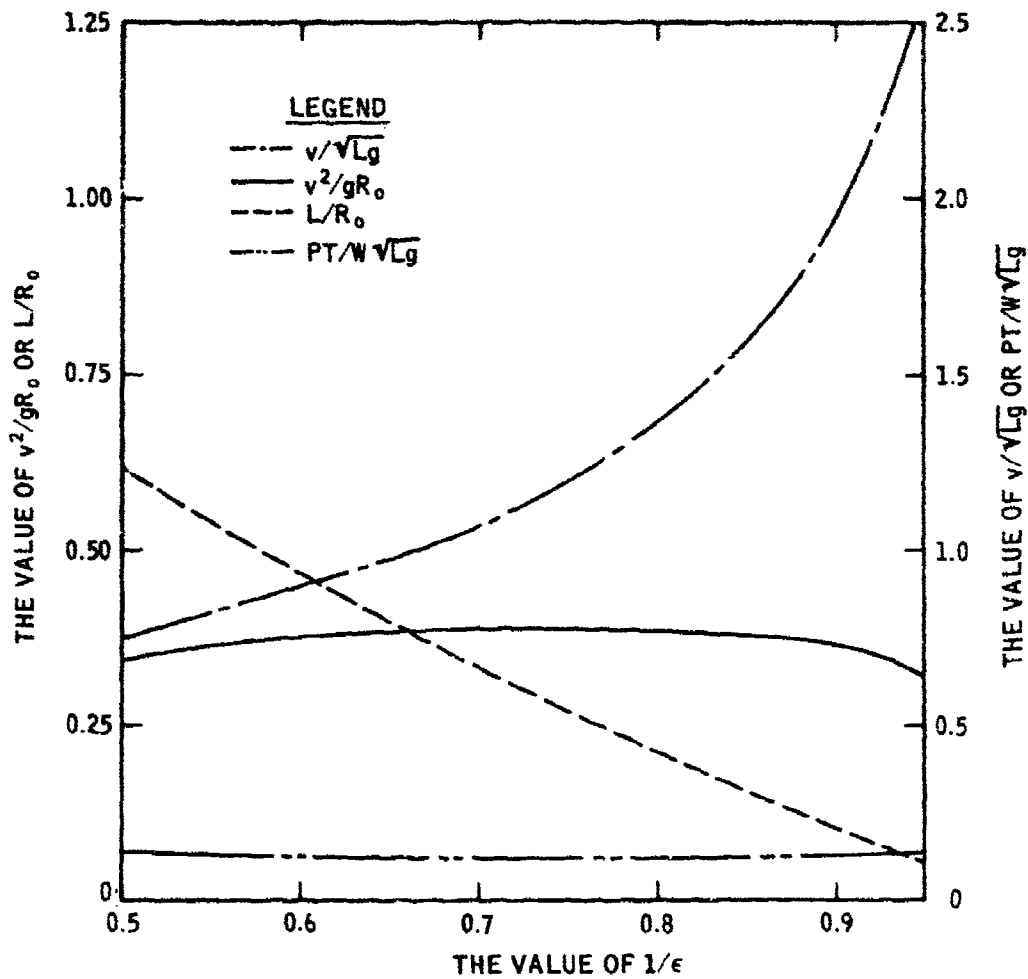


Figure 27. Relationships between steering ratio and turning radius, lateral acceleration, vehicle speed, and power requirement for firm surface (case 6)

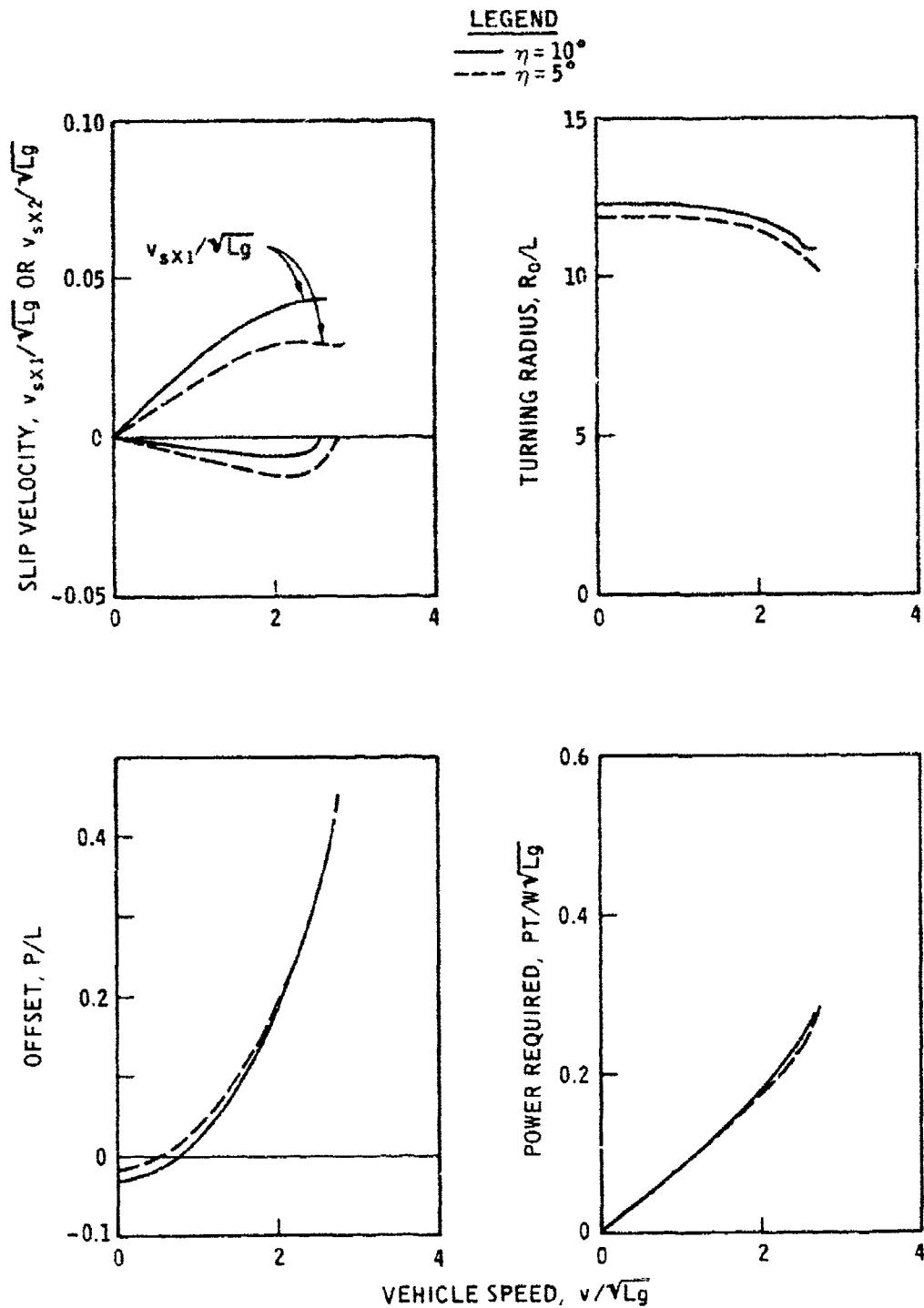
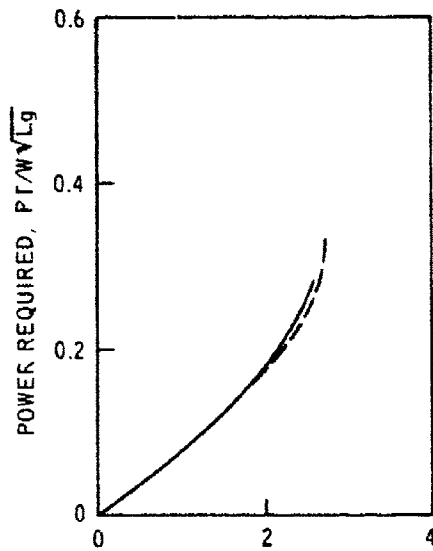
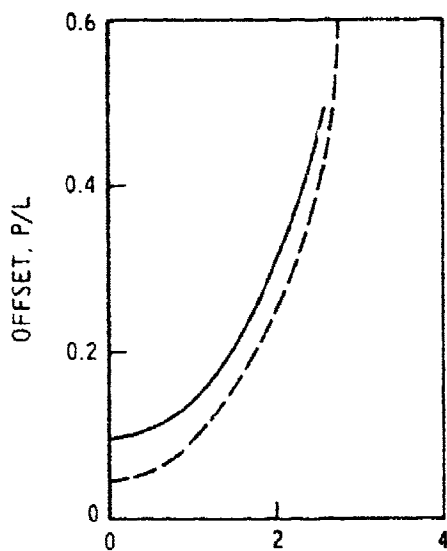
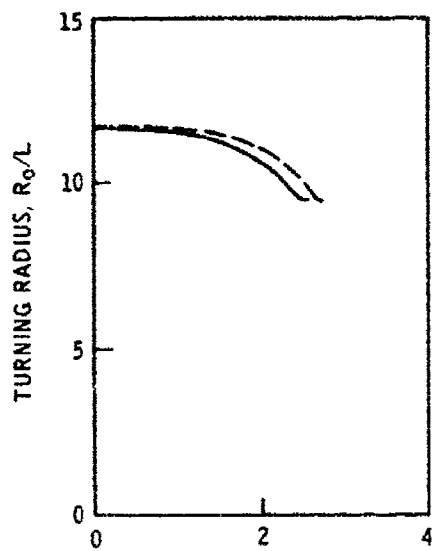
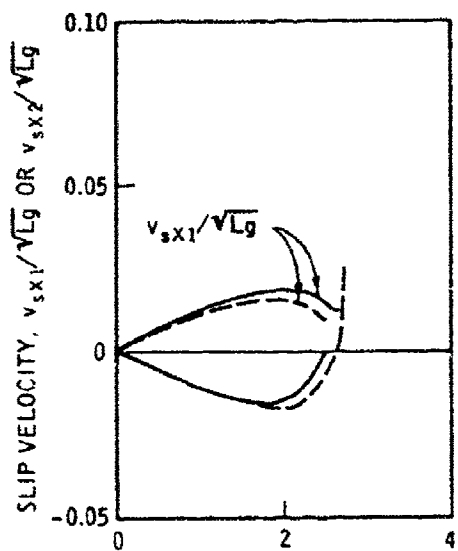


Figure 28. Effect of terrain slope on the relationships between vehicle speed and slip velocity, turning radius, offset, and power requirement (case 4, $\epsilon = 1.1$, $\chi = 0^\circ$)

LEGEND

— $\eta = 10^\circ$
 - - - $\eta = 5^\circ$



VEHICLE SPEED, v/\sqrt{Lg}

Figure 29. Effect of terrain slope on the relationships between vehicle speed and velocity, turning radius, offset, and power requirement (case 4, $\epsilon = 1.1$, $\chi = 90^\circ$)

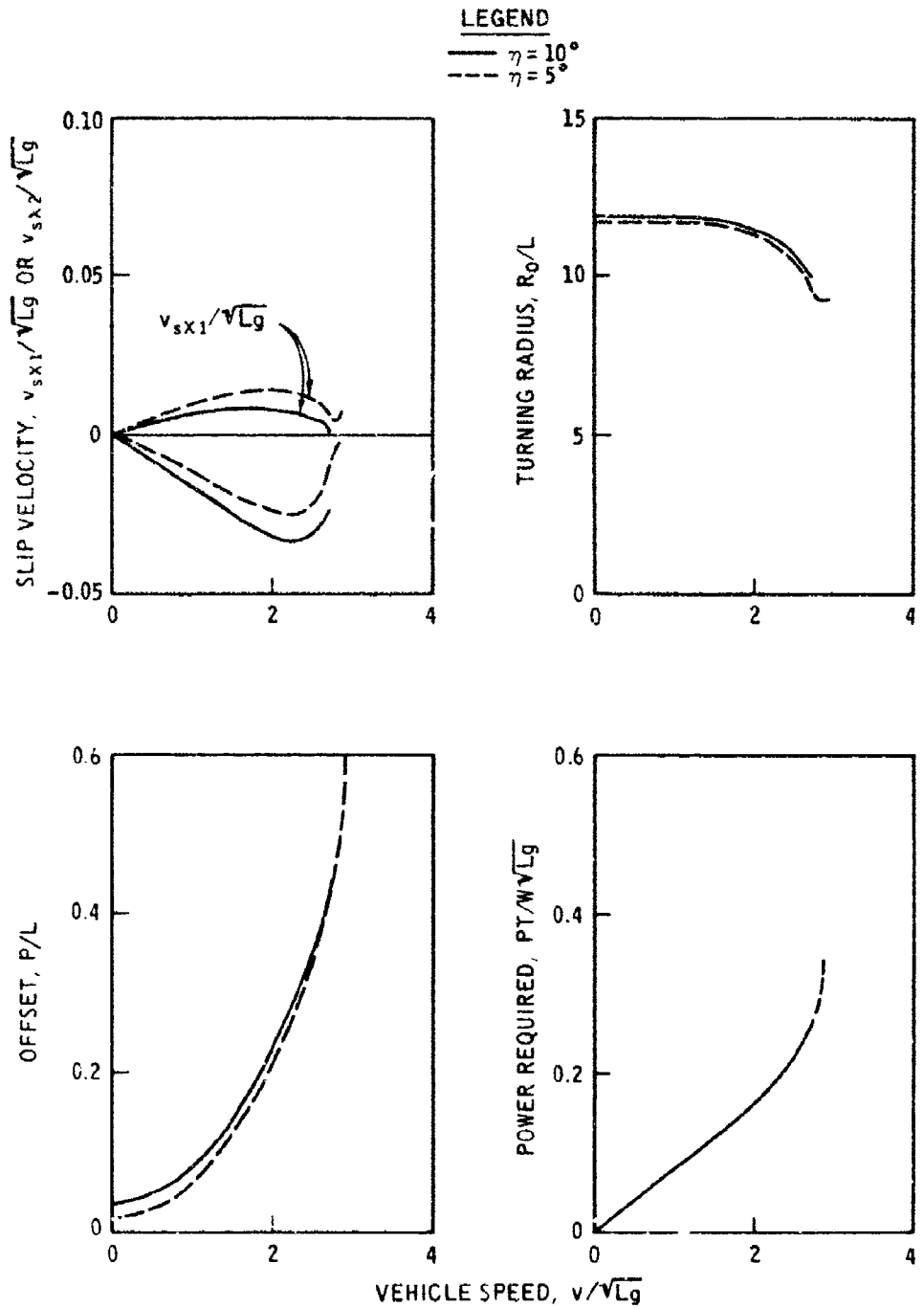


Figure 30. Effect of terrain slope on the relationships between vehicle speed and slip velocity, turning radius, offset, and power requirement (case 4, $\epsilon = 1.1$, $\chi = 180^\circ$)

LEGEND

— $\eta = 10^\circ$
 - - - $\eta = 5^\circ$

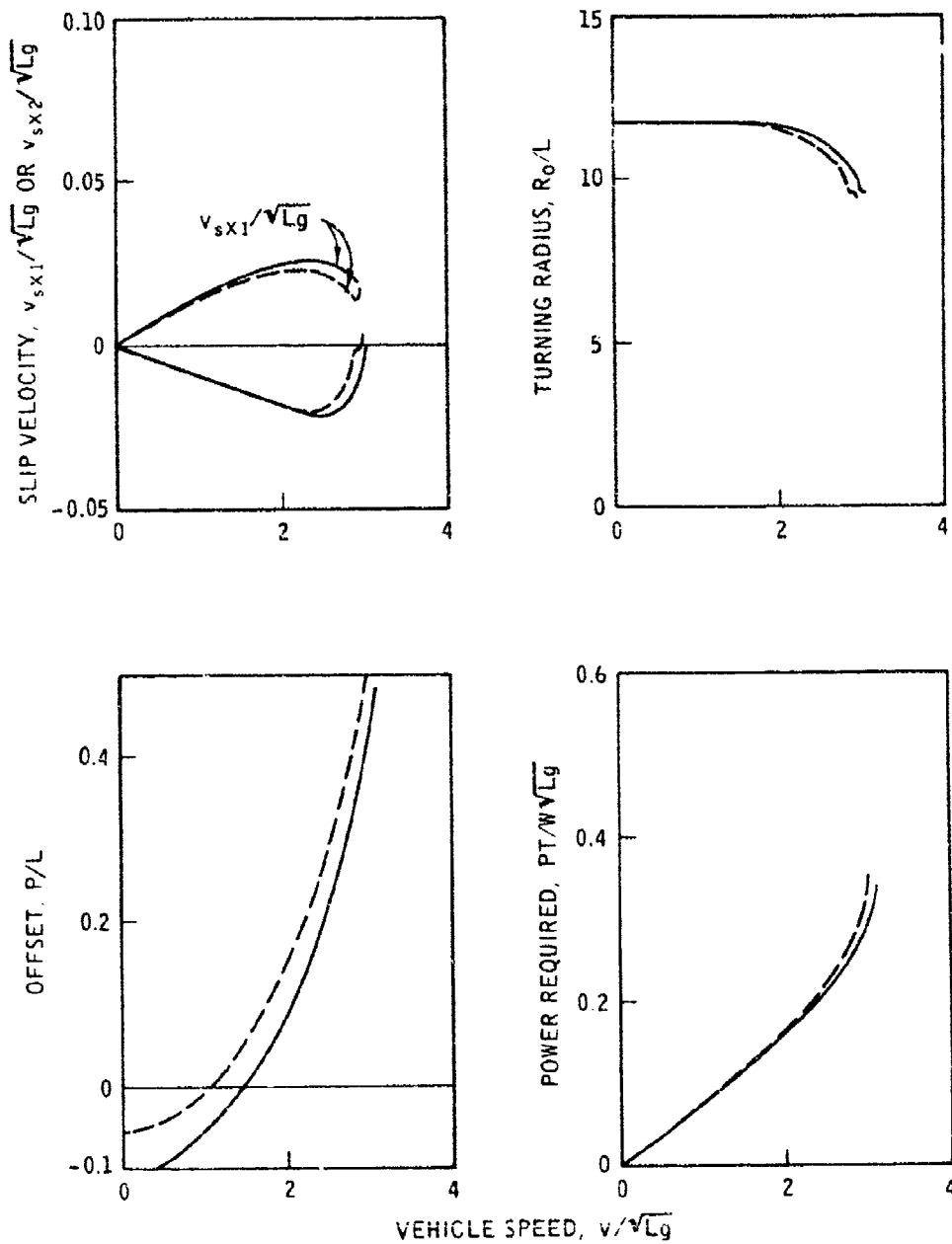


Figure 31. Effect of terrain slope on the relationships between vehicle speed and slip velocity, turning radius, offset, and power requirement (case 4, $\epsilon = 1.1$, $\chi = 270^\circ$)

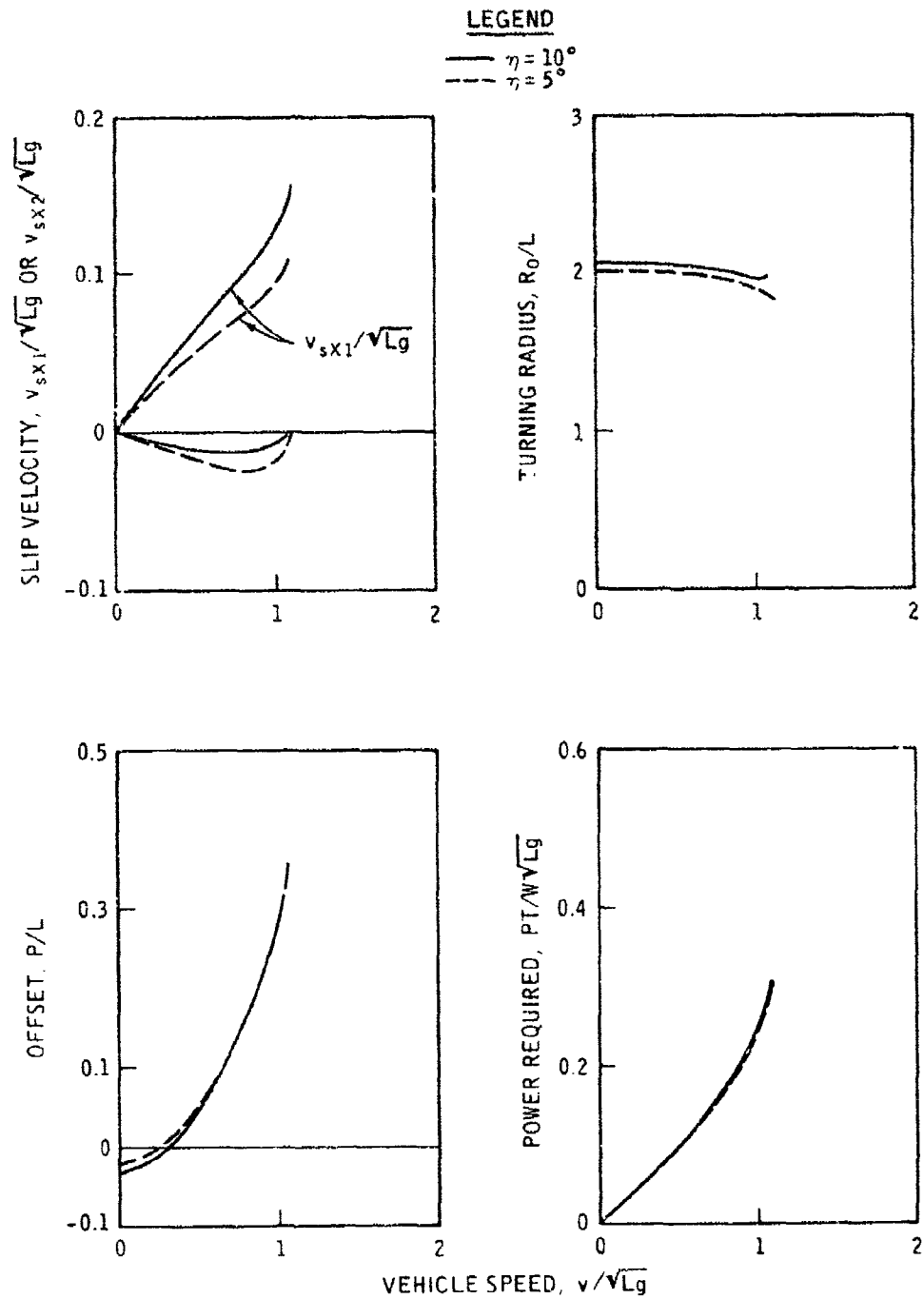


Figure 32. Effect of terrain slope on the relationships between vehicle speed and slip velocity, turning radius, offset, and power requirement (case 4, $c = 1.75$, $\chi = 0^\circ$)

LEGEND

— $\eta = 10^\circ$
 - - - $\eta = 5^\circ$

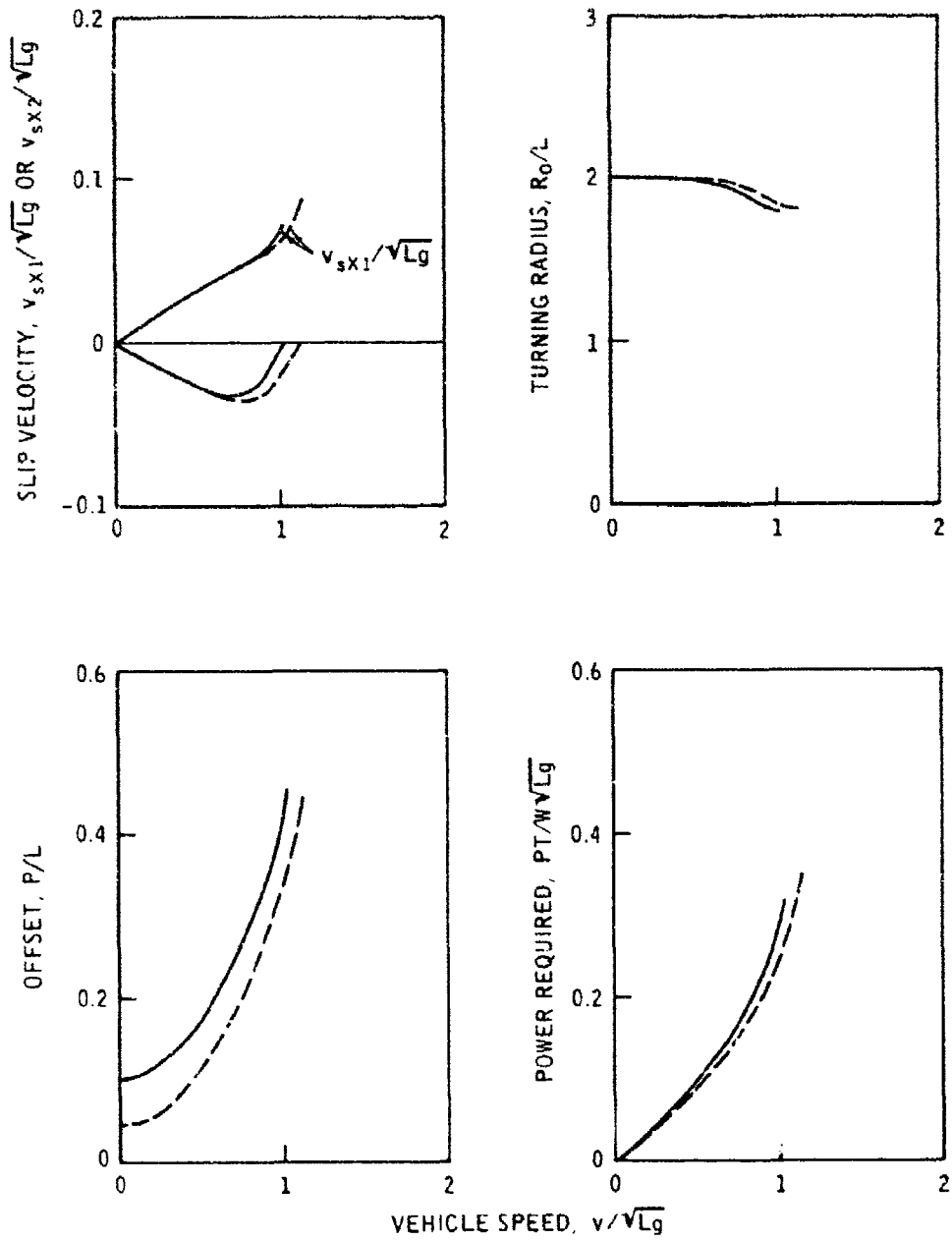


Figure 33. Effect of terrain slope on the relationships between vehicle speed and slip velocity, turning radius, offset, and power requirement (case 4, $\epsilon = 1.75$, $\chi = 90^\circ$)

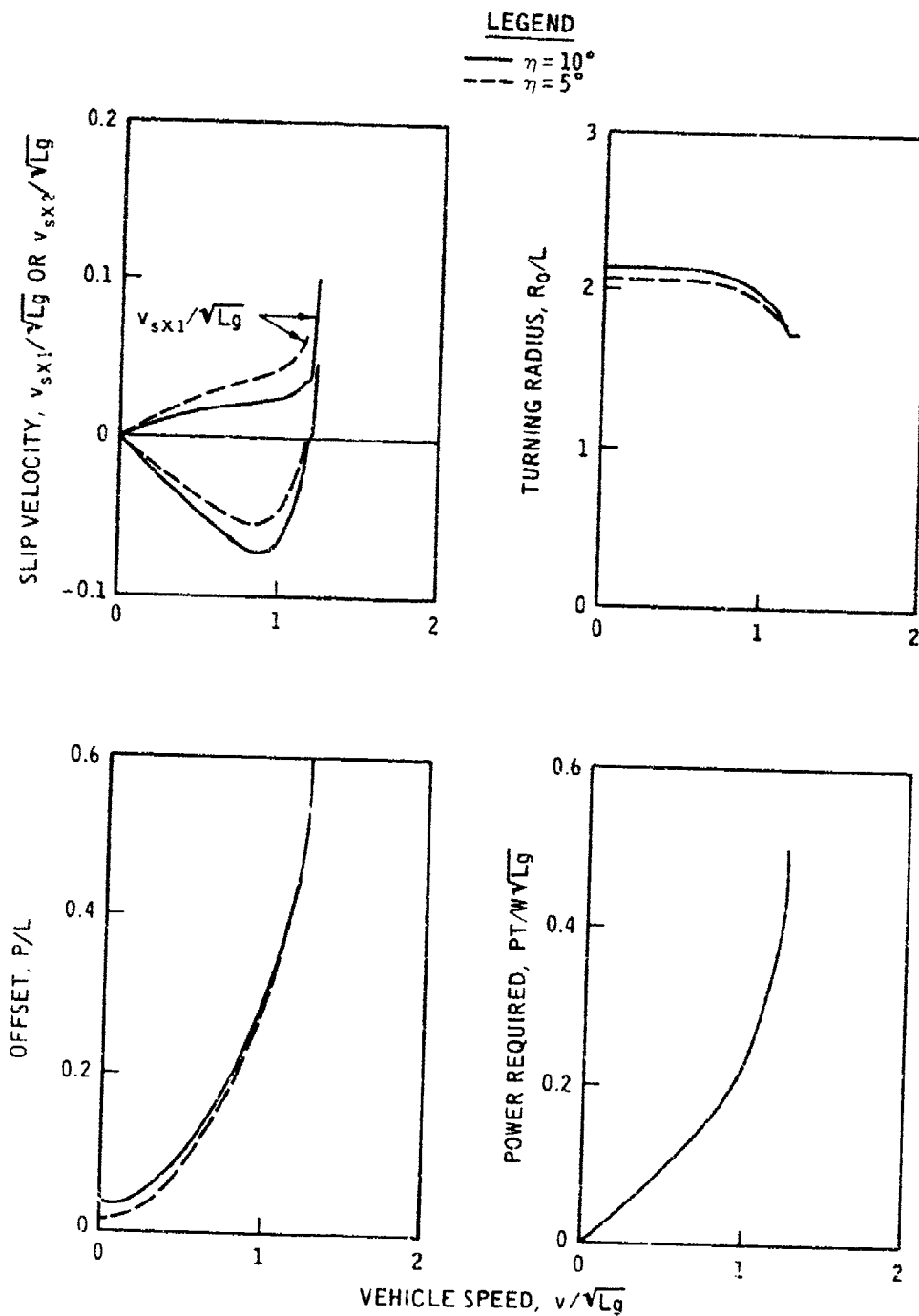


Figure 34. Effect of terrain slope on the relationships between vehicle speed and slip velocity, turning radius, offset, and power requirement (case 4, $\epsilon = 1.75$, $\chi = 180^\circ$)

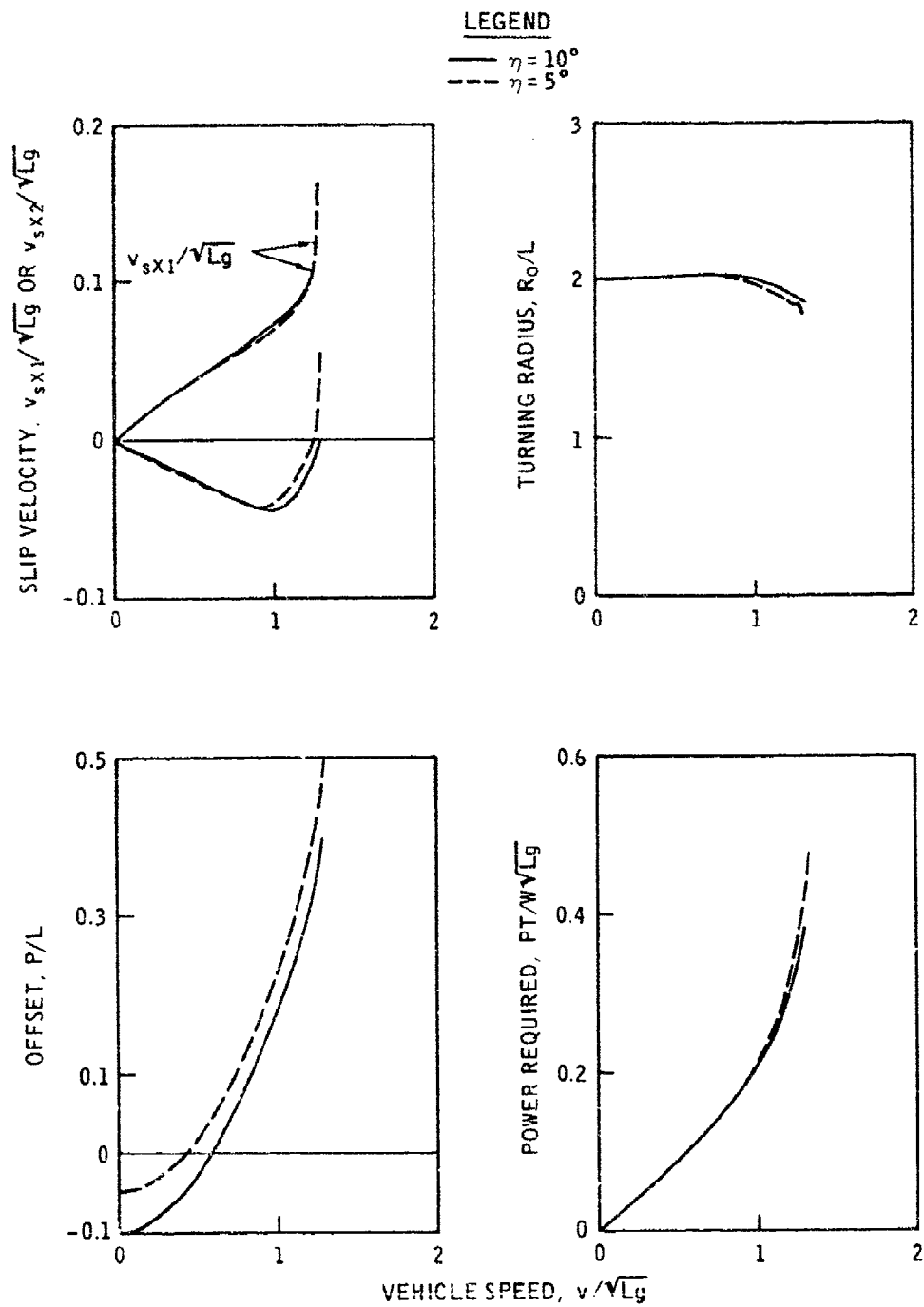


Figure 35. Effect of terrain slope on the relationships between vehicle speed and slip velocity, turning radius, offset, and power requirement (case 4, $\epsilon = 1.75$, $\chi = 270^\circ$)

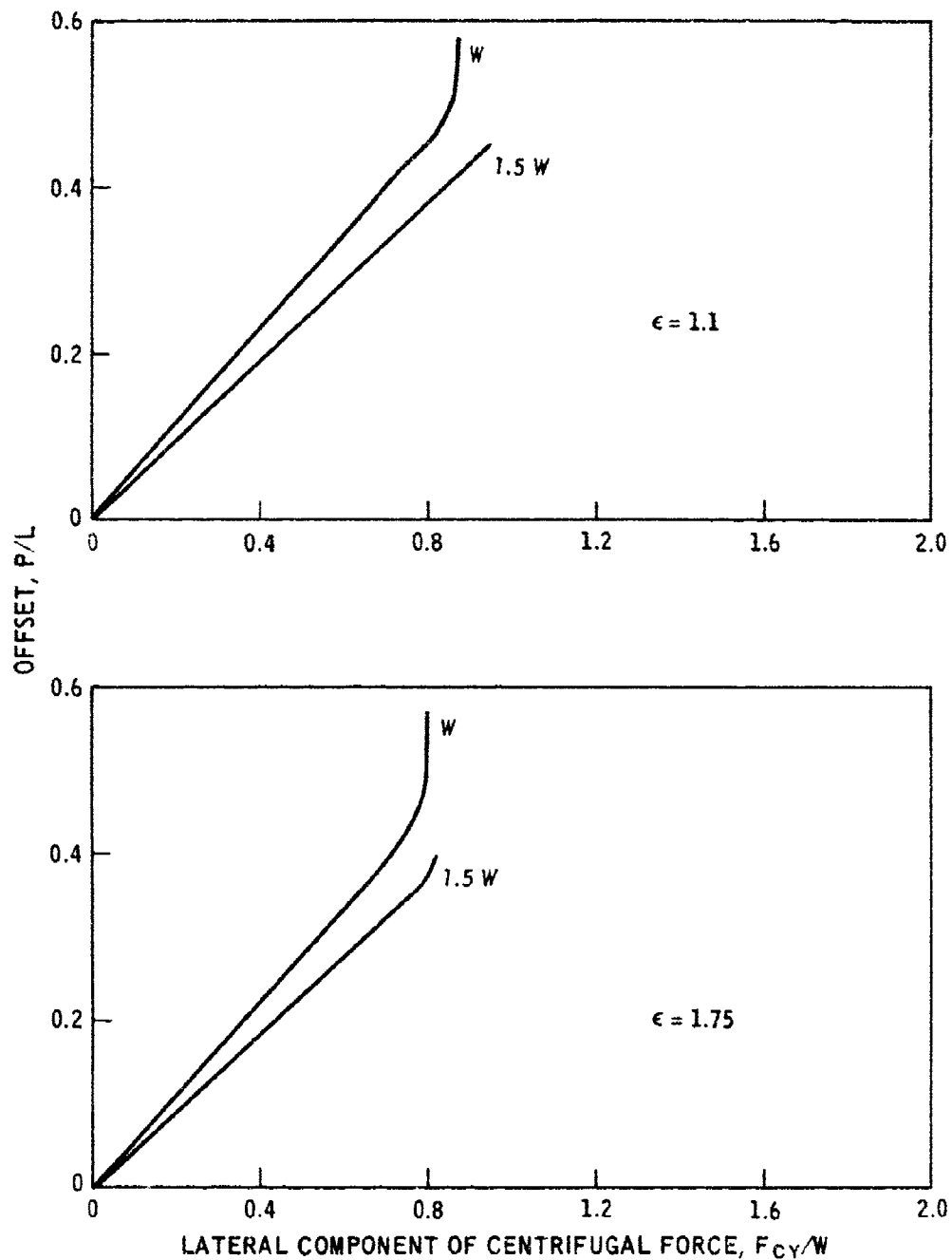


Figure 26. Effect of vehicle weight on the relationships between offset and lateral component of centrifugal force for mixed soil without rate effect (case 4)

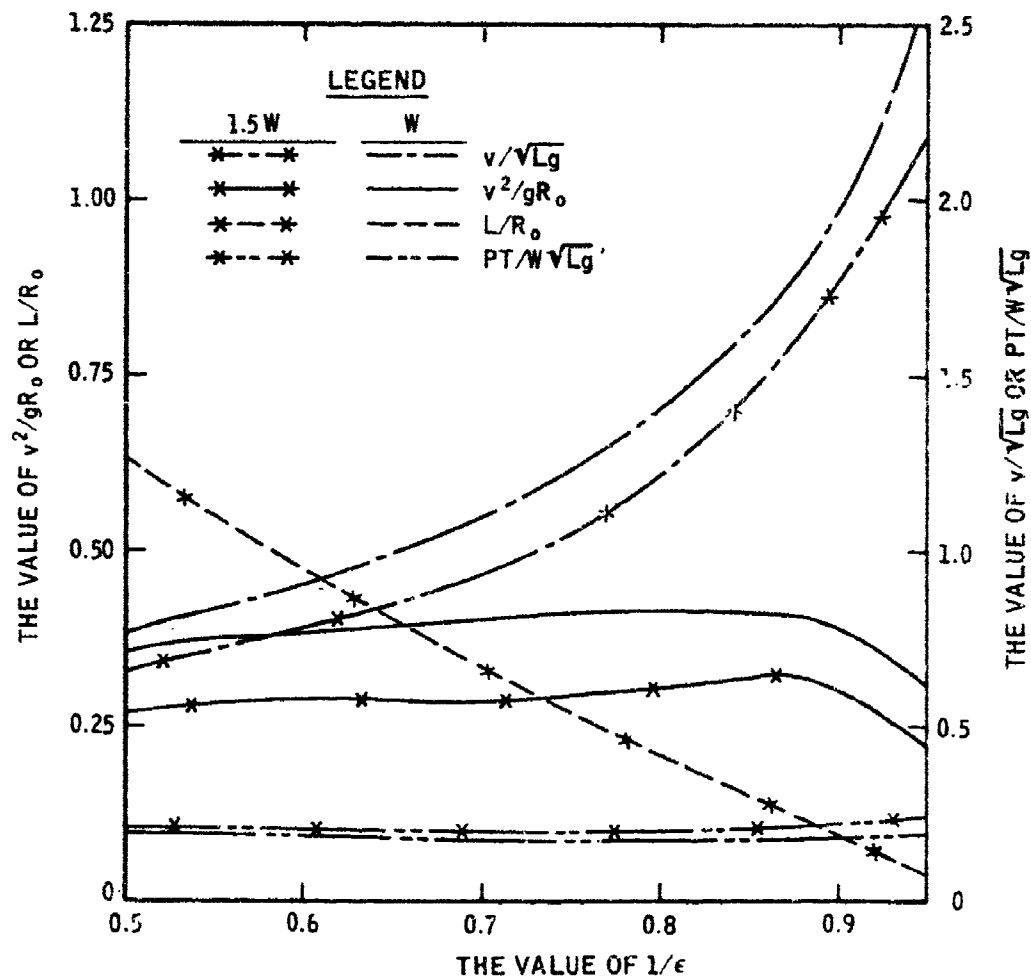


Figure 37. Effect of vehicle weight on the relationships between steering ratio and turning radius, lateral acceleration, vehicle speed, and power requirement for mixed soil without rate effect (case 4)

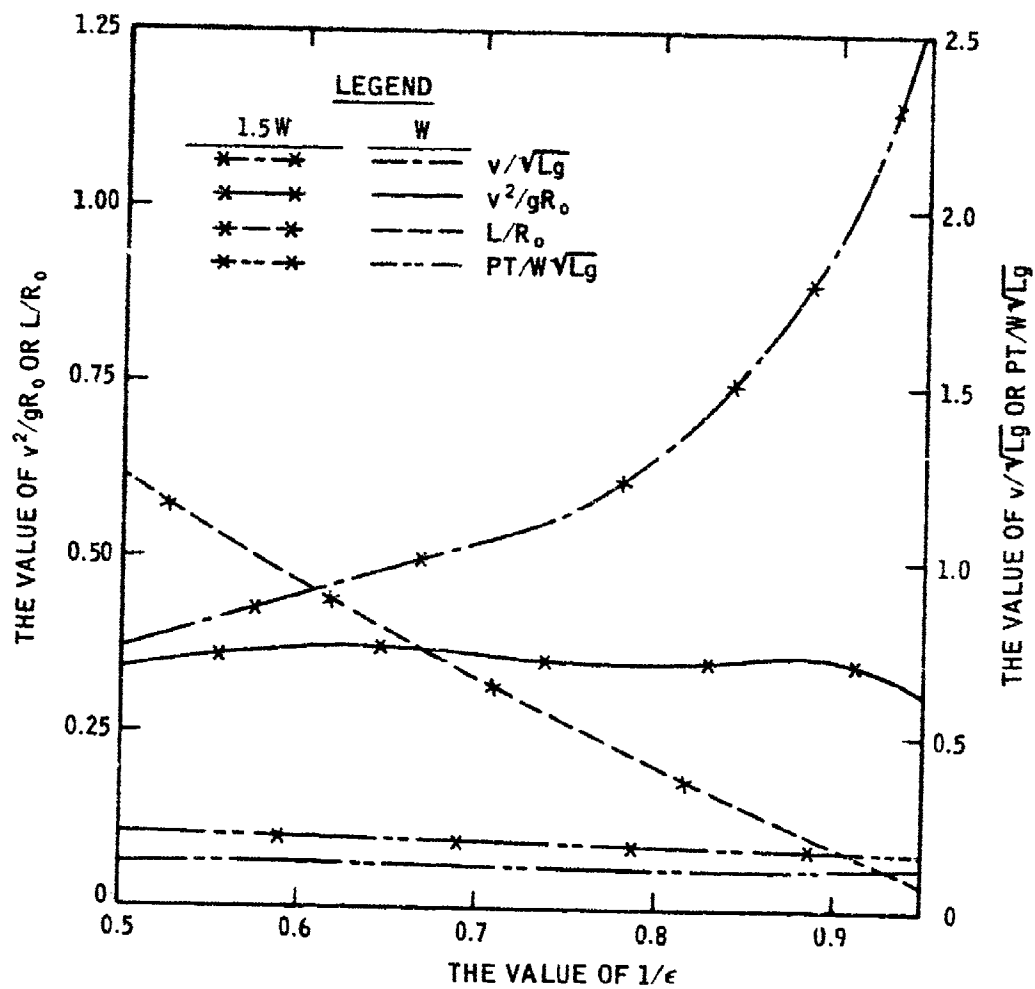


Figure 38. Effect of vehicle weight on the relationships between steering ratio and turning radius, lateral acceleration, vehicle speed, and power requirement for firm surface (case 6)

LEGEND

— $L = L$ (TRACK LENGTH BASELINE, TABLE 1)
 - - - $L = 1.5L$

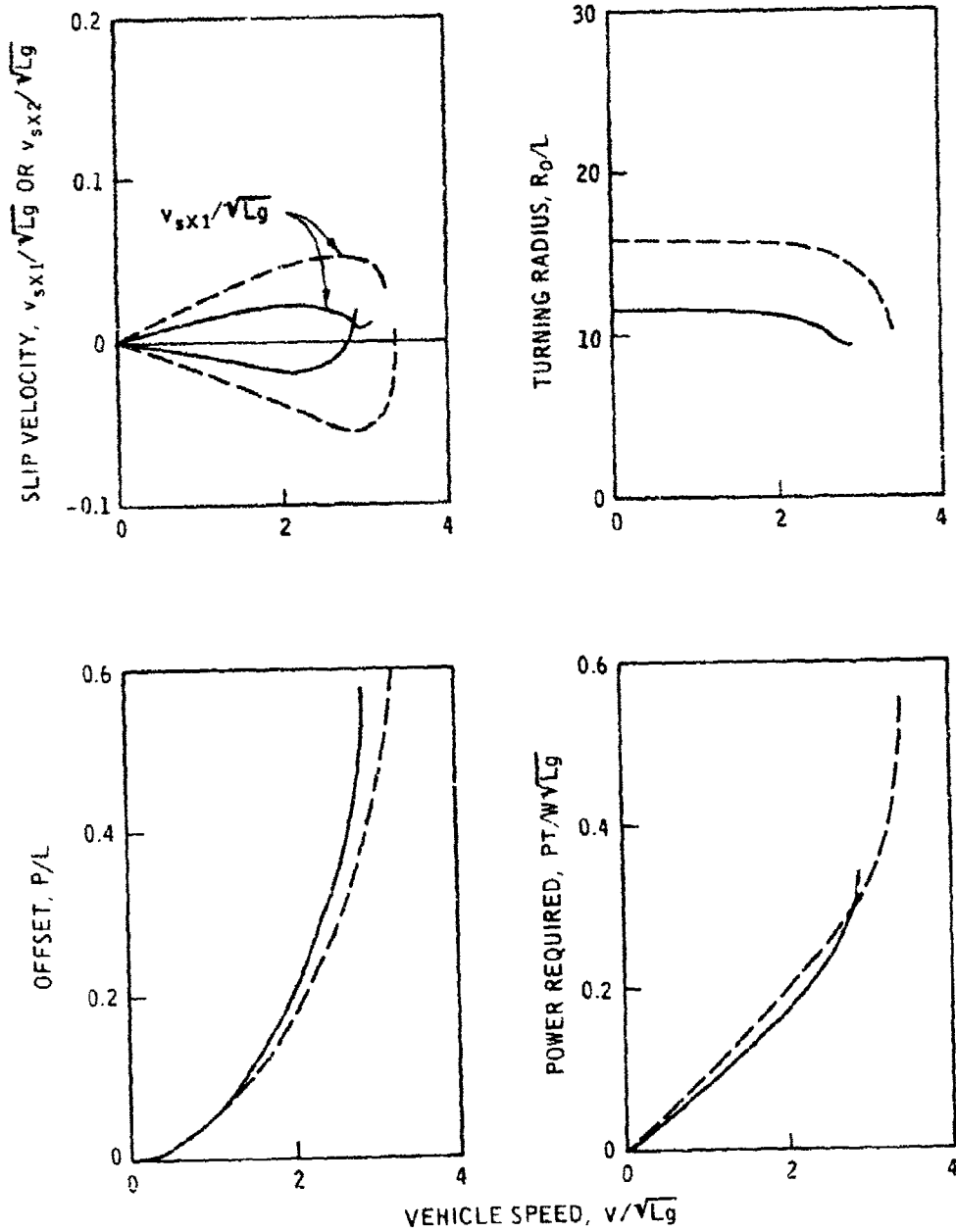


Figure 39. Effect of vehicle track length on the relationships between vehicle speed and slip velocity, turning radius, offset, and power requirement (case 4, $\epsilon = 1.1$)

LEGEND

— $L = L$ (TRACK LENGTH BASELINE, TABLE 1)
 - - - $L = 1.5L$

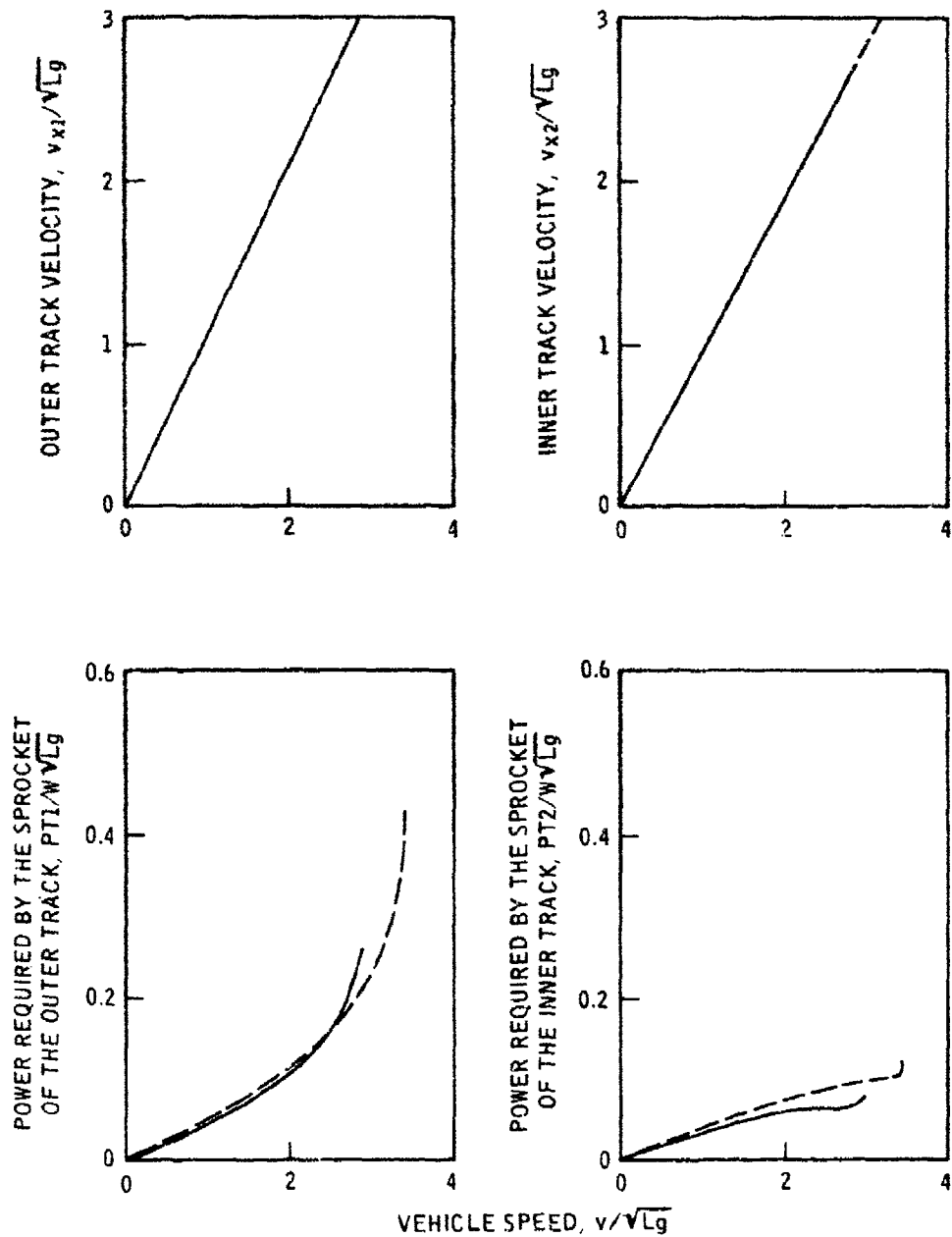


Figure 40. Effect of vehicle track length on the relationships between vehicle speed and track velocity, and power requirement (case 4, $\epsilon = 1.1$)

LEGEND

— $L = L$ (TRACK LENGTH BASELINE, TABLE 1)
 - - - $L = 1.5L$

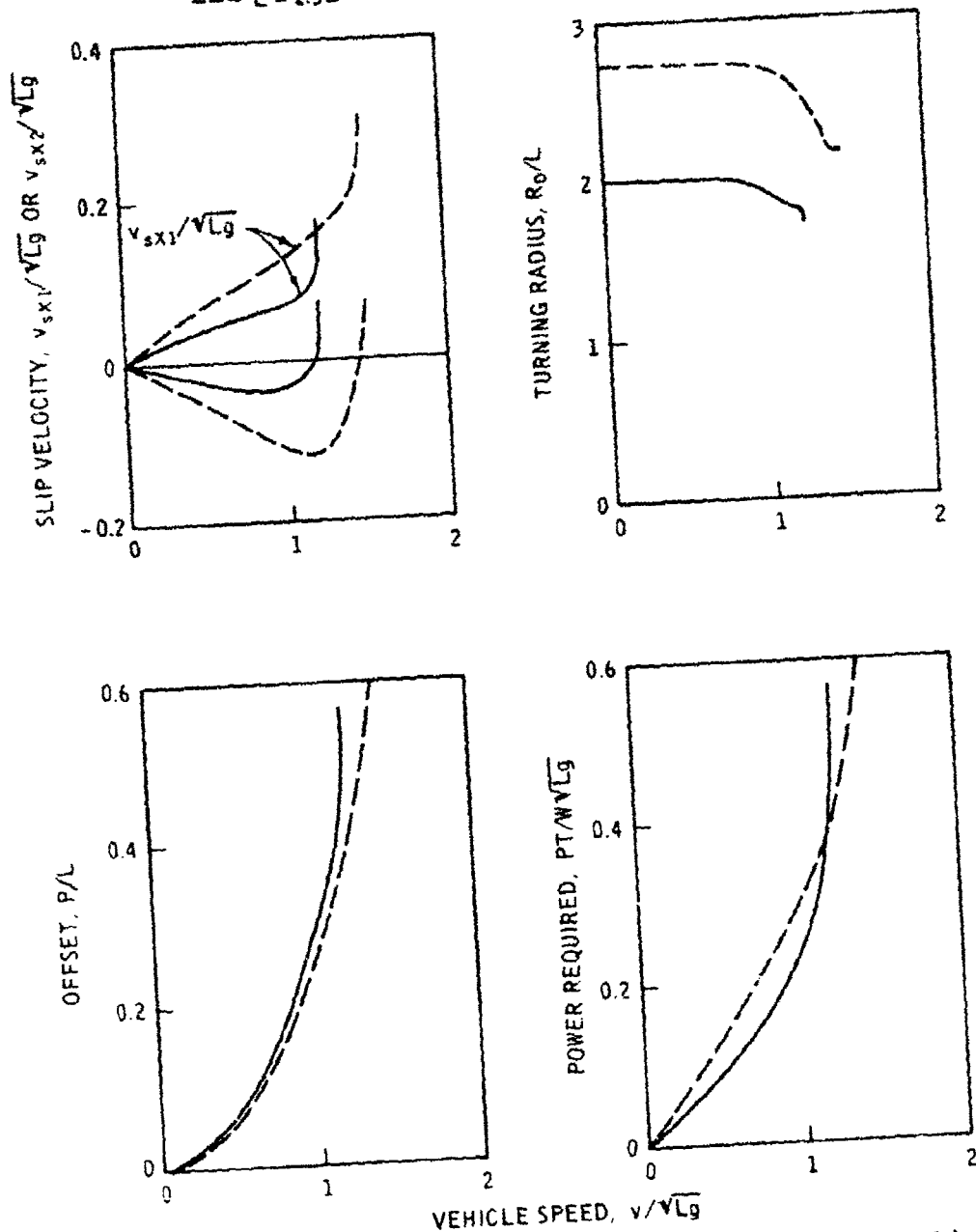


Figure 41. Effect of vehicle track length on the relationships between vehicle speed and slip velocity, turning radius, offset, and power requirement (case 4, $\epsilon = 1.75$)

LEGEND

— $L = L$ (TRACK LENGTH BASELINE, TABLE 1)
 - - - $L = 1.5L$

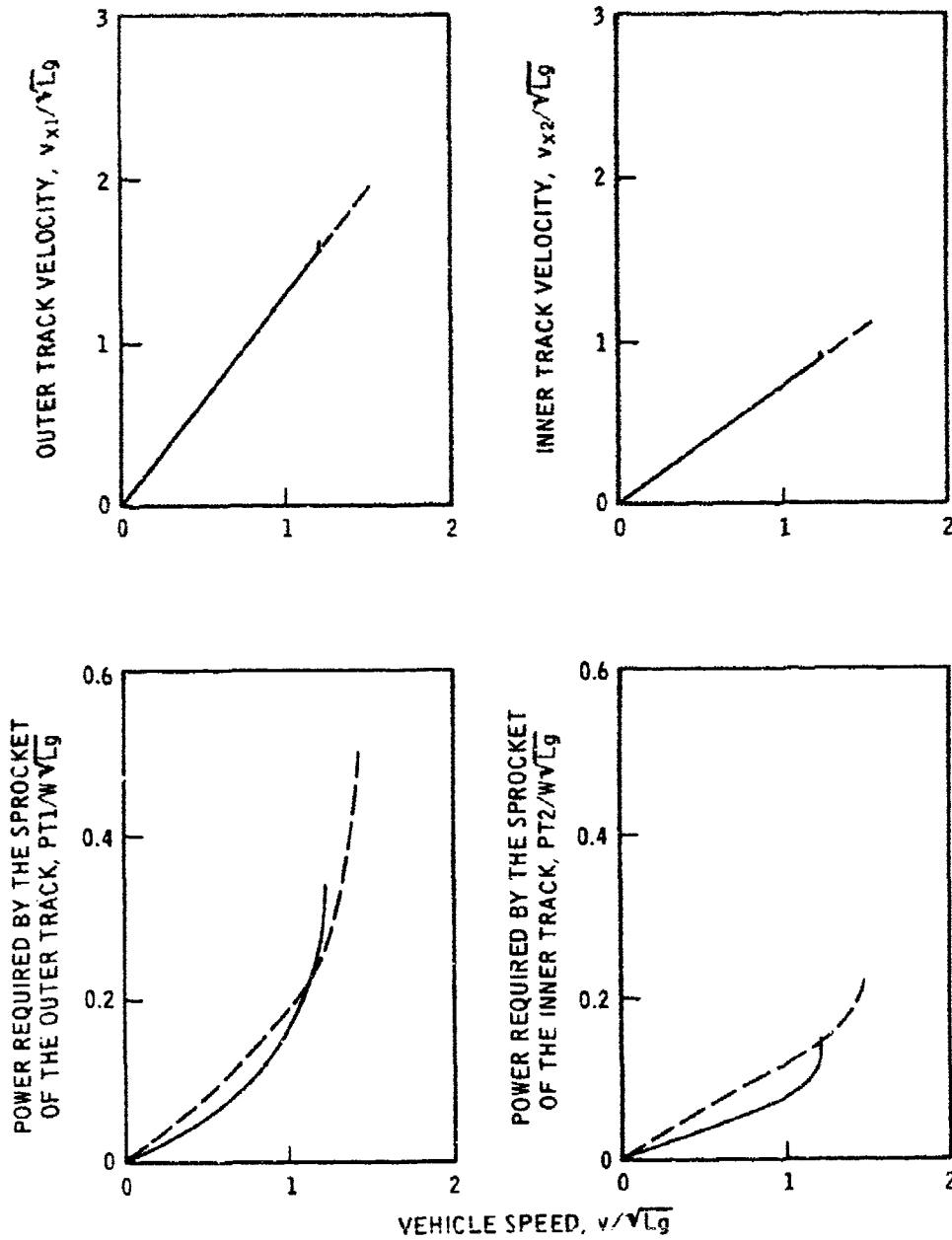


Figure 42. Effect of vehicle track length on the relationships between vehicle speed and track velocity, and power requirement (case 4, $\epsilon = 1.75$)

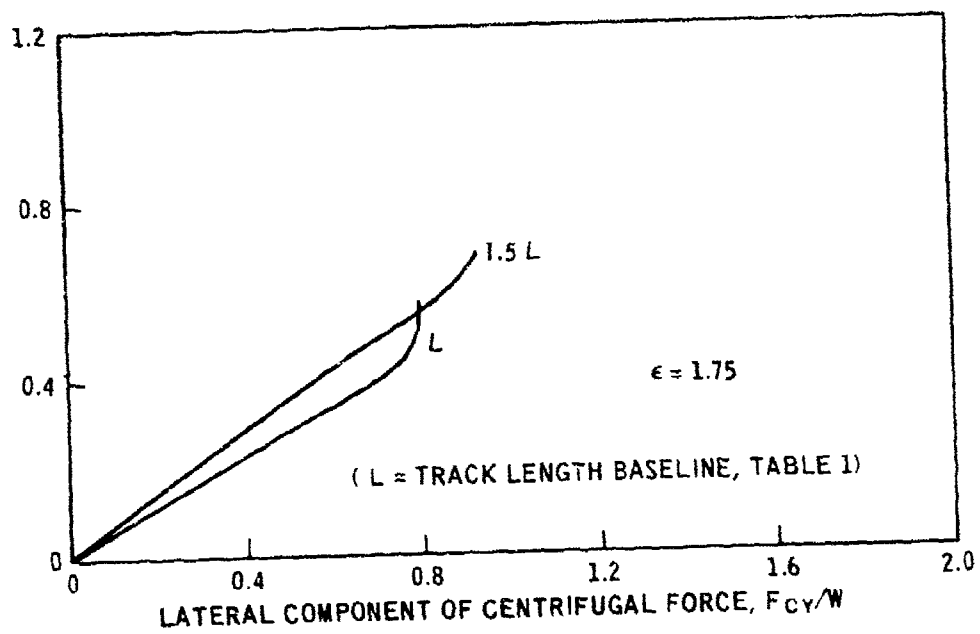
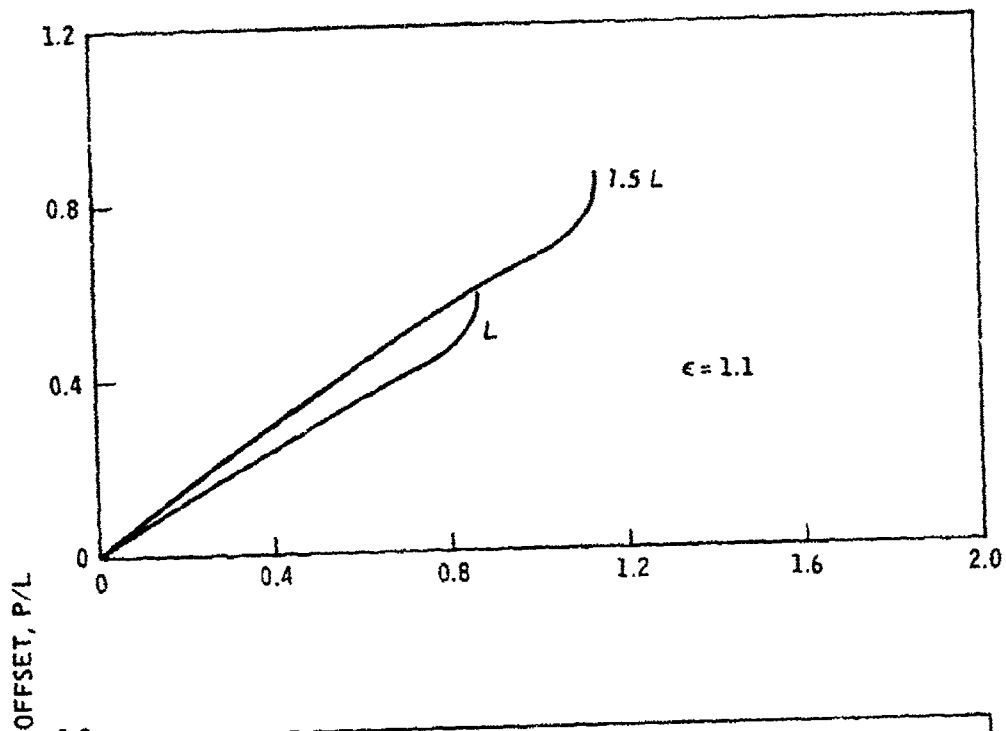


Figure 43. Effect of vehicle track length on the relationships between offset and lateral component of centrifugal force (case 4)

LEGEND

— D = D (TRACK WIDTH BASELINE, TABLE 1)
 - - - D = 1.5D

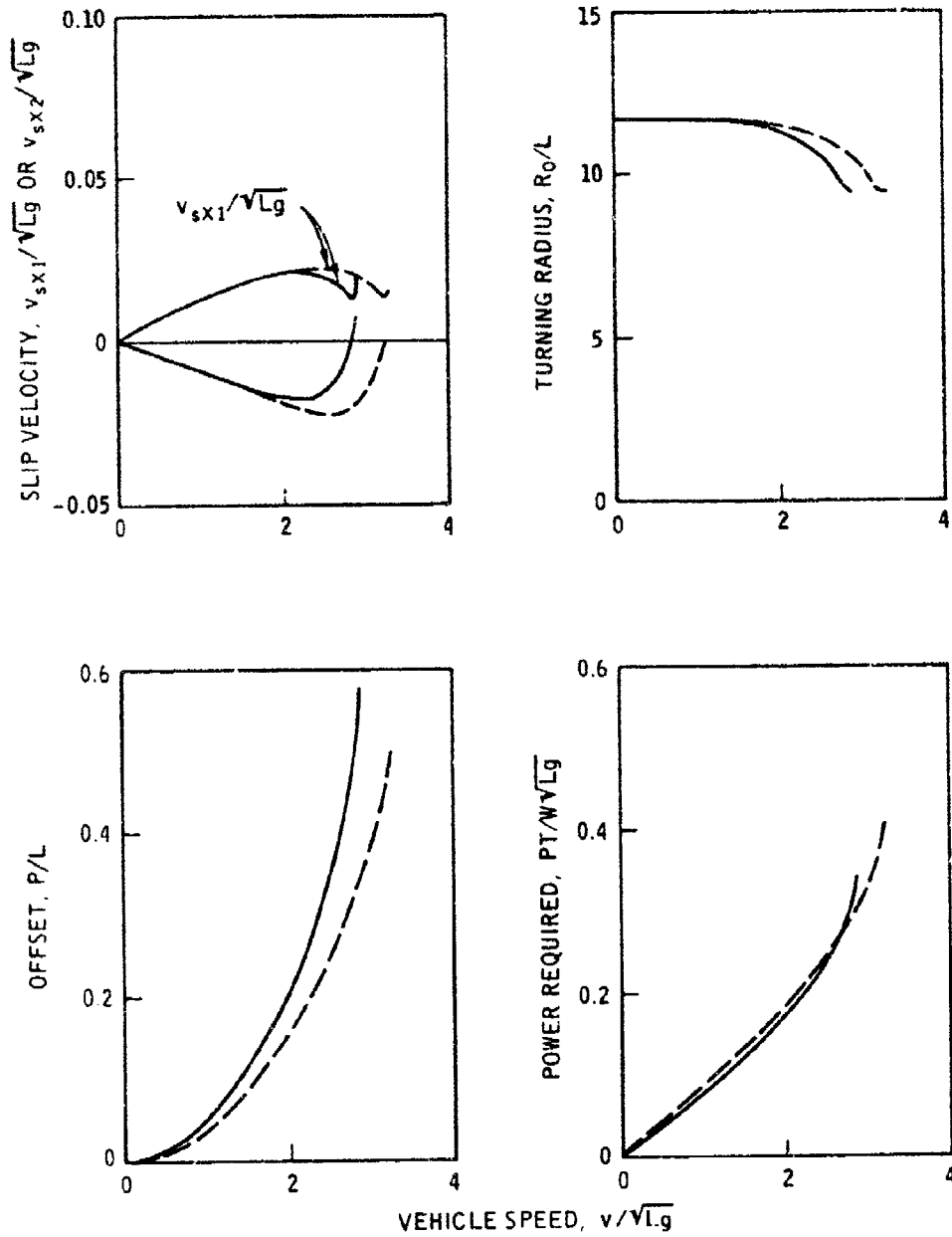


Figure 44. Effect of vehicle track width on the relationships between vehicle speed and slip velocity, turning radius, offset, and power requirement (case 4, $c = 1.1$)

LEGEND

— $D = D$ (TRACK WIDTH BASELINE, TABLE 1)
 - - - $D = 1.5D$

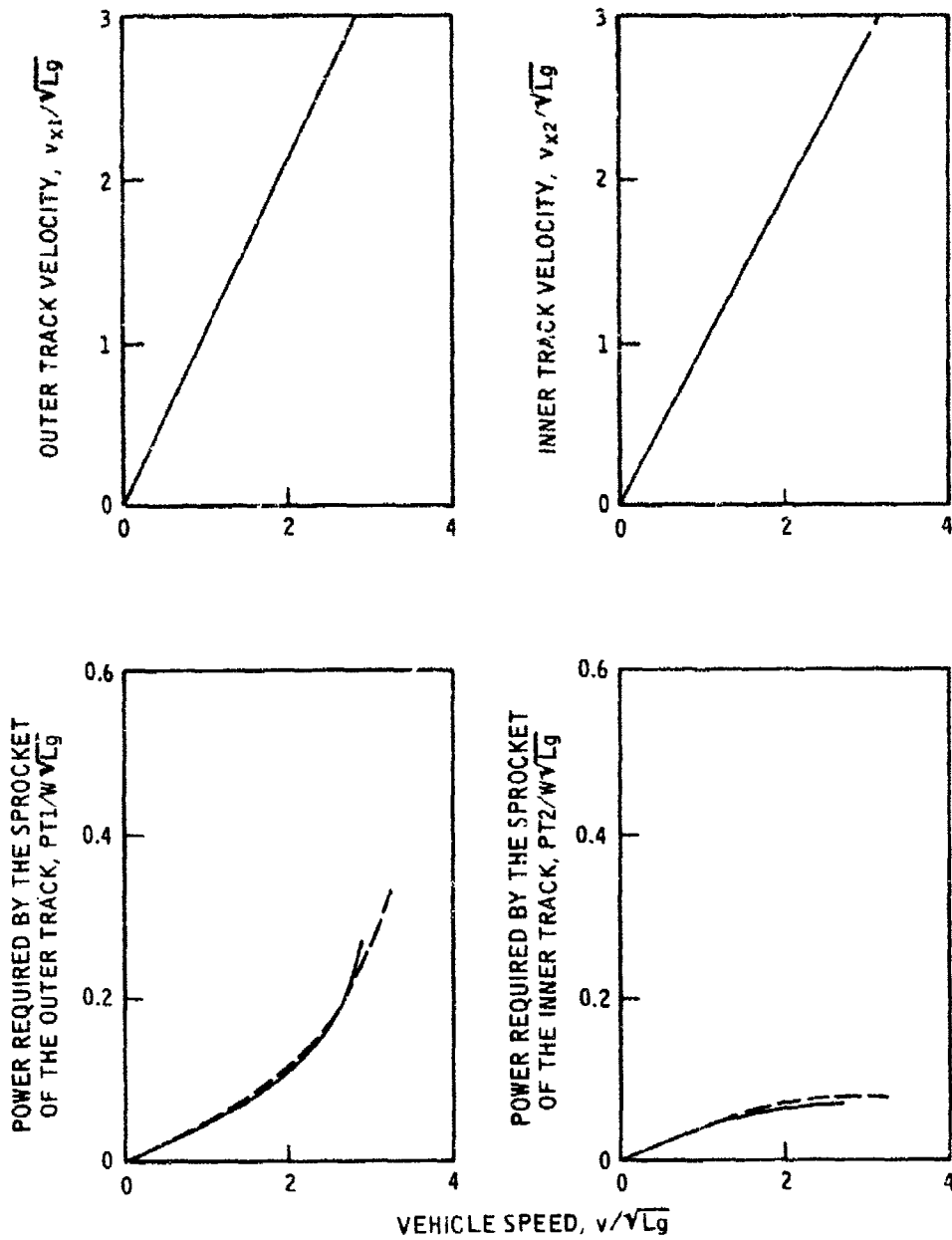


Figure 45. Effect of vehicle track width on the relationships between vehicle speed and track velocity, and power requirement (case 4, $\epsilon = 1.1$)

LEGEND

— D = D (TRACK WIDTH BASELINE, TABLE 1)
 - - - D = 1.5D

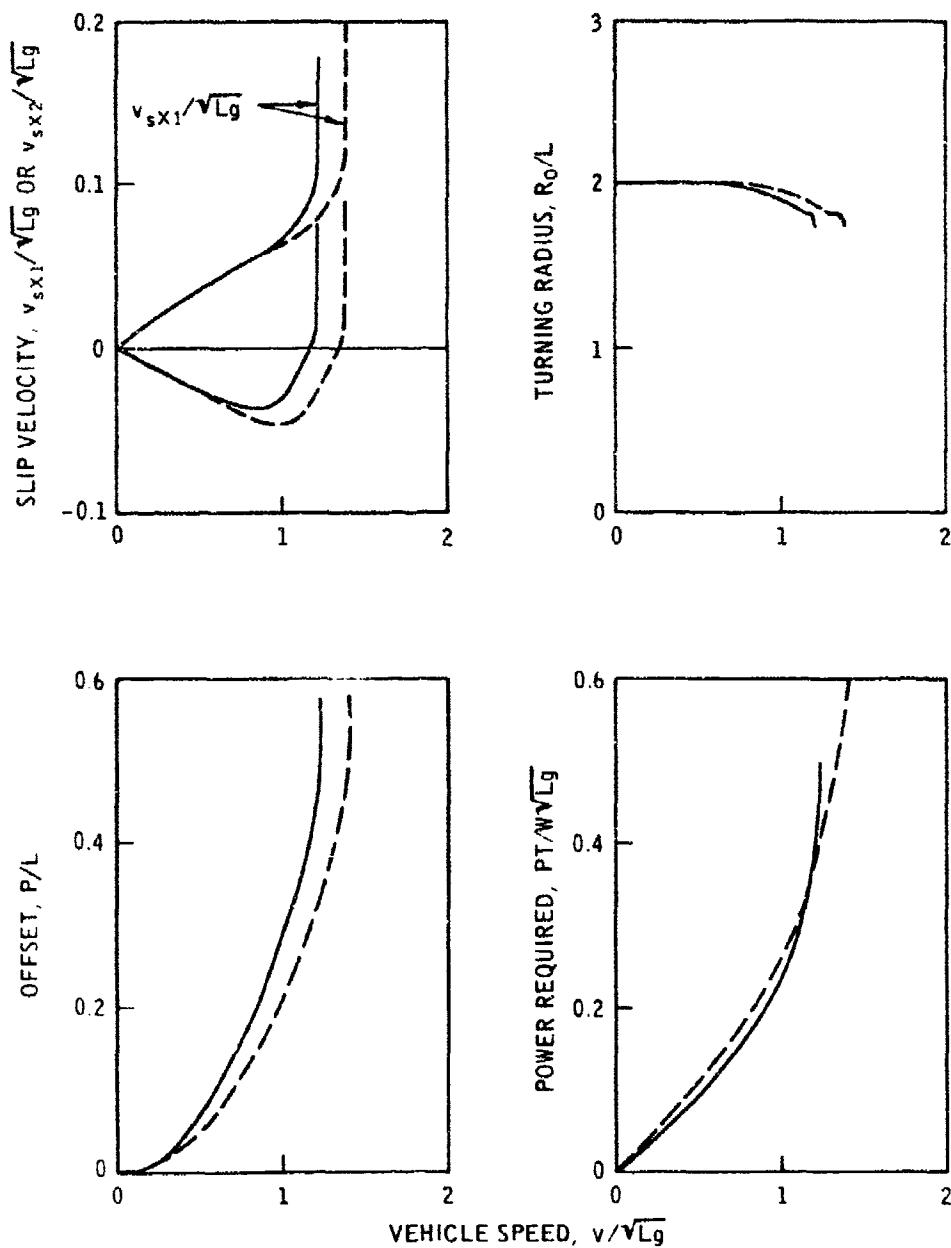


Figure 46. Effect of vehicle track width on the relationships between vehicle speed and slip velocity, turning radius, offset, and power requirement (case 4, $\epsilon = 1.75$)

LEGEND

— D = D (TRACK WIDTH BASELINE, TABLE 1)
 - - - D = 1.5D

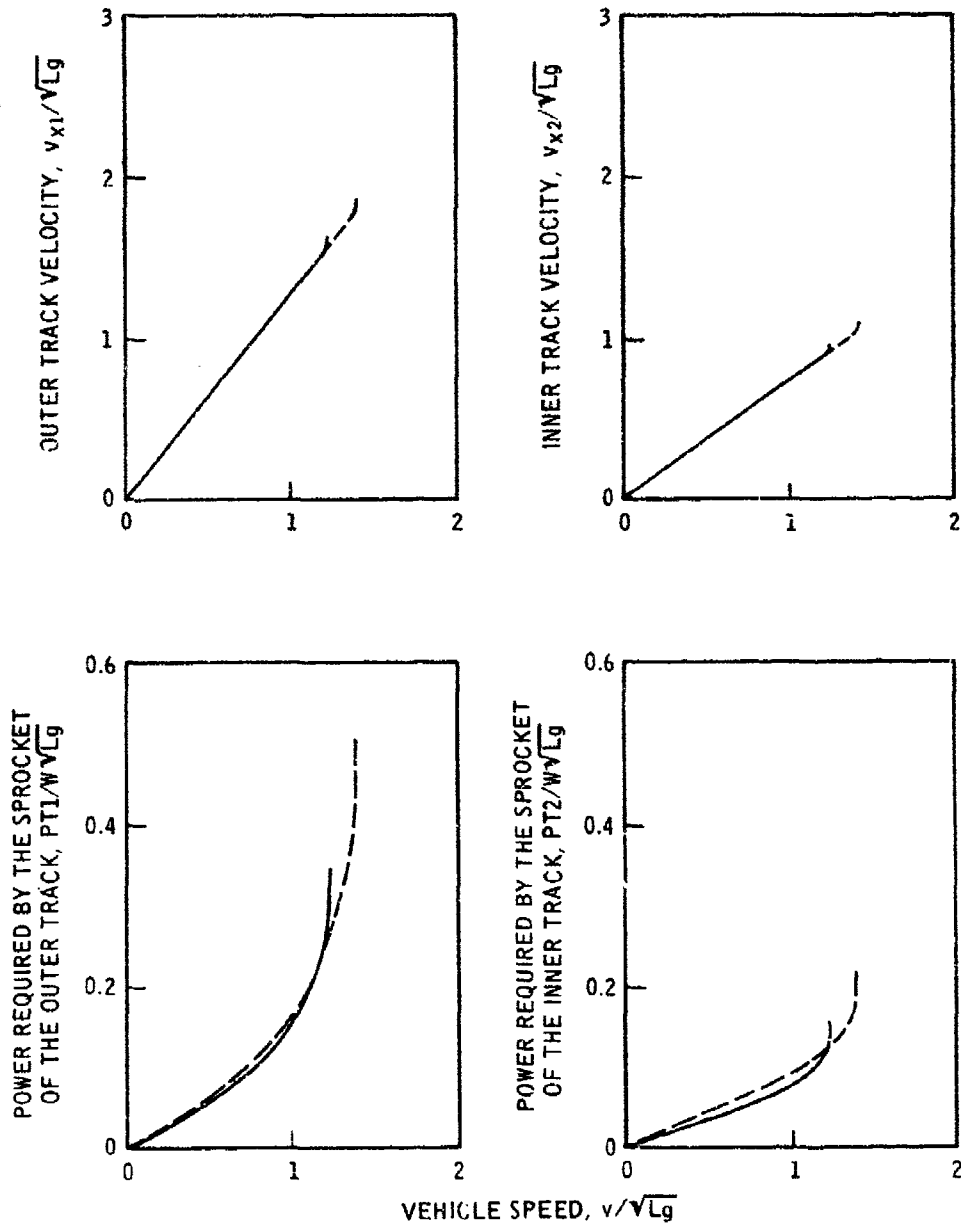


Figure 47. Effect of vehicle track width on the relationships between vehicle speed and track velocity, and power requirement (case 4, $\epsilon = 1.75$)

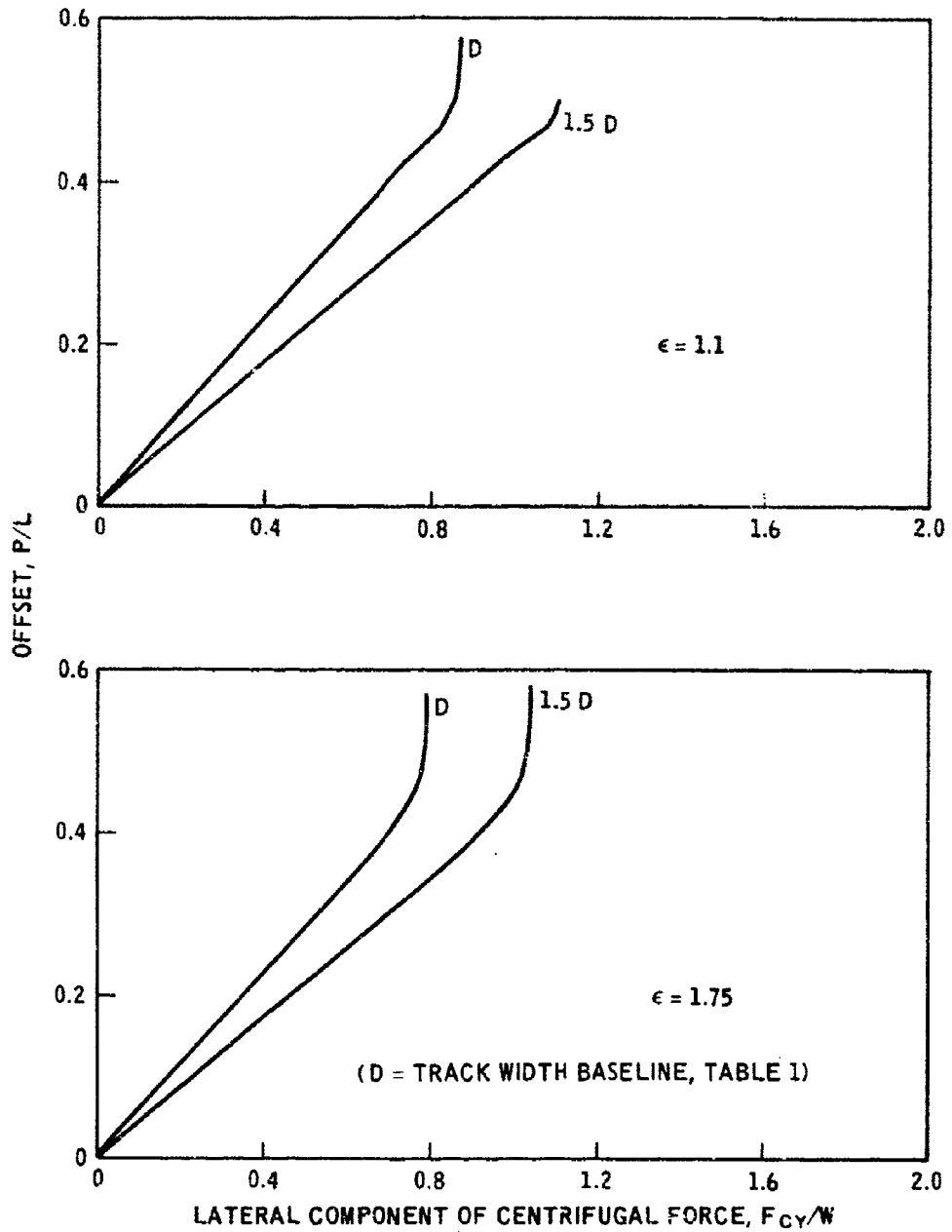


Figure 48. Effect of vehicle track width on the relationship between offset and lateral component of centrifugal force (case 4)

LEGEND

— 3 - B (TRACK TREAD BASELINE, TABLE 1)
 - - - B = 2B/3

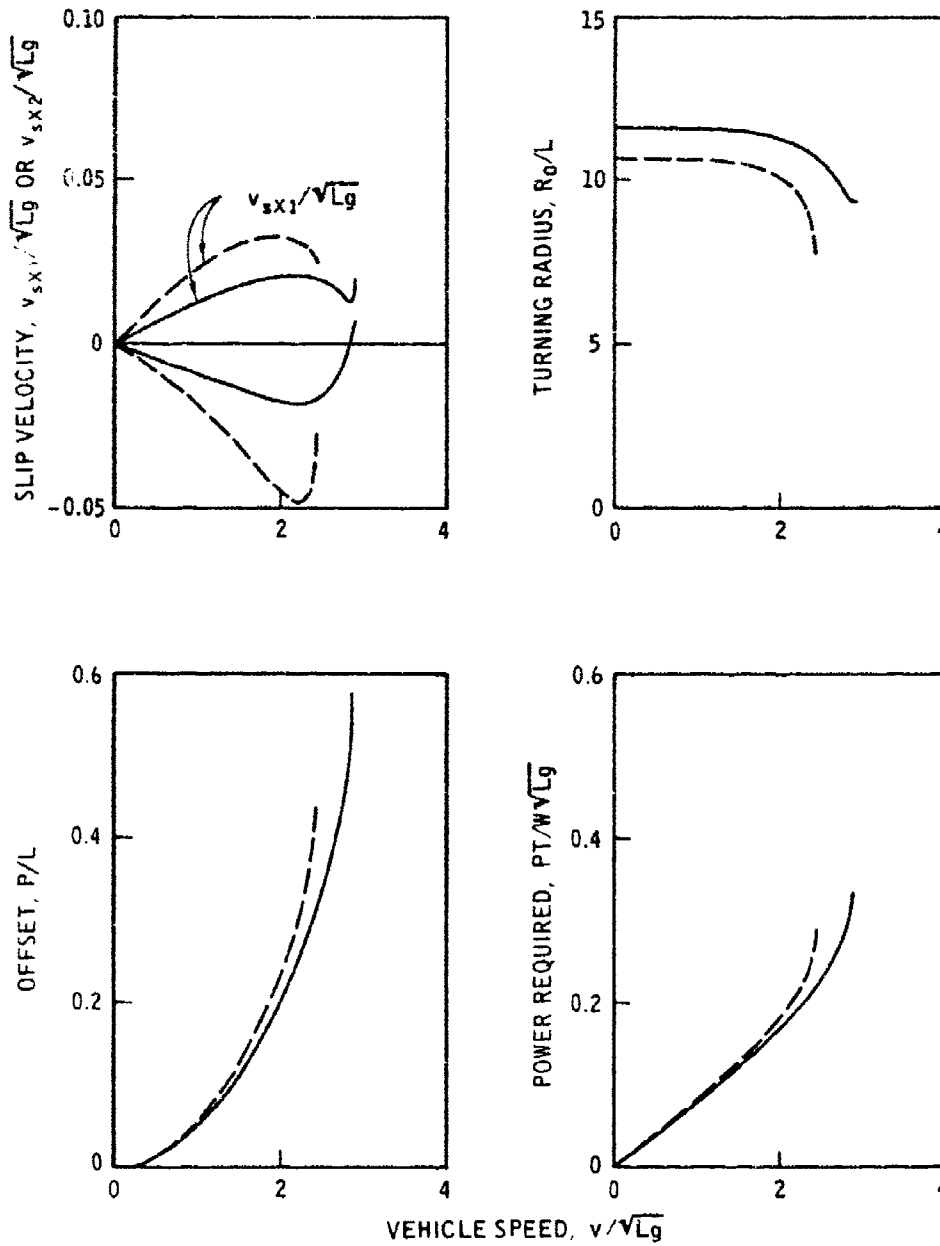


Figure 49. Effect of vehicle track tread on the relationships between vehicle speed and slip velocity, turning radius, offset, and power requirement (case 4, $\epsilon = 1.1$)

LEGEND

— B = B (TRACK TREAD BASELINE, TABLE 1)
- - - B = 2B/3

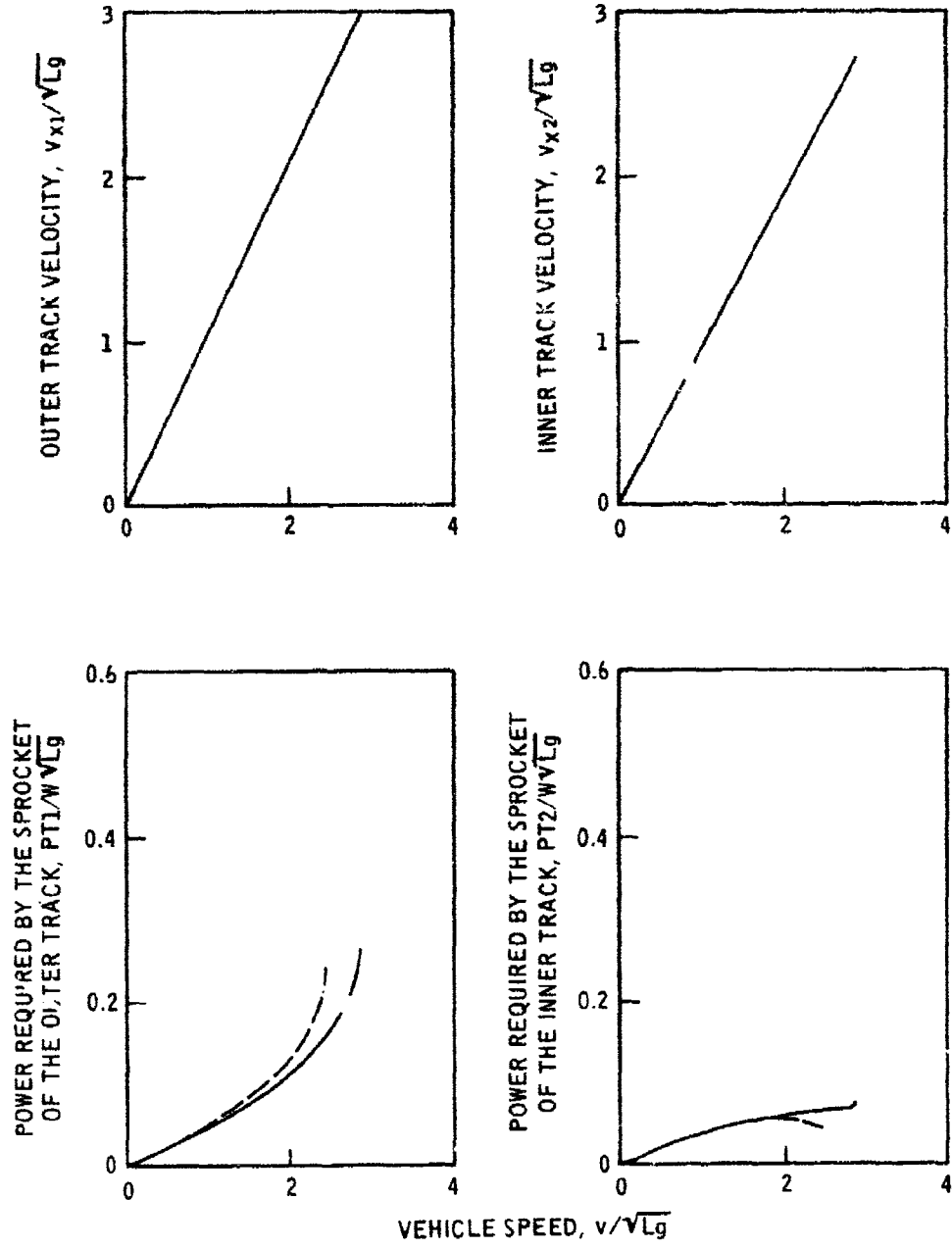


Figure 50. Effect of vehicle track tread on the relationships between vehicle speed and track velocity, and power requirement (case 4, $\epsilon = 1.1$)

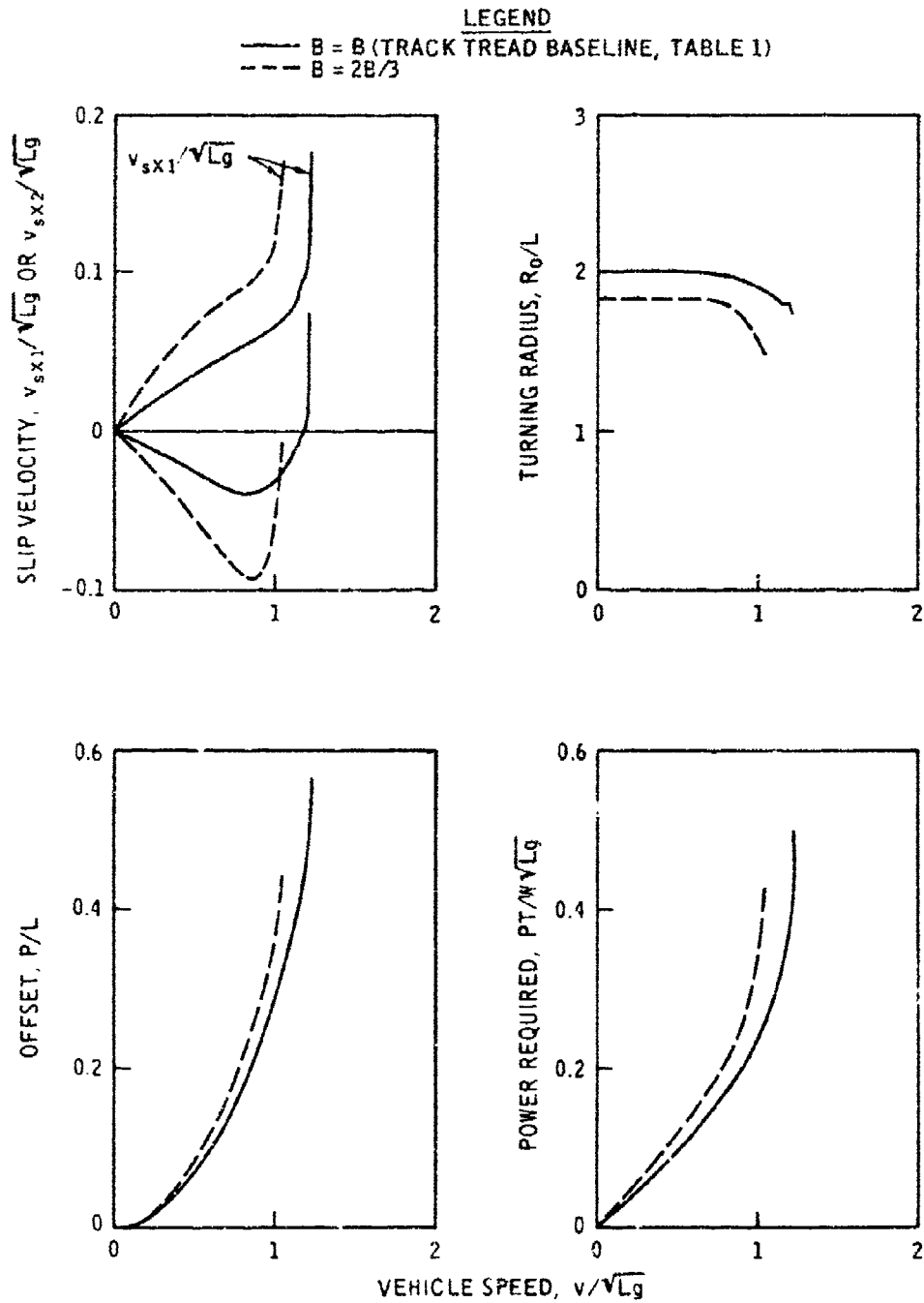


Figure 51. Effect of vehicle track tread on the relationships between vehicle speed and slip velocity, turning radius, offset, and power requirement (case 4, $\epsilon = 1.75$)

LEGEND

— B = B (TRACK TREAD BASELINE, TABLE 1)
 - - - B = 2B/3

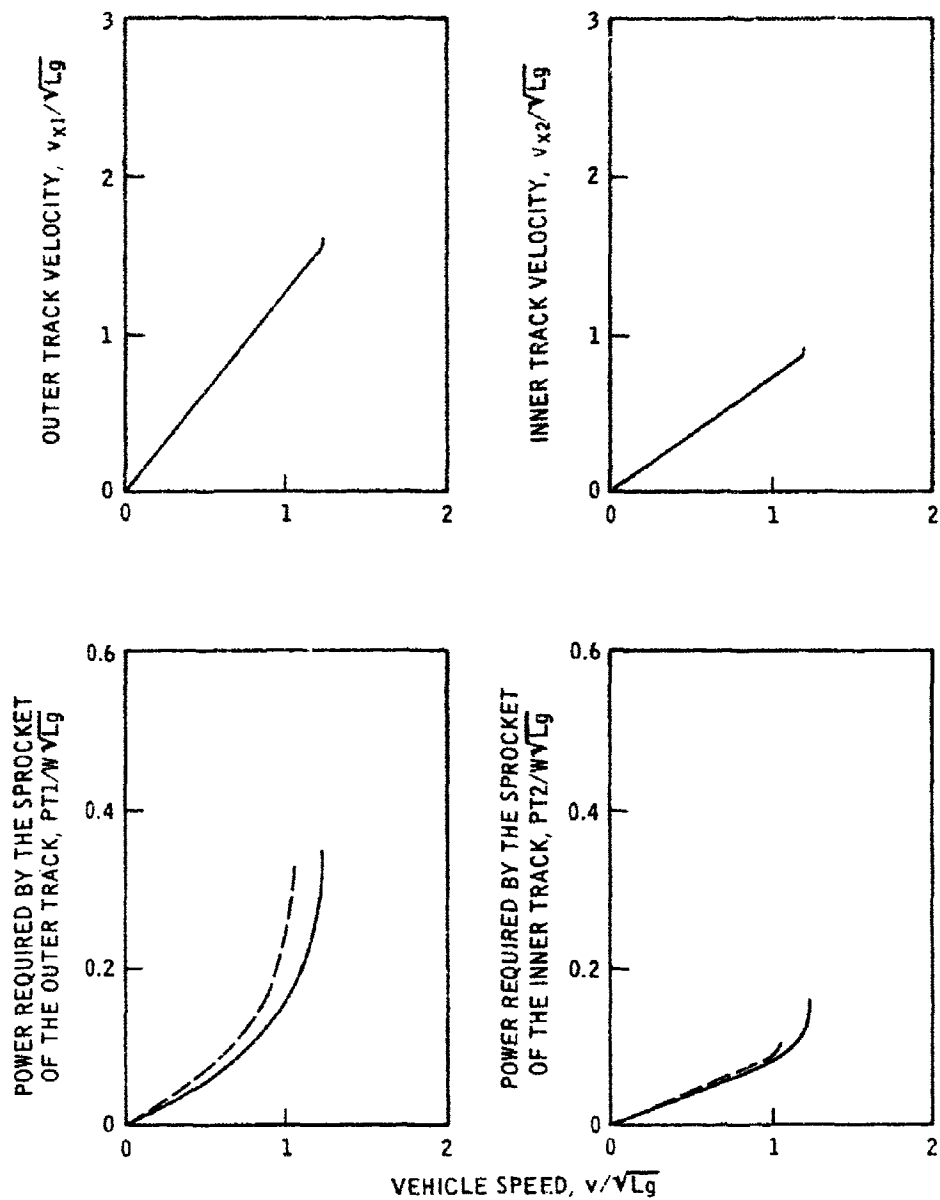


Figure 52. Effect of vehicle track tread on the relationships between vehicle speed and track velocity, and power requirement (case 4, $\epsilon = 1.75$)

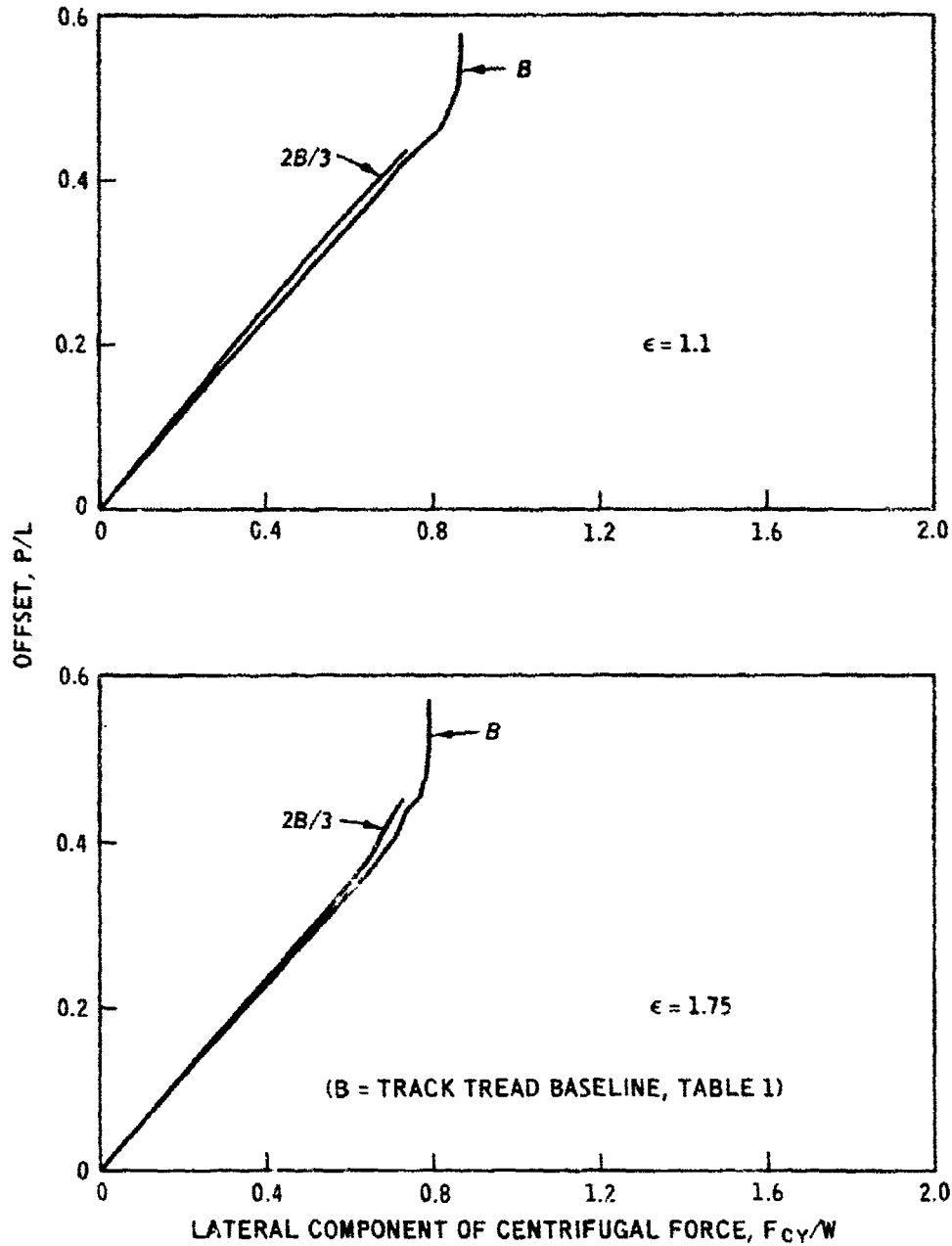


Figure 53. Effect of vehicle track tread on the relationship between offset and lateral component of centrifugal force (case 4)

LEGEND

- H/L = 0.610
- · - H/L = 0.367
- - - H/L = 0.122

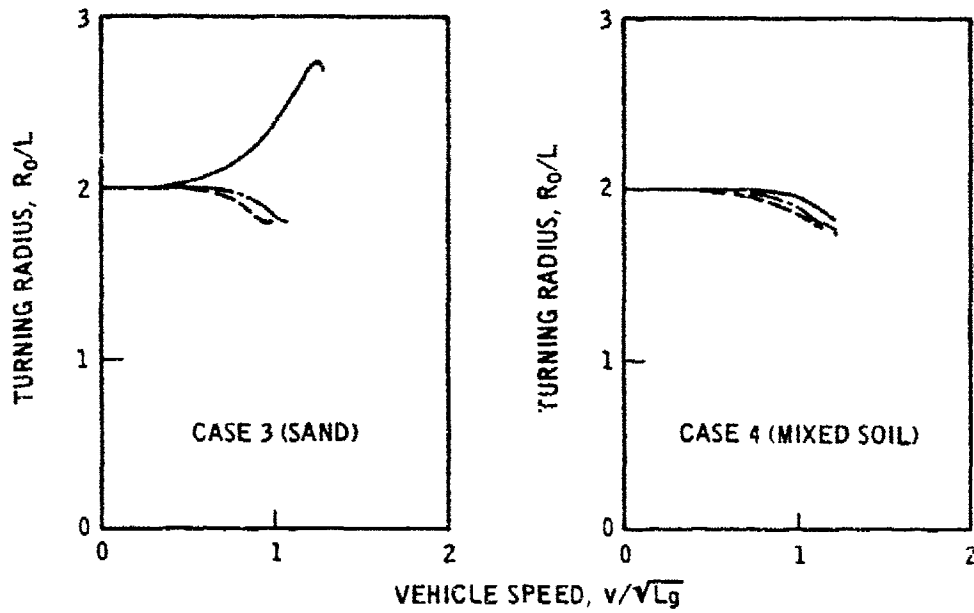


Figure 54. Effect of height of the center of gravity on the relationship between vehicle speed and turning radius ($c = 1.75$)

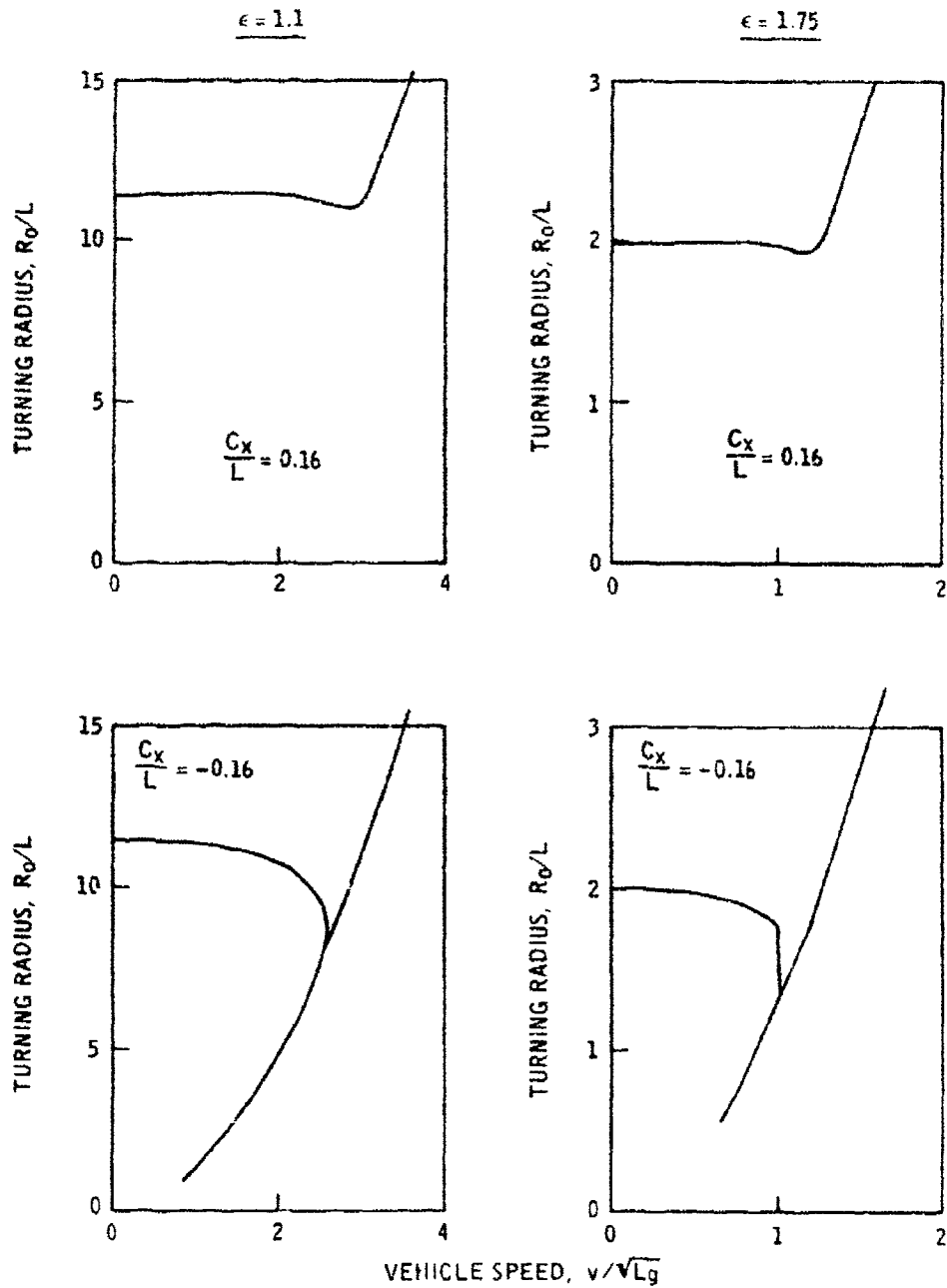


Figure 55. Effect of location of center of gravity of the vehicle on the relationship between vehicle speed and turning radius for mixed soil without rate effect (case 4)

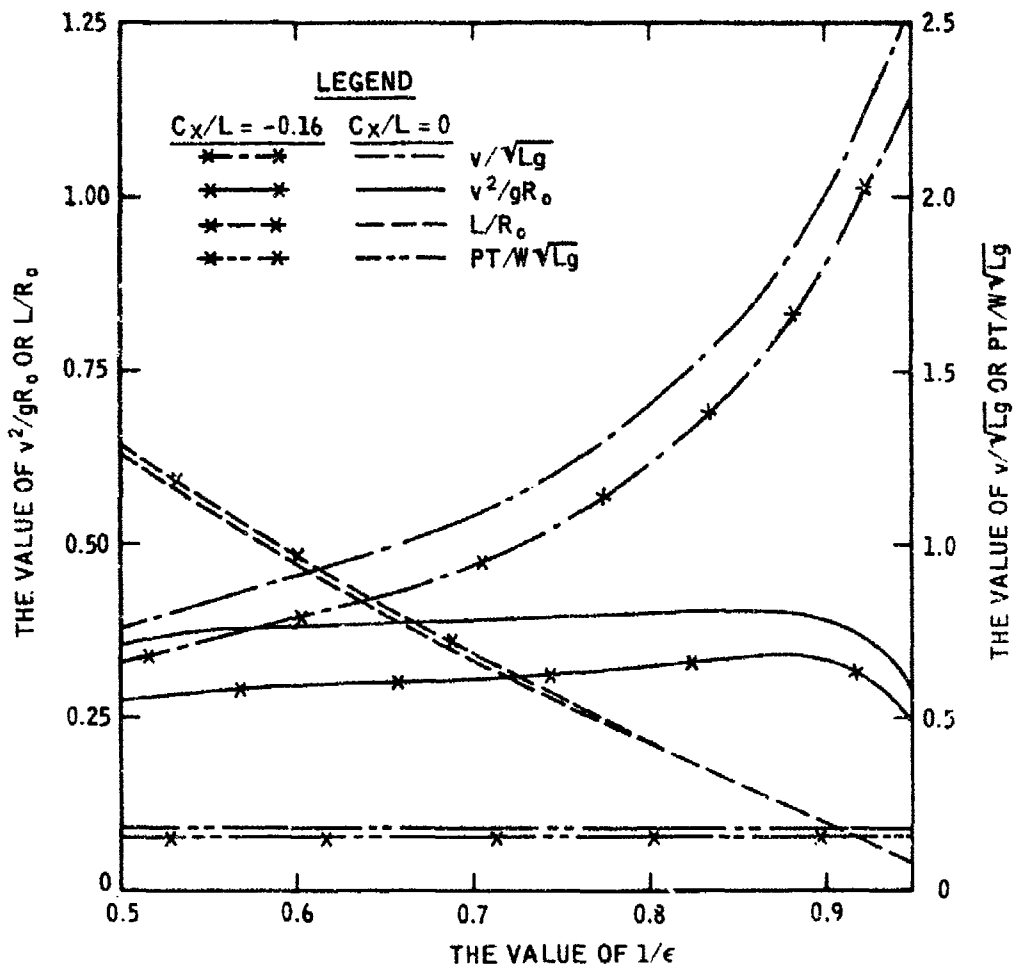


Figure 56. Effect of location of the center of gravity of the vehicle on the relationships between steering ratio and turning radius, lateral acceleration, vehicle speed, and power requirement for mixed soil without rate effect (case 4)

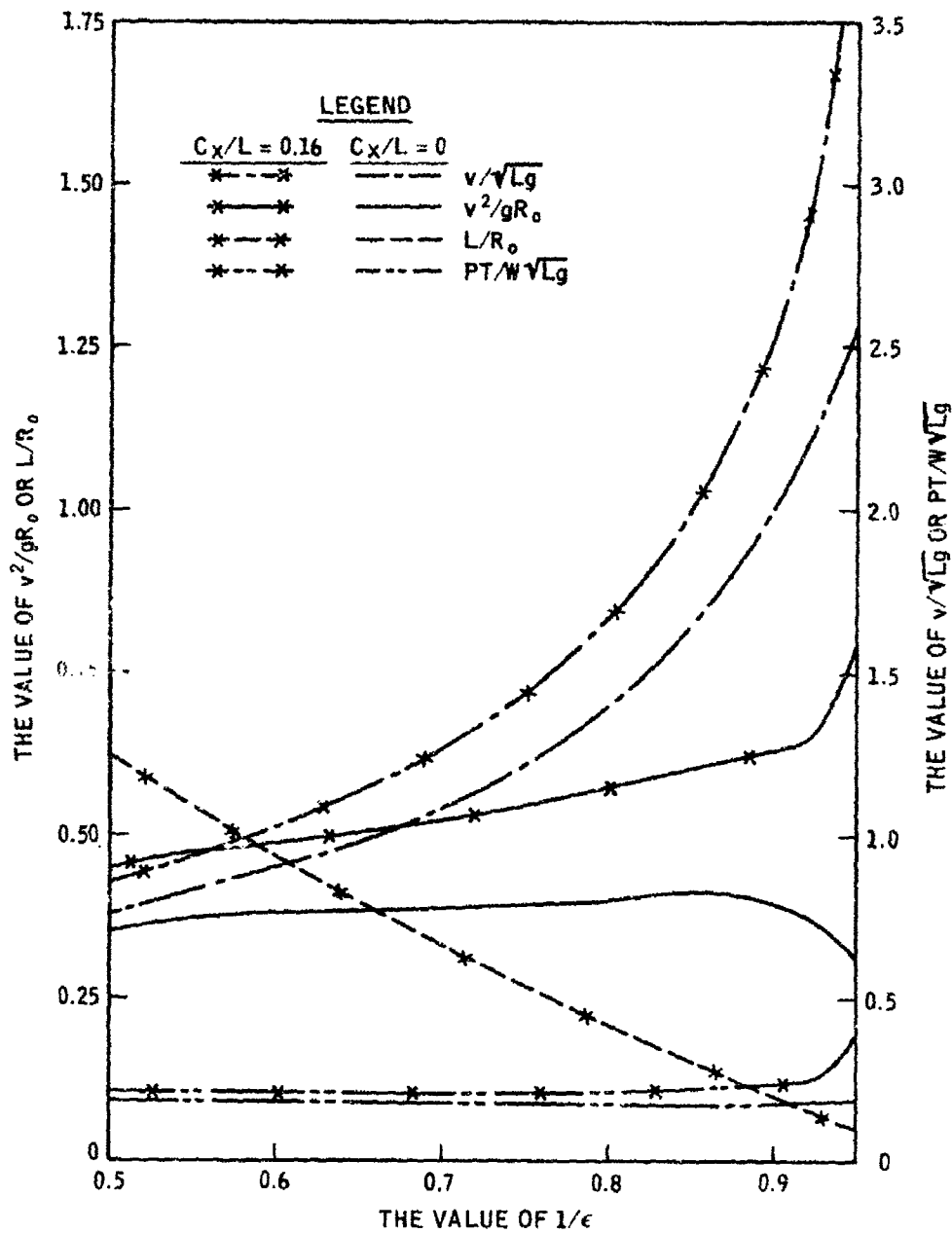


Figure 57. Effect of location of the center of gravity of the vehicle on the relationships between steering ratio and turning radius, lateral acceleration, vehicle speed, and power requirement for mixed soil without rate effect (case 4)

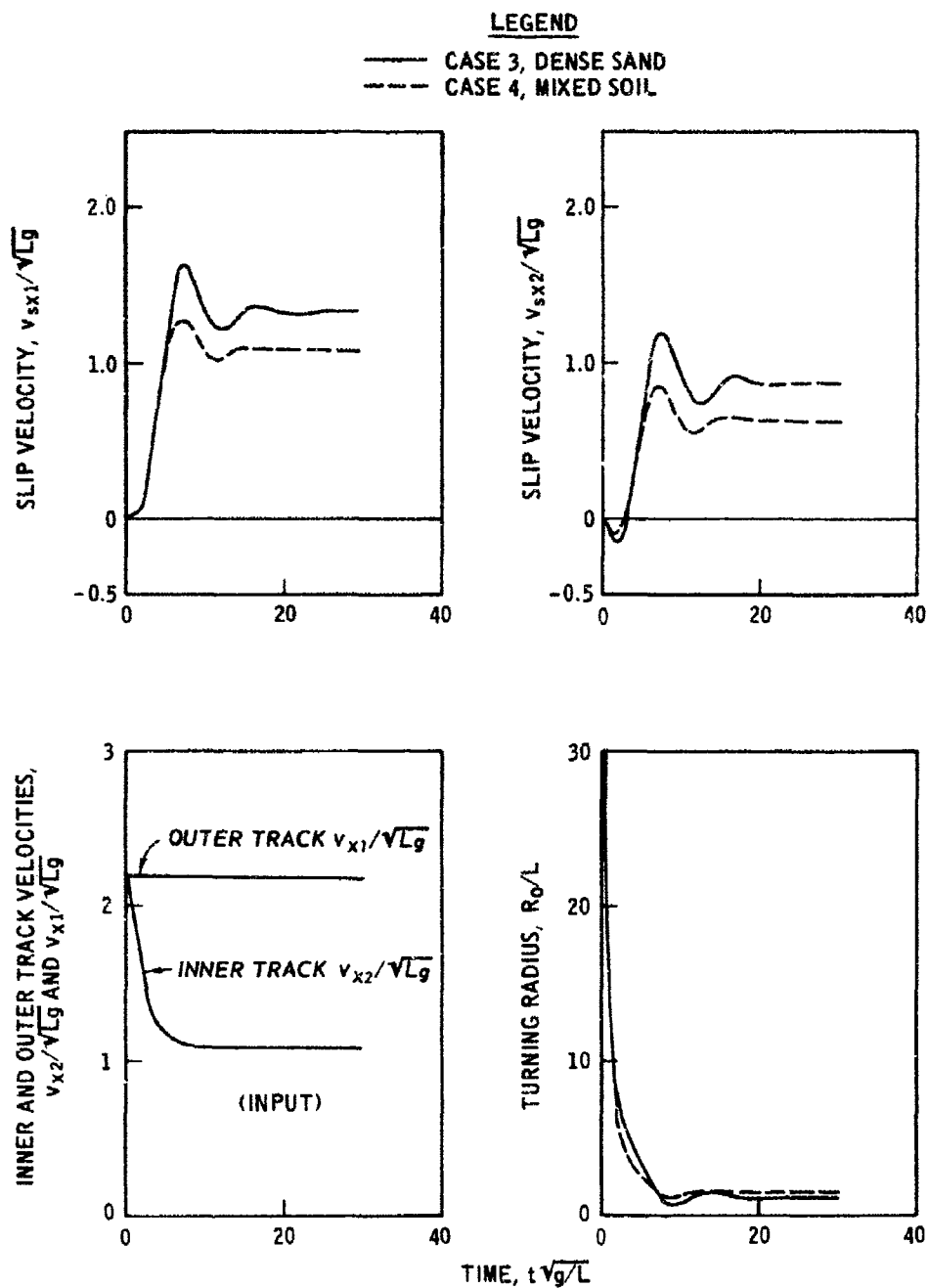


Figure 58. Time histories of slip velocities, track velocities, and turning radius

LEGEND

— CASE 3, DENSE SAND
- - - CASE 4, MIXED SOIL

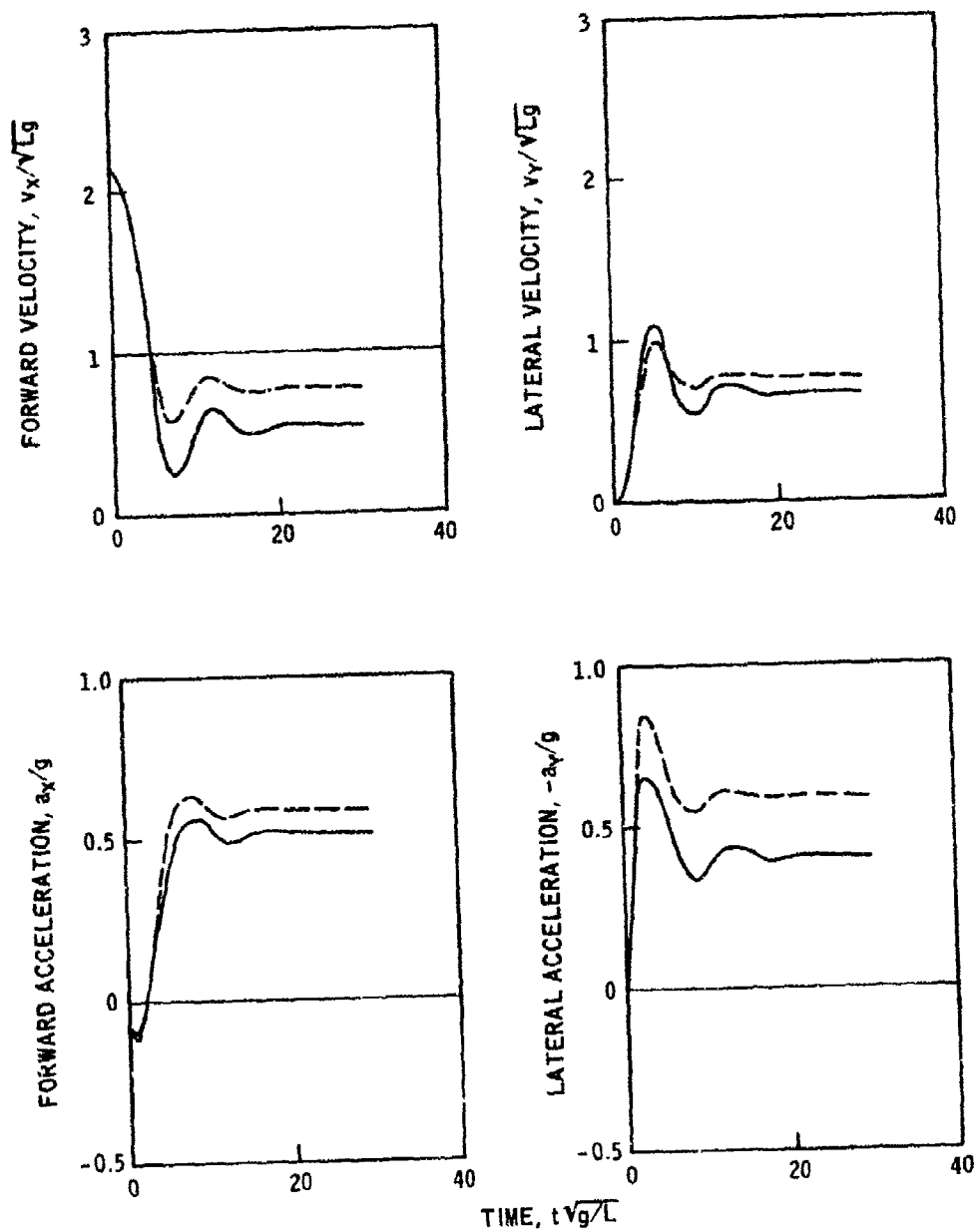


Figure 59. Time histories of forward and lateral velocities and accelerations

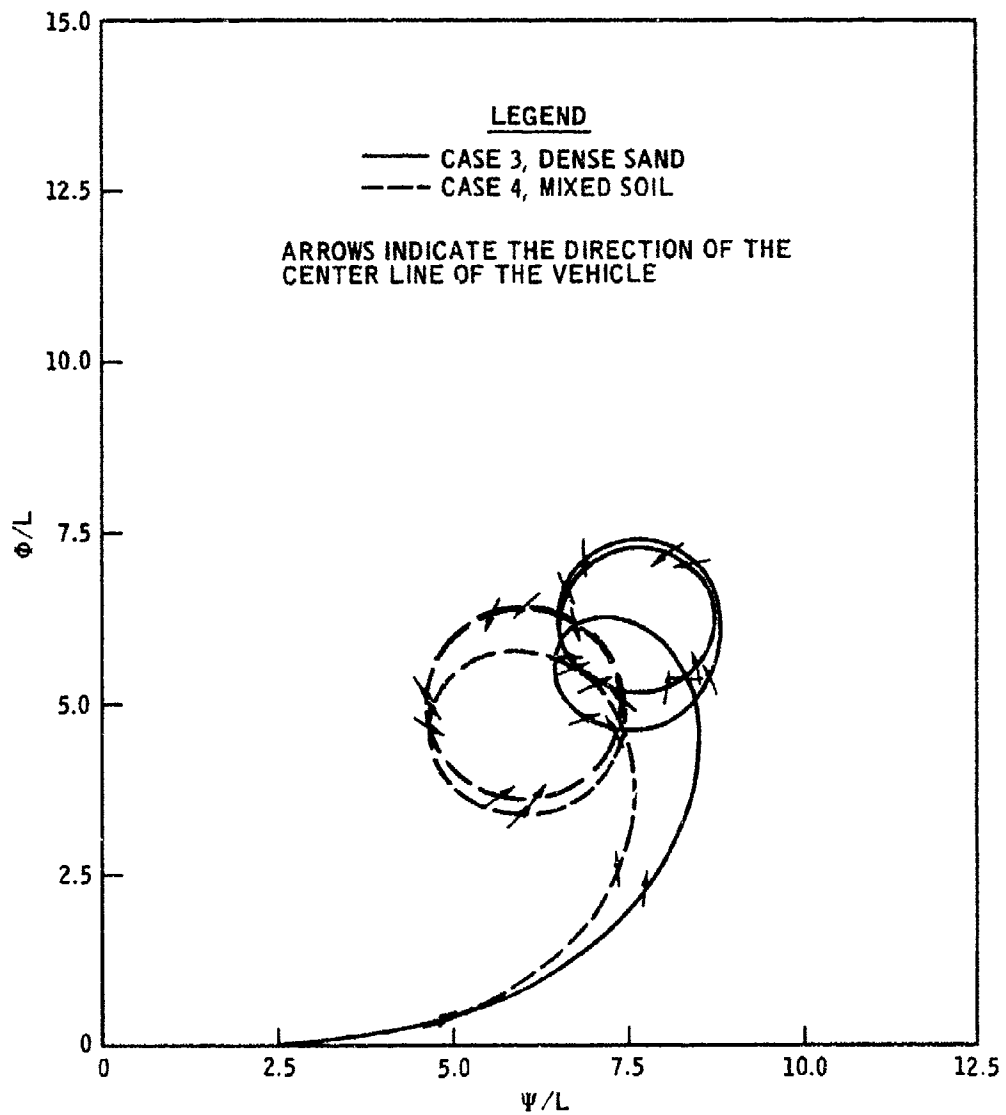


Figure 60. Trajectory of motion at initial forward velocity of 25 mph

LEGEND

— CASE 3, DENSE SAND
- - - CASE 4, MIXED SOIL

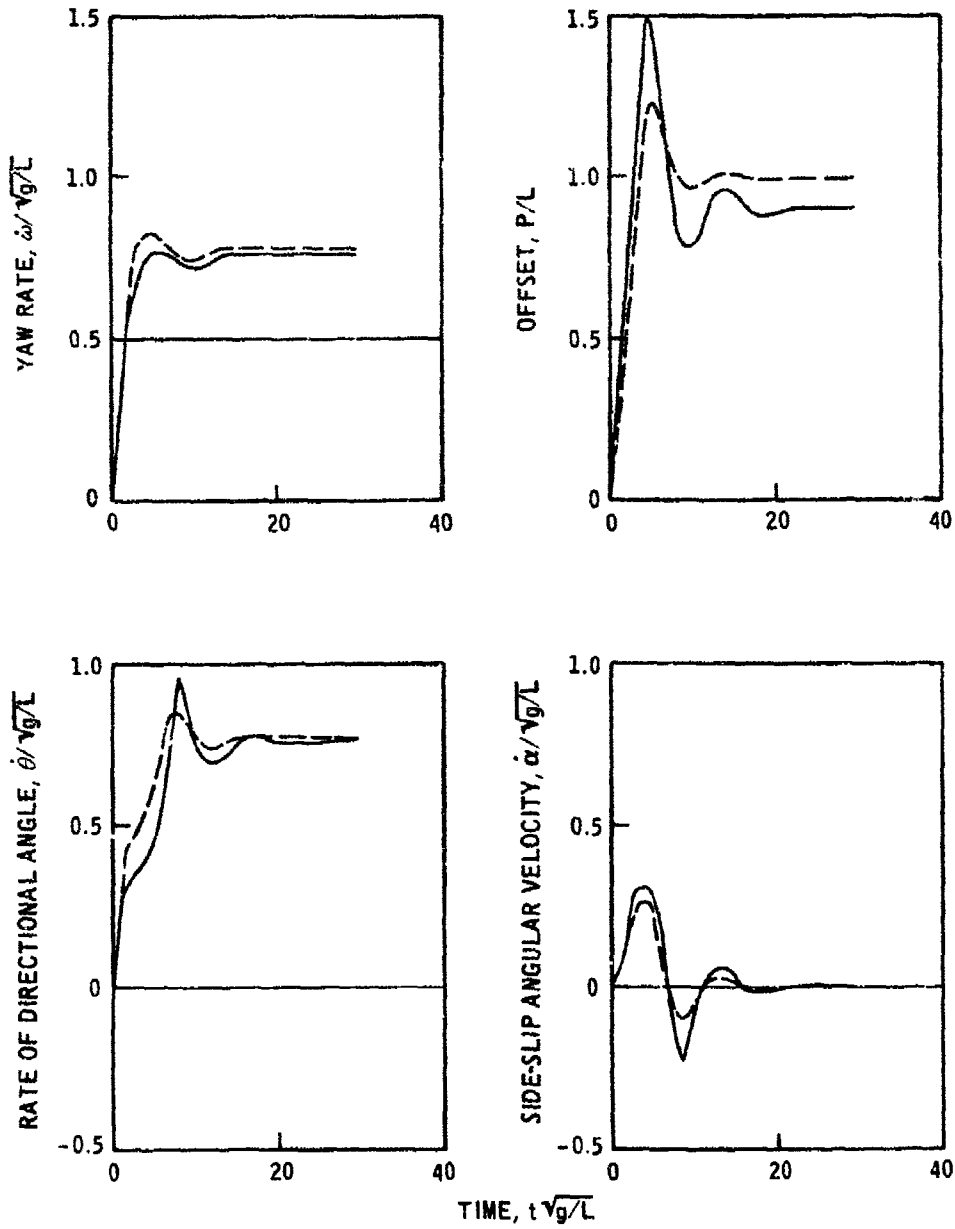


Figure 61. Time histories of yaw rate, offset, rate of directional angle, and side-slip angular velocity

LEGEND

- CASE 3, DENSE SAND
- - - CASE 4, MIXED SOIL

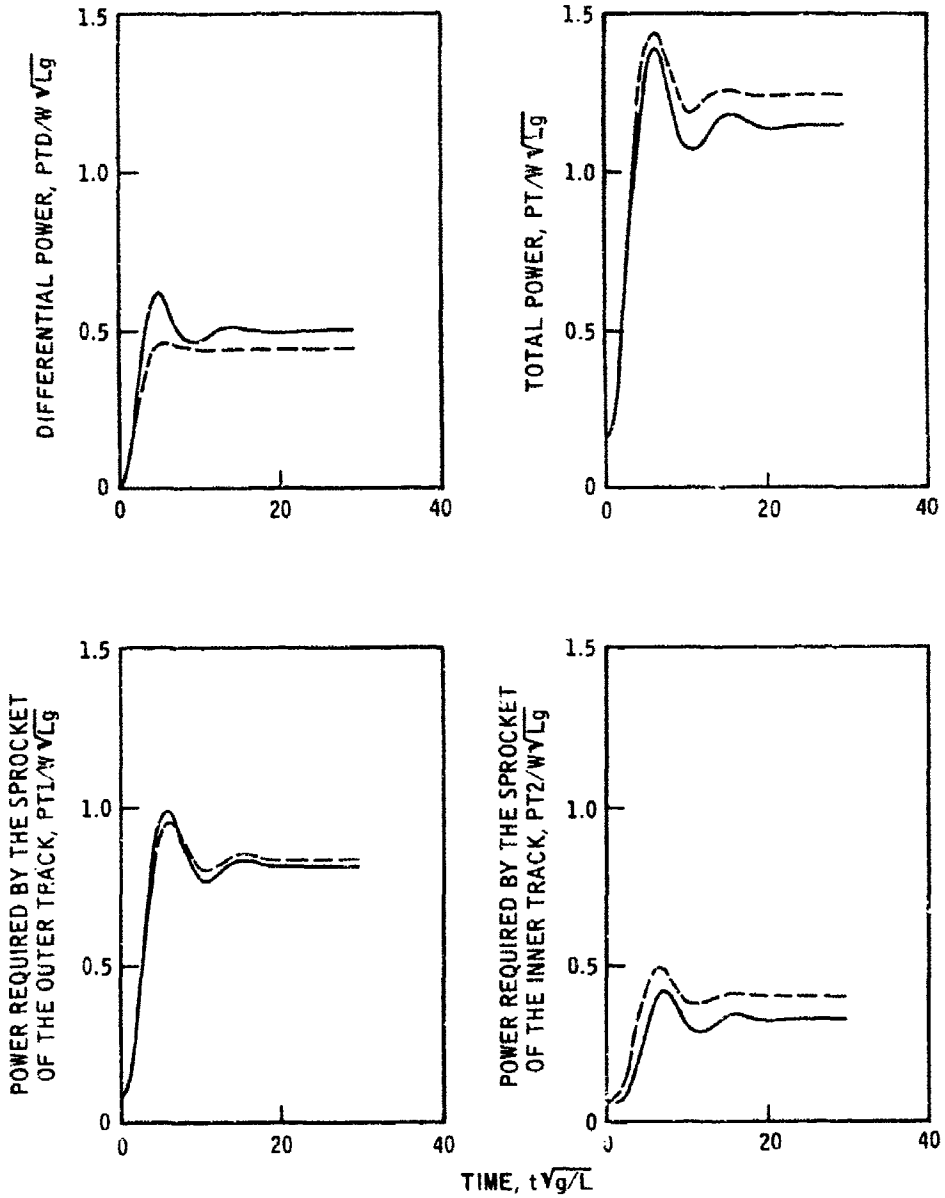


Figure 62. Time histories of differential and total power and power required by the sprocket of the inner and outer tracks

LEGEND

— WITHOUT TRACK TENSION
 - - - WITH TRACK TENSION

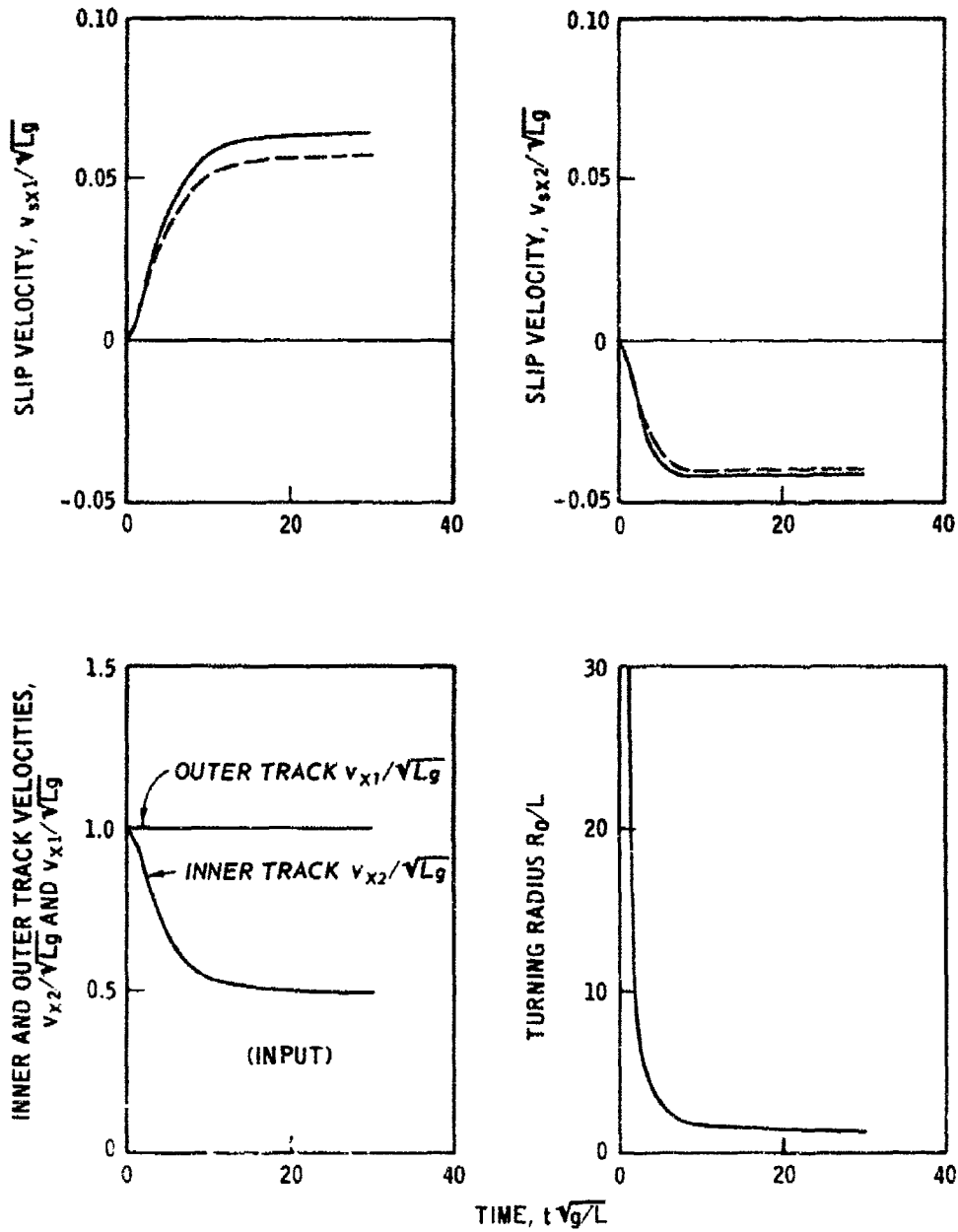


Figure 63. Time histories of slip velocities, track velocities, and turning radius (case 4)

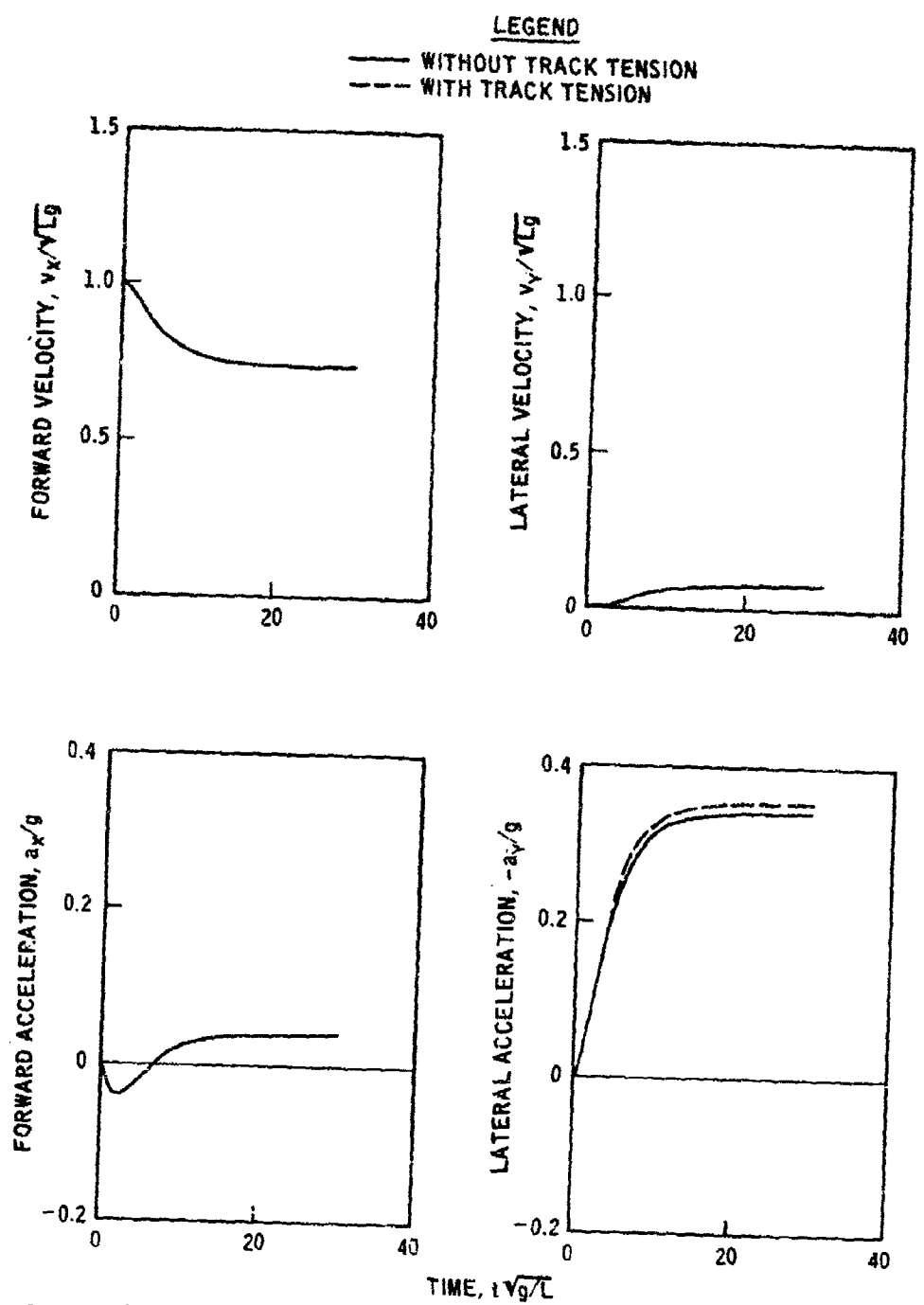


Figure 64. Time histories of forward and lateral velocities and accelerations (case 4)

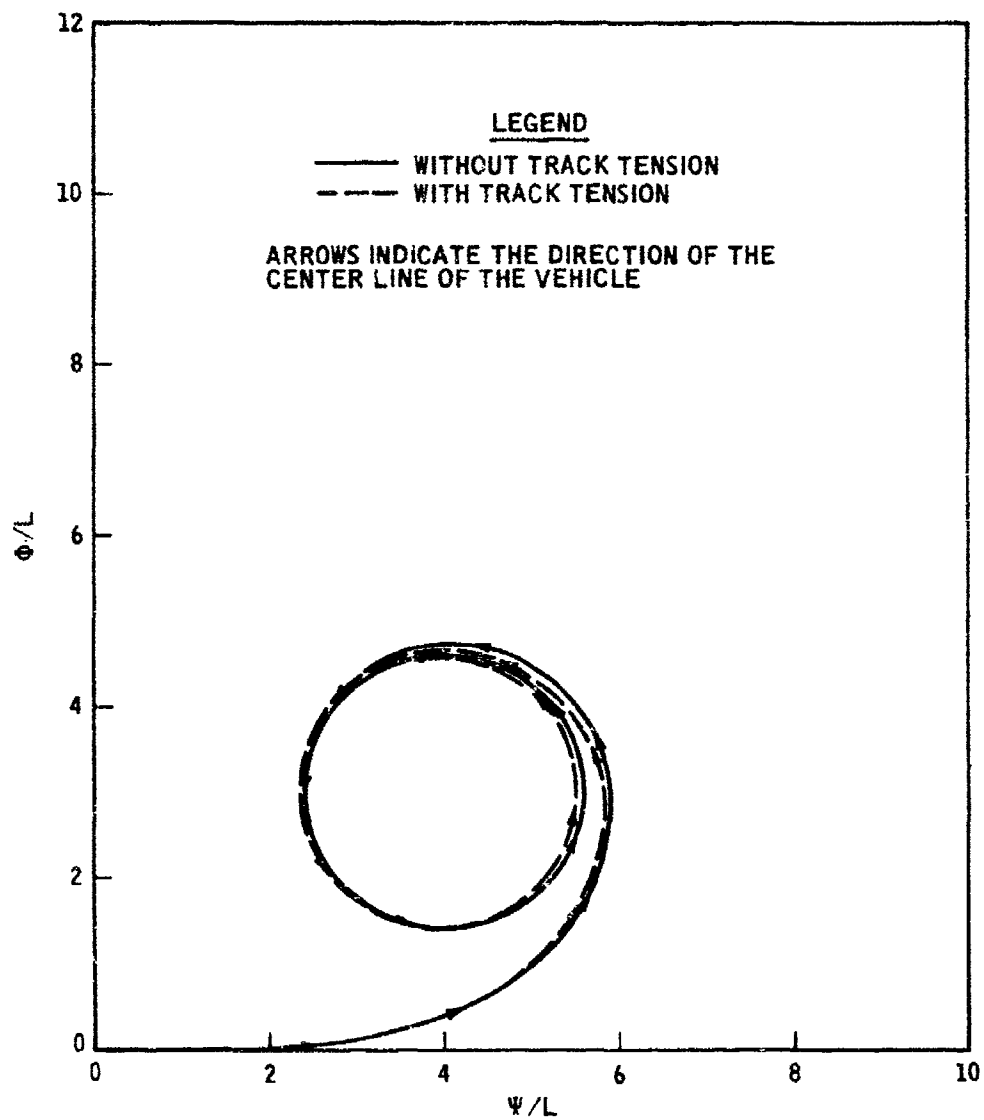


Figure 65. Trajectory of motion at initial forward velocity of 11.4 mph (case 4)

LEGEND

— WITHOUT TRACK TENSION
- - - WITH TRACK TENSION

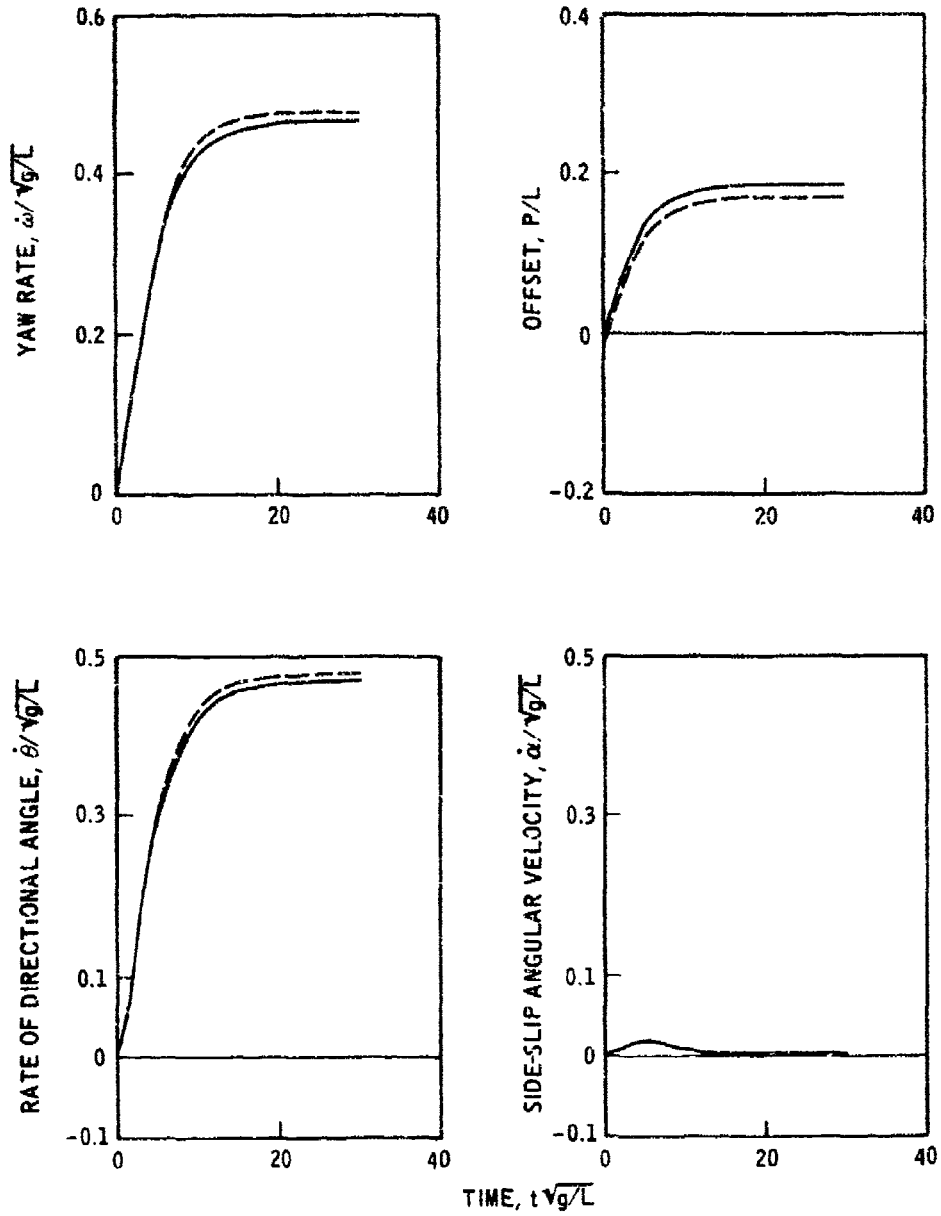


Figure 66. Time histories of yaw rate, offset, rate of directional angle, and side-slip angular velocity (case 4)

LEGEND

— WITHOUT TRACK TENSION
- - - WITH TRACK TENSION

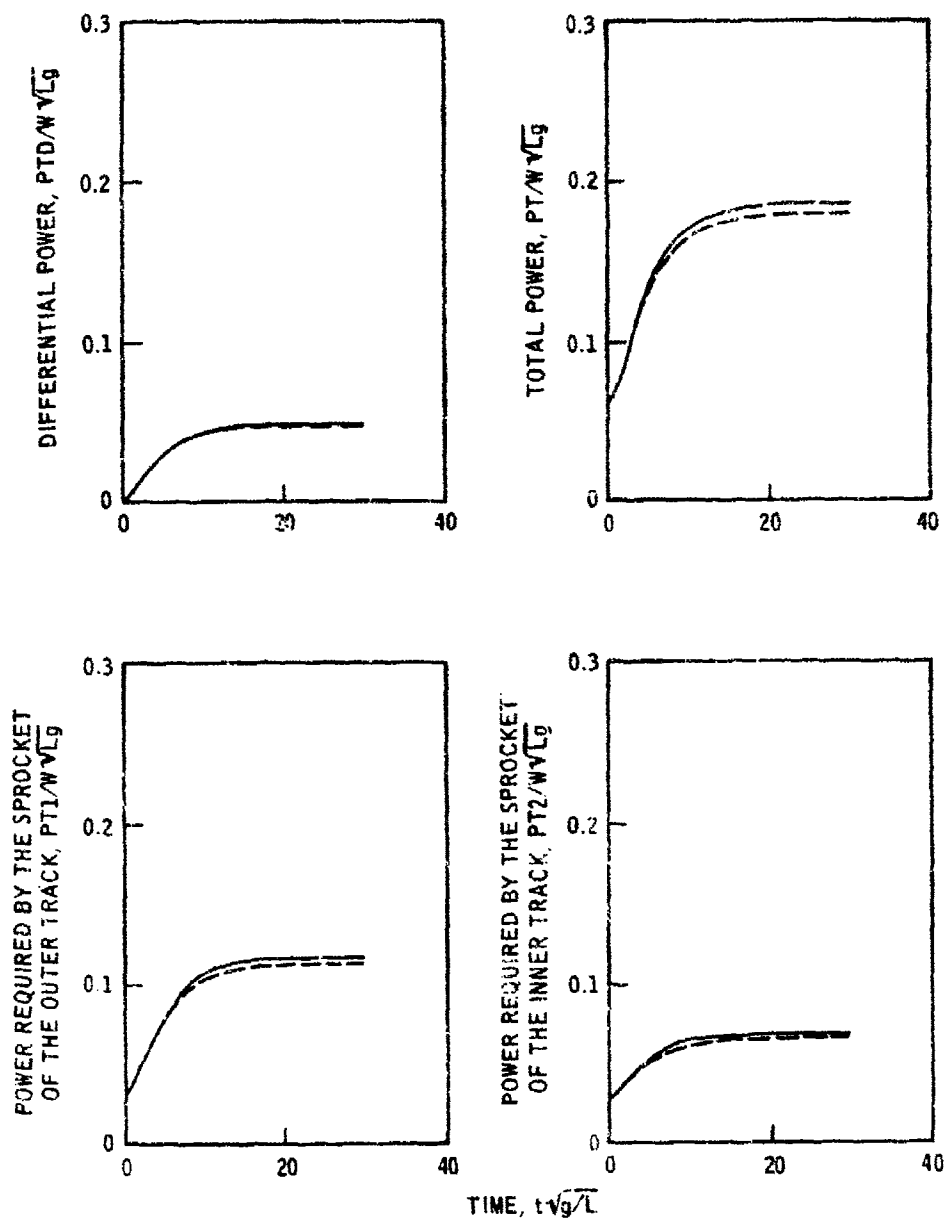


Figure 67. Time histories of differential and total power and power required by the sprocket of the inner and outer tracks (case 4)

APPENDIX A: PROCEDURE FOR DETERMINING THE
COEFFICIENT OF ROLLING RESISTANCE

1. An empirical procedure for determining the coefficient of rolling resistance f in terms of the vehicle characteristics and the WES* cone index is given by Rula and Nuttall (1971).** The procedure involves the following steps:

- a. Determine the mobility index (MI) for the tracked vehicle of interest using the following expression:

$$\text{Mobility index} = \left\{ \frac{\text{contact pressure factor} \times \text{weight factor}}{\text{track factor} \times \text{grouser factor}} + \text{bogie factor} - \text{clearance factor} \right\} \times \left\{ \text{engine factor} \right\} \times \left\{ \text{transmission factor} \right\}$$

where

$$\text{Contact pressure factor} = \frac{\text{gross weight, lb}}{\text{area of tracks in contact with ground, in.}^2}$$

Weight factor: Less than 50,000 lb = 1.0
 50,000 to 69,999 lb = 1.2
 70,000 to 99,999 lb = 1.4
 100,000 lb or greater = 1.8

$$\text{Track factor} = \frac{\text{track width, in.}}{100}$$

Grouser factor: Grousers less than 1.5 in. high = 1.0
 Grousers more than 1.5 in. high = 1.1

$$\text{Bogie factor} = \frac{\text{gross weight, lb, divided by 10}}{(\text{total number of bogies on tracks in contact with ground}) \times (\text{area, in.}^2, \text{ of 1 track shoe})}$$

* U. S. Army Engineer Waterways Experiment Station (WES).
 ** Sources are listed in the References section at the end of the main text.

$$\text{Clearance factor} = \frac{\text{clearance, in.}}{10}$$

$$\text{Engine factor: } \begin{cases} \geq 10 \text{ hp/ton of vehicle wt} = 1.00 \\ < 10 \text{ hp/ton of vehicle wt} = 1.05 \end{cases}$$

Transmission factor: Automatic = 1.0; manual = 1.05

- b. Determine the vehicle cone index VCI_1 for one-pass traffic using the expression

$$VCI_1 = 7.0 + 0.2 MI - \left(\frac{39.2}{MI + 5.6} \right)$$

- c. The coefficient of rolling resistance is then determined by the following equation:*

$$\delta = 0.045 + \left(\frac{2.3075}{CI - VCI_1 + 6.5} \right)$$

where CI is the WES cone index for the particular terrain of interest. Note that CI must be equal to or greater than VCI_1 in order for the vehicle to complete one pass.

2. The value of CI must be determined experimentally. However, if such measurement is not available, CI can be estimated from the parameters C and ϕ in the soil model. The following empirical relation is often used to relate CI to C and ϕ :

$$CI = 12C \text{ (in psi)} + 4\phi \text{ (in degrees)}$$

* In Rula and Nuttall (1971), the rating cone index RCI rather than cone index CI is used to calculate δ . RCI is the product of measured cone index and remolding index RI, and is a valid description only for fine-grained soils and for sands with fines, poorly drained. RI is a ratio that expresses the change in strength of a fine-grained soil or a sand with fines, poorly drained, that may occur under traffic of a vehicle.

APPENDIX B: RECOMMENDED STABILITY CRITERIA FOR
UNIFORM TURNING MOTION

1. The vehicle is assumed to be unstable if one of the following conditions prevails:

- a. Rapid change in the slip velocity of the inner or the outer track.
- b. The pivot point moves outside the front edge of the track-ground contact area (i.e., the offset equals $0.5 L$ when the center of gravity and center of geometry of the vehicle coincide).
- c. Rapid decrease or increase in the turning radius.

2. These instability conditions usually take place at different vehicle velocities (Figure B1). The unstable vehicle velocity is chosen as the minimum of these velocities, as shown by the heavy line in Figure B1. Figure B2 shows a typical example of steering performance of a tracked vehicle at its critical turning speed (heavy line in Figure B1). This figure contains relationships between steering ratio and turning radius, lateral acceleration, vehicle speed, and power requirement for mixed soil (see Table 2).

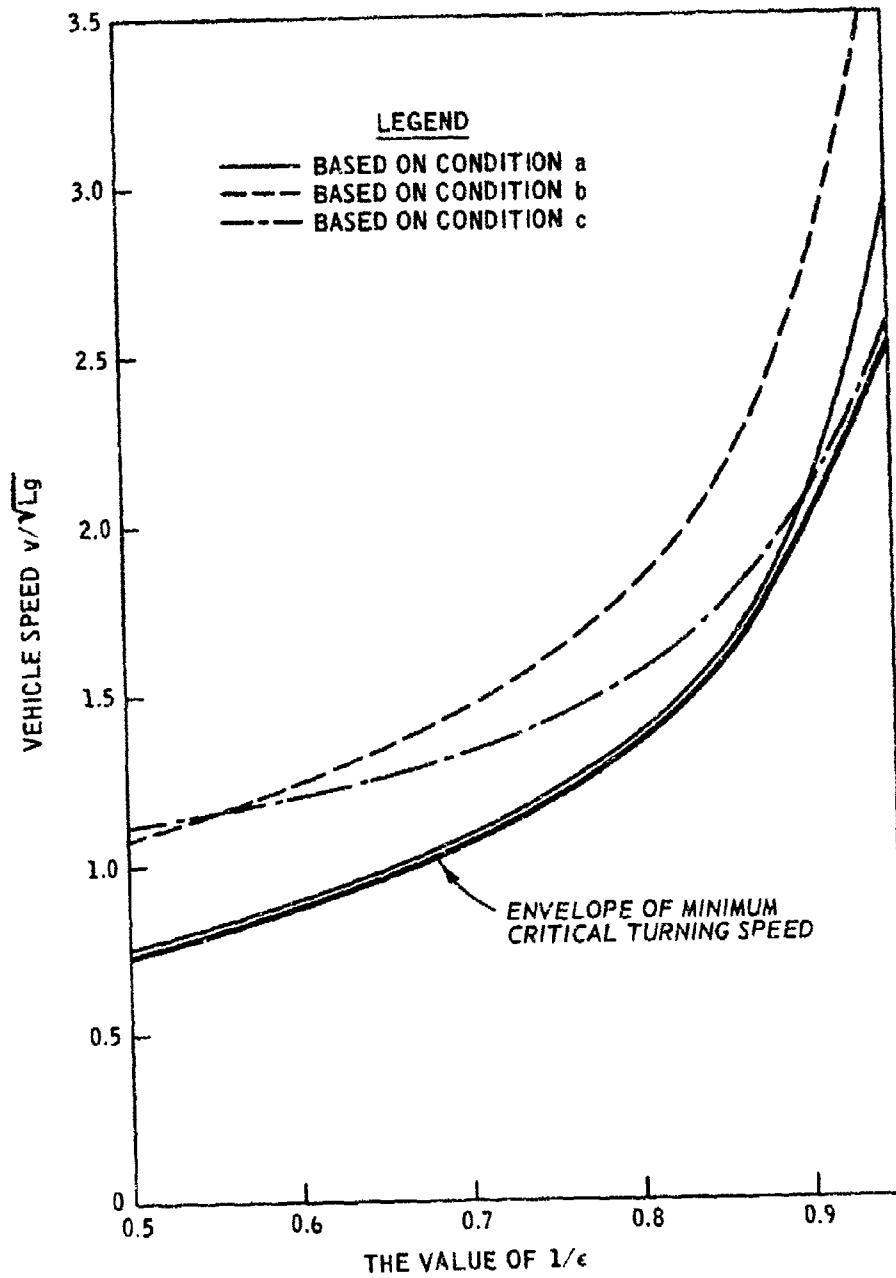


Figure B1. Relationship between steering ratio and critical turning speed (case 4)

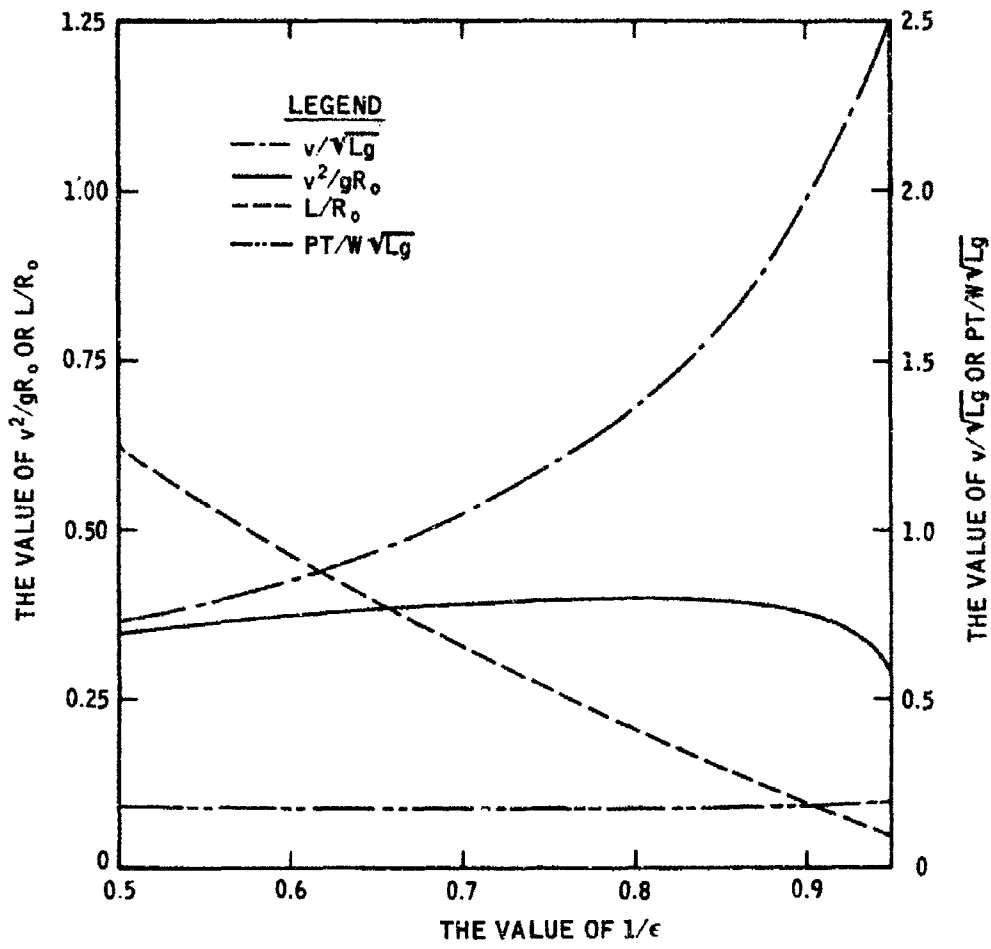


Figure B2. Relationship between steering ratio and turning radius, lateral acceleration, vehicle speed, and power requirement, at the minimum critical turning speed (case 4)

APPENDIX C: DESCRIPTION OF THE FIELD DIRECT SHEAR DEVICE

Background

1. The tracked vehicle agility model requires five soil parameters as input. They are (Figures 1 and 2 of main text):

- G , initial shear stiffness coefficient (assumed to be independent of rate of deformation)
- C , static soil cohesion
- C_d , increase in soil cohesion due to dynamic loading (maximum value achieved for loading rates of interest)
- ϕ , friction angle of soil (assumed to be independent of rate of deformation)
- Λ , material constant describing the effects of rate of deformation on the cohesive strength of soil

The soil parameters G , C , and ϕ can be determined from various existing laboratory test devices, such as the triaxial shear device or direct shear device. The triaxial shear and direct shear devices, however, may not yield the same values of G , C , and ϕ for identical specimens because of differences in test boundary conditions. The stress boundary conditions associated with the direct shear test more closely approximate the stress conditions experienced by the soil during steering of track-laying vehicles. It is, therefore, more appropriate to determine these parameters from direct shear tests. The parameters C_d and Λ can only be determined from special static and dynamic triaxial shear tests since dynamic direct shear devices are not presently available. Therefore, to adequately determine the five soil parameters, two separate test series may be required:

- a. Direct shear tests to define G , C , and ϕ .
- b. Static and dynamic triaxial shear tests to define C_d and Λ .

It should be noted that in determining C_d and Λ from triaxial tests rather than direct shear tests, it is assumed that these parameters are not sensitive to test boundary conditions. The validity of this assumption should, of course, be evaluated.

2. The most important consideration in conducting laboratory soil tests is that the undisturbed specimens be representative of the materials over which the vehicle must travel. This implies that the upper several inches of surface material must be sampled, trimmed to necessary specimen size, and tested in the laboratory. Water content, soil structure, density, and vegetation root systems, all of which affect material response, must be preserved. With this in mind, a field-operated direct shear device capable of testing a variety of in situ surface soils for normal loads of interest was designed and fabricated. The description of the device and the procedure by which the soil parameters can be determined are documented in this appendix.

Direct Shear Device

Design consideration

3. Previously proposed field devices were considered but rejected because of one or more of the following reasons: (a) some of the soil parameters could not be measured and hence required additional tests, (b) the necessary support equipment was too massive to be easily field transportable, or (c) specimen disturbances were encountered prior to testing. The idea of creating a new type of test was also rejected because any new device would contain inherent boundary problems, all of which would have to be evaluated with time and usage. The direct shear device, on the other hand, has been used extensively, and it is a fairly simple test to run. Furthermore, the three basic soil parameters (G , C , and ϕ) could be measured rather directly from this test. Figure C1 shows a sketch of the field device that was fabricated as a result of this project. Photographs taken of the device during the conduct of actual field tests are shown in Figure C2.

Specimen container

4. Specimen configuration was the first consideration made in the design of the device. It was assumed that in many cases the in situ soil could not be sampled without disturbance; therefore, the specimen container would have to be placed around the soil. A round ring similar

to a coring device would afford the least chance of soil disturbance. However, the stress distribution along a plane of a circular specimen is not uniform, and for this reason a square-shaped specimen container was selected.

5. A 4-in. by 4-in. box was selected in order to keep the shear and normal loads within limits of interest to analysis of track-laying vehicles and at the same time retain a reasonably large specimen size. The use of deadweights is the simplest way to produce normal load, but use of more than 200 lb in weights is awkward for field testing. Therefore, with the weight requirement below the 200-lb limit, normal stress of up to 12 psi can be produced on a 4-in. by 4-in., or 16-sq in., specimen. However, the largest particle or grain size permissible with a 4-in. by 4-in. specimen is probably 1/2 in., which is a reasonable limit for most terrains of interest.

6. The overall specimen height was controlled by the depth of the desired shear plane as directed by grouser depth ranging from approximately 3/4 in. to 1-1/2 in. The compressibility of soil could significantly alter this depth, but for estimation purposes the depth was assumed to be no greater than 2 in. Therefore, the height of the upper box portion was set at 2 in., permitting testing of depths from approximately 1/4 in. to 2 in. This, of course, can be altered should particular site conditions dictate. The lower box portion was set at 1-1/4-in. height, including the cutting edge. A 1/8-in. wall thickness was used for both boxes.

7. Figure C3 presents a series of sketches of the specimen container showing the various stages of placement. To minimize specimen disturbance, it was decided to use the specimen cutting box as the device container rather than removing the cutting and placing a container over the specimen. The box consists of three parts: (a) a lower portion with knife-sharp edges to aid in cutting the soil, (b) an upper portion, and (c) an outer holder to keep the lower and upper portions in alignment. The box is alternately pushed and trimmed into the soil to the desired depth. Once in place, the outer holder can be carefully removed, leaving the two boxes on the specimen with the joint between

the lower and upper box portion forming the shear test plane.

Base

8. A relatively narrow 1-in.-thick aluminum plate was used to construct the base with a square hole at one end to fit around the 4-in. by 4-in. lower specimen containers (Figure C1). The shear loader was attached to the other end of the plate. A second 1-in.-thick aluminum yoke was constructed to fit over the upper specimen container. Set screws through the yoke serve to raise the yoke off the base plate, thus minimizing friction between the surfaces. The shear loader attached by cable to the yoke pulls the upper specimen while the base reacts against the lower specimen container. Guide rails along the edge of the base insure that no torsional shear or twisting is applied to the specimen.

Shear loader

9. An electric 12-volt boat winch was incorporated into the base as the shear loader. This is the simplest approach for providing a shear loader. (If necessary, the winch can be replaced with a more sophisticated loader custom-built for this device.) Currently, the winch is capable of pulling loads up to 2000 lb. Static loading rates can be applied by manually turning the winch via a socket-ratchet arrangement. Fast loading rates (approximately 300-600 msec time to peak load) can be applied using the electric feature of the winch. The power is supplied by a 12-volt car battery, which is also used as the instrumentation power supply.

Instrumentation

10. A 2-in. travel film potentiometer is attached to the base and records relative movement between the upper specimen holder and the base. A strain gaged load cell attaching the winch cable to the specimen yoke is used to measure shear load. A compact, two-channel DC instrumentation amplifier is used for signal conditioning. Output is recorded in the form of a shear load versus deflection plot on a commercially available DC-operated X-Y plotter. As previously mentioned, a simple car battery is the main power supply. All initial testing was done by recording the data on a time base light beam strip chart. This

was later dropped since the loading times remained fairly constant on the soils tested. A time base can be added at a later date through the use of a frequency oscillatory and an X-Y-Z recorder.

Normal load

11. A series of steel weights, the largest weighing 57 lb and the smallest weighing 8-1/2 lb, was fabricated for use with the device. Guide holes and studs permit stacking and centering of the weights on the specimen surface. Although a variety of load combinations is possible, most tests have been conducted using weights totalling approximately 8-1/2, 88, and 180 lb (i.e., normal stress levels of 0.5, 5.6, and 11.25 psi).

Measurement of Soil Parameters

12. A series of two or more tests is required at a site to define the necessary soil parameters. A typical testing program may call for the conduct of three fast and three slow tests at normal stresses of 0.5, 5.6, and 11.25 psi. For each test an X-Y data record of shear load versus deflection is obtained. In addition, measurements of soil density and water content are made on each test specimen (generally on the posttest specimen contained in the upper and/or lower specimen holders).

13. For each test a plot of shear stress versus deflection is obtained. The initial slope of the plot defines G , the peak stress defines the maximum shear stress, and the deflection at peak stress divided by time to peak stress defines the deflection rate. A table listing of each test is used to summarize the data and contains specimen number, wet density, water content, dry density, normal load/stress, maximum shear load/stress, initial G , deflection at peak stress, and deflection rate. A presentation of test results obtained from the series of field tests conducted at a given site is shown in Figure C4.

14. A graphical presentation of the analysis plots is shown in Figure C5. A summary plot of shear stress versus normal stress is made to obtain C and ϕ ; if differences are noted between the data

from the slow and fast tests, different values of C and ϕ are obtained for each rate. A plot of C versus deflection rate may be constructed from which the value of C_d can be obtained. Since the present model requires single numerical values for each parameter, judgment must be applied to the analysis plot to derive the most representative values for G , ϕ , C , and C_d .

Limitation

15. One deficiency of the device is the limitation of the electric winch to produce loading rates comparable to those experienced by soil during steering of tracked vehicles at maximum speed. Analyses of the agility model output indicate that time-to-peak shear load is generally in the range of 10 msec. The current loading time of 300-600 msec is not only the limit of the winch but is also the limitation of the instrumentation recording system.

16. There are three possible courses of action to remedy the limitation: (a) provide a new loader and recording system capable of both slow and very rapid loading time, (b) develop a secondary index test that would provide a direct or indirect measure of C_d and Λ , or (c) use the present device with some rationale for estimating C_d and Λ . The first course of action is possible since many specialized laboratory test devices currently operate within the loading time of 10 msec. However, the requirement of support equipment (such as compressed gas to operate the dynamic loaders, sophisticated electronics to time-sequence the loader and recording device, and the size of recording equipment) makes it impractical for field tests. A means of compacting such equipment would have to be investigated. Development of a secondary test or index measurement might be possible; however, a fairly extensive field evaluation program would have to accompany the development of such a device. The third course may be the most practical. Limited experience with the agility model has indicated that the parameters C_d and Λ do not have great influence on steering performance for soils with high shear strength (i.e., soils with cone

index values approximately above 300).^{*} Also, for loading rates of interest, sands do not have significant rate effects. Therefore, sites containing these materials could be adequately defined with the existing equipment by measuring only the parameters G , C , and ϕ . But soft soils, such as wet clay, are known to be rate-sensitive with factors of two or more and to increase in stiffness and in strength over static values. The parameters C_d and Λ , therefore, become important input to the agility model. The possibility of rate effect of a given soil can be identified by comparison of results obtained from both slow and fast tests with the current direct shear device. If rate effect is present, then static and dynamic triaxial shear tests could be conducted to define C_d and Λ . This approach was taken during the actual field investigation conducted at two vehicle test areas at Fort Knox, Kentucky, and appeared to be satisfactory.

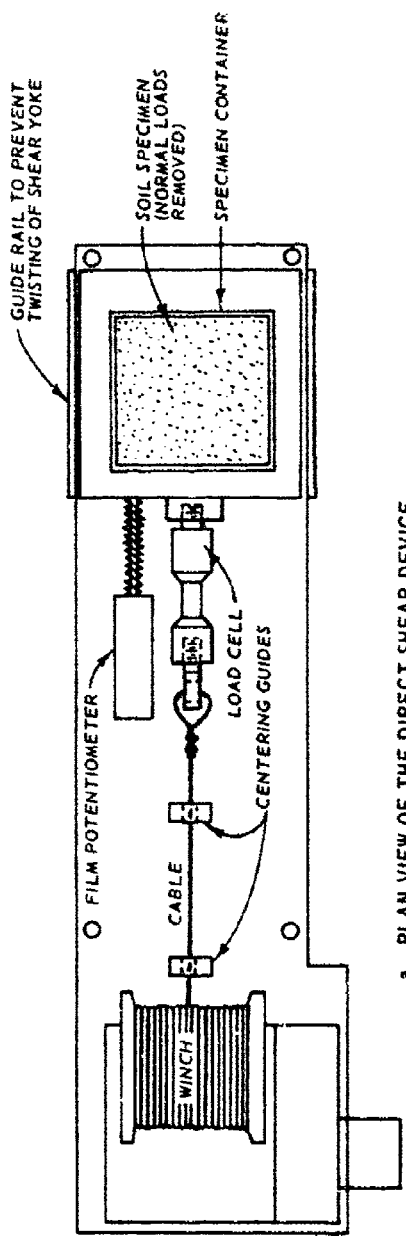
Conclusions

17. A new agility model for track-laying vehicles was developed that required soil parameter input not commonly obtained during mobility studies. It was realized that field sampling and laboratory testing would not always be possible because of the nature of very near-surface soil deposits. An approach was taken to use a conventionally accepted test to define the parameters. A field operable direct shear device and necessary instrumentation were built at WES. The equipment is fairly compact (can easily fit into a car or truck), operates off of a car battery, is relatively simple to use, saves operation time compared with comparable laboratory tests, and is capable of directly accessing the soil parameters G , C , and ϕ .

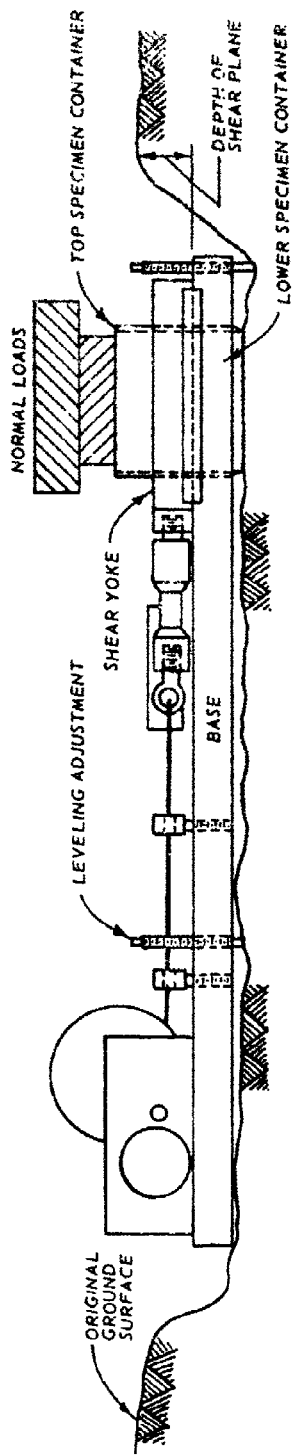
18. The device has been used to conduct some 40 tests at different locations at Fort Knox, Kentucky. Some of the near-surface soils encountered were very friable and impossible to sample and test in the laboratory by conventional means without excessive disturbance.

* The cone index corresponds to WES cone index.

However, the direct shear device performed quite well, only requiring extra care by the test operator not to disturb the specimen during placement of the device base over the sample box containing the soil specimen. The time required to perform a test was approximately one hour. This time is especially reasonable when compared with the time it takes to prepare and test a comparable sample in the laboratory, excluding the time spent obtaining the sample in the field.

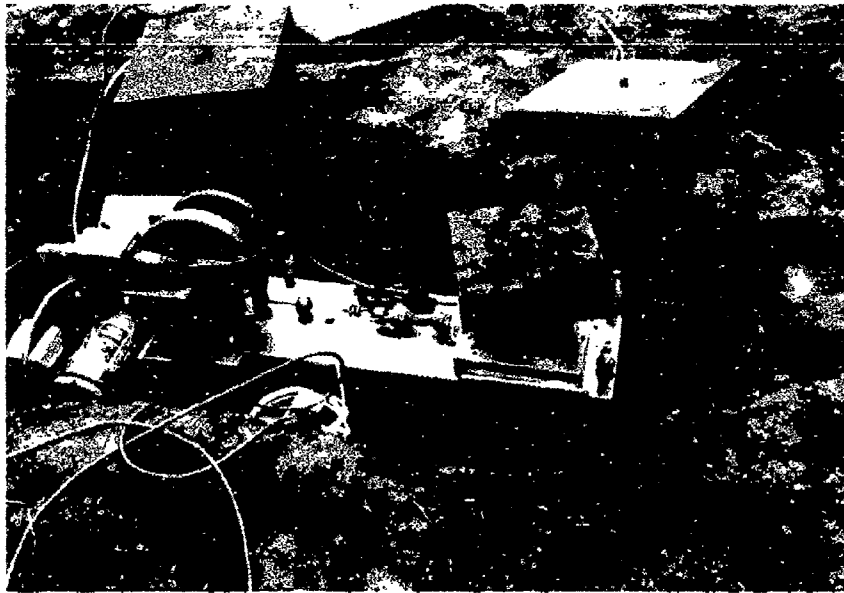


a. PLAN VIEW OF THE DIRECT SHEAR DEVICE

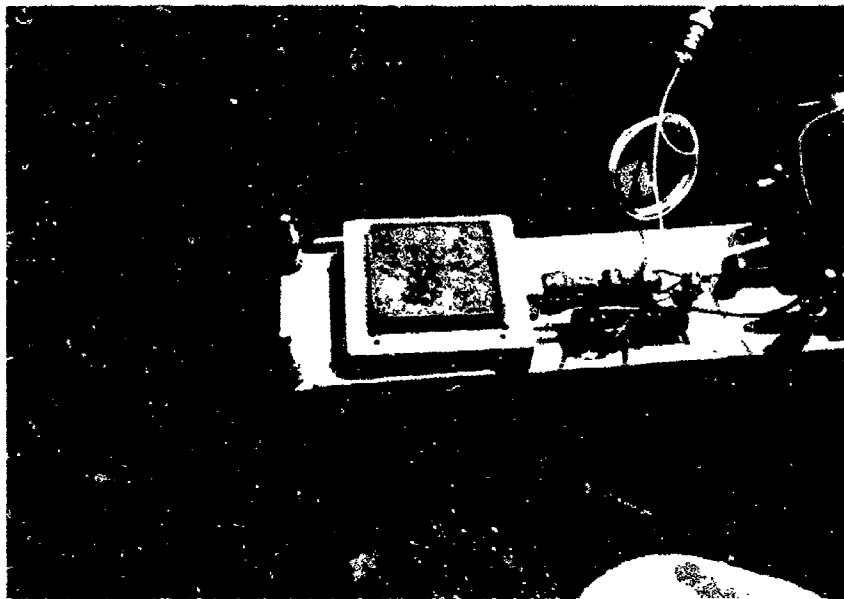


b. PROFILE VIEW OF THE DIRECT SHEAR DEVICE IN PLACE

Figure C1. Plan and profile views of the direct shear device

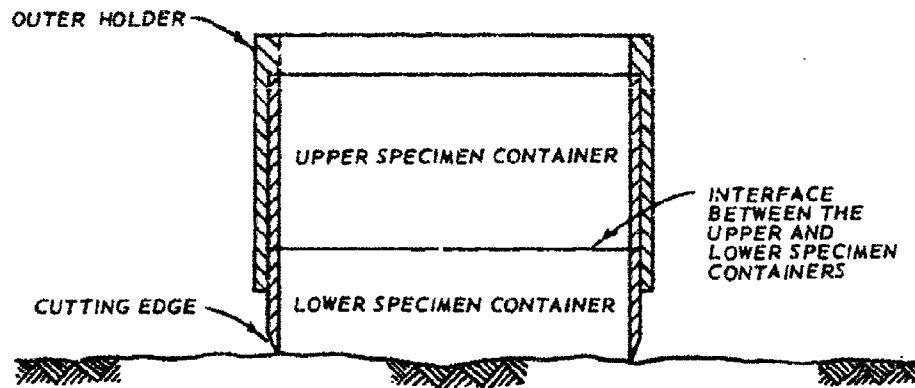


a. Direct shear device assembled for test

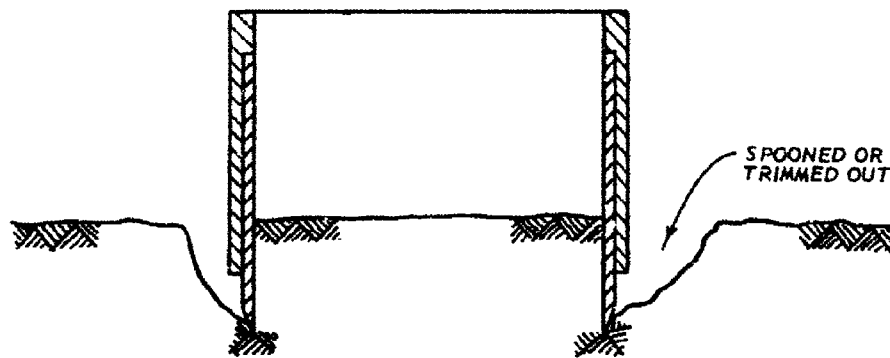


b. Specimen immediately following test with normal loads removed

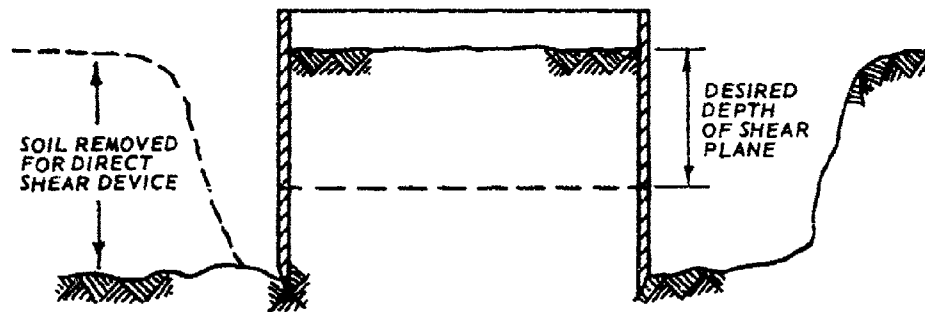
Figure C2. Photographs of the direct shear device taken during actual field testing



a. CONTAINER WITH OUTER HOLDER ON SOIL SURFACE

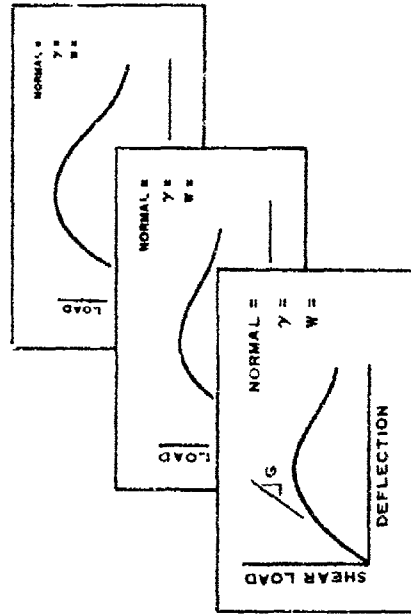


b. CONTAINER DURING PLACEMENT - ALTERNATELY PUSHED AND EXCESS MATERIAL SPOONED (OR TRIMMED) OUT

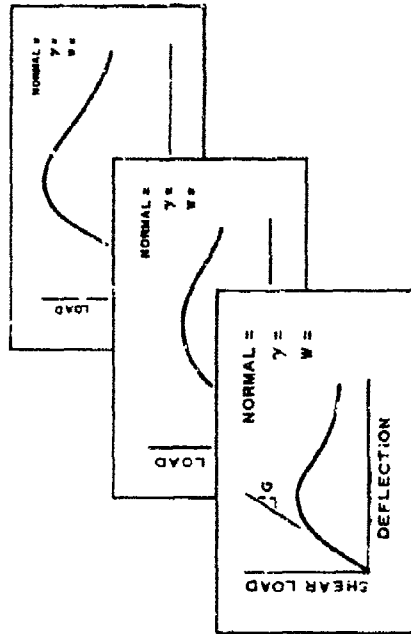


c. CONTAINER AT DESIRED DEPTH - OUTER HOLDER REMOVED AND READY FOR PLACEMENT OF DIRECT SHEAR DEVICE

Figure C3. Cross sections through the specimen container showing various stages of placement



DATA FROM A SERIES OF FAST TESTS



DATA FROM A SERIES OF SLOW TESTS

SITE	TEST	WET DENSITY	WATER CONTENT	DRY DENSITY	RATE	INITIAL MODULUS	NORMAL LOAD STRESS	SHEAR LOAD STRESS	DEFLECTION	AT PEAK		REMARKS
										LOAD STRESS	DEFLECTION	
A	S10S	108.0	16.1	93.0	0.002	100	8.5	0.54	34.9	2.18	0.064	GOOD TEST
A	S15S	109.0	15.0	94.7	0.002	190	90.0	5.6	121.9	7.83	0.071	
A	S110S	106.0	17.0	93.7	0.002	250	186.0	11.25	241.3	15.08	0.053	γ MAY BE QUEST
A	S10F	107.0	16.1	92.2	0.2	113						
A	S15F											

TABLE SUMMARIZING PERTINENT DATA FROM TESTS CONDUCTED AT A GIVEN SITE

Figure C4. Presentation of test results obtained from the direct shear device

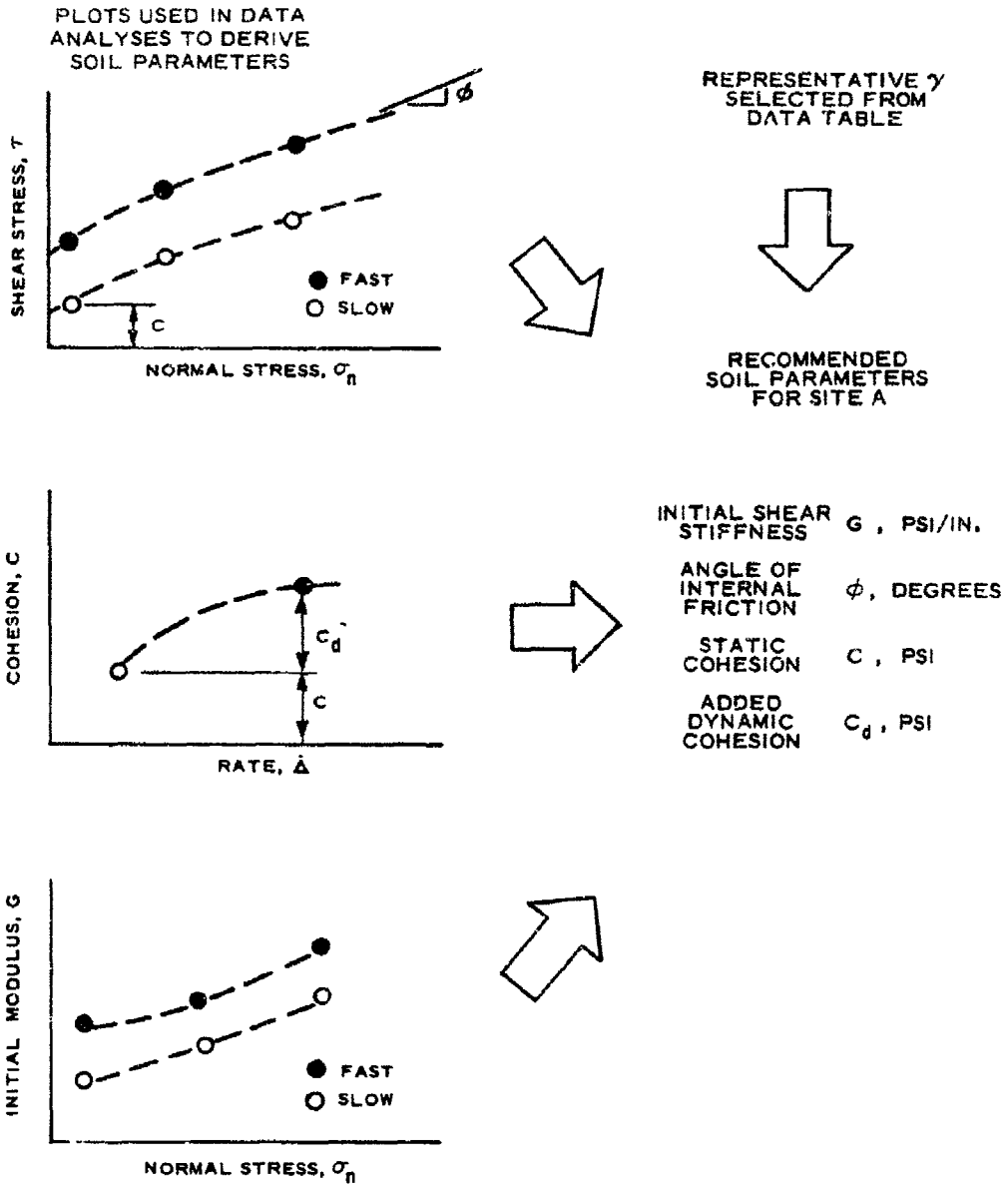


Figure C5. Graphical presentation of the selection of recommended soil parameters based on the field data

APPENDIX D: NOTATION

a_X	Forward acceleration of the vehicle
a_Y	Lateral acceleration of the vehicle
a_ϕ	Acceleration of the vehicle along the ϕ axis
a_ψ	Acceleration of the vehicle along the ψ axis
b	B/L
B	Track tread
c	CL^2/W
c_d	$C_d L^2/W$
c_X	C_X/L
C	Static cohesive component of shear strength
C_d	Added cohesive strength due to dynamic loading
C_X	Abscissa of the center of gravity of the vehicle
C_1	Slip radius of the outer track
C_2	Slip radius of the inner track
CG	Center of gravity of the vehicle
CI	WES cone index
CR	Center of rotation of the vehicle
d	D/L
D	Track width
f_{CX}	F_{CX}/W
f_{CY}	F_{CY}/W
F_C	Inertial force
F_{CX}	Longitudinal component of inertial force
F_{CY}	Transverse component of inertial force

f	Coefficient of rolling resistance
g	Acceleration due to gravity
G	Initial shear stiffness coefficient
h	H/L
H	Height of center of gravity
I_z	Mass moment of inertia of the vehicle about an axis passing through its center of gravity and parallel to the Z axis
IC_1	Center of slip rotation of the outer track
IC_2	Center of slip rotation of the inner track
ICR	Instantaneous center of rotation of the vehicle
l	Distance between two adjacent wheels
L	Contact length of track
MI	Mobility index
n_1	Vertical component of \bar{T}_1
n_2 or n'_2	Vertical component of \bar{T}_2
$N_1(X)$	Lifting stress due to the outer track tension
$N_2(X)$	Lifting stress due to the inner track tension
p	P/L
P	Offset (distance from center of gravity to pivot point of vehicle)
PT	Total power = $PT1 + PT2$
$PT1$	Power required by the sprocket of the outer track
$PT2$	Power required by the sprocket of the inner track
PTD	Differential power = $PT1 - PT2$
$q_1(x)$	$dL^2 Q_1(x)/W$
$q_2(x)$	$dL^2 Q_2(x)/W$

$Q_1(X)$	Transverse component of shear stress along the outer track
$Q_2(X)$	Transverse component of shear stress along the inner track
$r_1(x)$	$dL^2 R_1(x)/W$
$r_2(x)$	$dL^2 R_2(x)/W$
\tilde{R}	Ordinate of the instantaneous center of rotation of the vehicle
R_0	Radius of the trajectory of the center of gravity of the vehicle
R_s	Rolling resistance
$R_1(X)$	Normal stress under the outer track
$R_2(X)$	Normal stress under the inner track
R_I	Instantaneous radius of curvature
t	Time
$t_1(x)$	$dL^2 T_1(x)/W$
$t_2(x)$	$dL^2 T_2(x)/W$
\bar{T}_1	Track tension in the inner track
\bar{T}_2	Track tension in the outer track
$T_1(X)$	Longitudinal component of shear stress along the outer track
$T_2(X)$	Longitudinal component of shear stress along the inner track
v	Velocity of the vehicle
v_e, v_{ex}, v_{ey}	Instantaneous velocity of an arbitrary point of the hull and its components along X and Y coordinates
v_{s1}	Total slip velocity of the outer track
v_{s2}	Total slip velocity of the inner track
v_{sX1}	Longitudinal component of slip velocity of the outer track

v_{sX2}	Longitudinal component of slip velocity of the inner track
v_{sY1}	Transverse component of slip velocity of the outer track
v_{sY2}	Transverse component of slip velocity of the inner track
v_X	Longitudinal component of velocity of the vehicle
v_{X1}	Longitudinal component of velocity of the outer track
v_{X2}	Longitudinal component of velocity of the inner track
v_Y	Transverse component of velocity of the vehicle
v_ϕ	Component of velocity of the vehicle along the ϕ axis
v_ψ	Component of velocity of the vehicle along the ψ axis
VCI_1	Vehicle cone index for one pass
W	Weight of the vehicle
W_N	Component of weight of the vehicle normal to the terrain
W_T	Component of weight of the vehicle parallel to the terrain
x	X/L
X, Y, Z	Local coordinate system
y	Y/L
z	Z/L
α	Side-slip angle
β	ℓ/L
γ_1	Angle of slip direction of the outer track
γ_2	Angle of slip direction of the inner track
Δ	Shearing deformation
Δ_{I1}	Initial displacement of the outer track
Δ_{I2}	Initial displacement of the inner track
Δ_1	Shearing deformation of soil under the outer track

$\dot{\Delta}_1$	Time rate of shearing deformation
Δ_2	Shearing deformation of soil under the inner track
$\dot{\Delta}_2$	Time rate of shearing deformation
δ_1	Δ_1/L
$\dot{\delta}_1$	$\dot{\Delta}_1/L$
δ_2	Δ_2/L
$\dot{\delta}_2$	$\dot{\Delta}_2/L$
ϵ	Steering ratio
η	Angle of sloping terrain
θ	Directional angle
θ_a	Approach angle of the track envelope
θ_d	Departure angle of the track envelope
Λ	Material constant related to rate effect
λ	ΛL
μ	GL^3/W
ξ_1	C_1/L
ξ_2	C_2/L
σ	Normal stress
τ	Shear stress
τ_M	Maximum shear strength
ϕ	Angle of internal friction
ψ, ϕ	Coordinate system fixed on level ground
ω	Yaw angle

In accordance with letter from DAEN-RDC, DAEN-ASI dated 22 July 1977, Subject: Facsimile Catalog Cards for Laboratory Technical Publications, a facsimile catalog card in Library of Congress MARC format is reproduced below.

Baladi, George Youssef

A terrain-vehicle interaction model for analysis of steering performance of track-laying vehicles / by George Y. Baladi and Behzad Rohani. Vicksburg, Miss. : U. S. Waterways Experiment Station ; Springfield, Va. : available from National Technical Information Service, 1979.

47, [93] p. : ill. ; 27 cm. (Technical report - U. S. Army Engineer Waterways Experiment Station ; GL-79-6)

Prepared for Office, Chief of Engineers, U. S. Army, Washington, D. C., under Project 4A161102AT24, Task A3/E3, Work Unit 003,

References: p. 47.

1. AGIL (Computer program). 2. Mathematical models. 3. Military vehicles. 4. Rheological models. 5. Soil-track interaction. 6. Terrain-vehicle interaction. 7. Track-laying vehicles. 8. Vehicle performance. I. Rohani, Behzad, joint author. II. United States. Army. Corps of Engineers. III. Series: United States. Waterways Experiment Station, Vicksburg, Miss. Technical report ; GL-79-6.
TA7.W34 no.GL-79-6